

Statistics of recent aftershock sequences in central and eastern North America and their implications for declustering

Will Levandowski*
Boulder Geophysics
BoulderGeophysics@gmail.com

*Also at TetraTech, Inc.
1100 S. McCaslin Blvd,
Superior, CO 80027
(303)448-7412
will.levandowski@tetrtech.com
Grant Time Period: May 16, 2021-May 16, 2022

Acknowledgment of Support:

This material is based upon work supported by the U.S. Geological Survey under Grant No. G21AP10312

Disclaimer: The views and conclusions contained in this document are those of the authors and should not be interpreted as representing the opinions or policies of the U.S. Geological Survey. Mention of trade names or commercial products does not constitute their endorsement by the U.S. Geological Survey.

Abstract

Aftershock clusters are transient so must be identified and culled—“declustered”—from earthquake catalogs to calculate reliable long-term seismicity rates. Because most of central and eastern North America (CENA) lacks discrete fault sources in the National Seismic Hazard Model (NSHM), such long-term seismicity rates are the sole meaningful sources for decadal peak ground motions and thus hazard levels. Despite this importance and the known differences between aftershock behavior in low strain-rate intraplate settings like CENA and tectonically active regions, the current NSHM declustering algorithm is based on 62 southern California earthquake sequences between 1932 and 1972. Here, data from 145 intraplate CENA earthquake sequences (1974–2021; mainshocks M_w 3.65–5.84) demonstrate that CENA aftershock sequences last several times longer than the current NSHM declustering window, yet they are confined to a smaller epicentral radius (\sim 15 km). Post-mainshock seismicity decays log-linearly with time, returning to pre-mainshock rates typically after a year ($M < 4.0$) to a decade or more ($M 5+$), but there is no evidence for millennial sequences that would invalidate the use of historic to instrumental seismicity catalogs in intraplate hazard assessment. The slope of log-rate vs time—Omori’s parameter p —varies significantly across CENA: Decay throughout most of southeastern Canada ($p > 1.0$) roughly parallels typical California behavior ($p \approx 1.07$), while central/eastern US (CEUS) sequences ($p \approx 0.85$) and aftershocks in the Charlevoix, Quebec, seismic zone ($p \approx 0.9$) die off more slowly. Average aftershock rates are determined as functions of epicentral distance and time since the mainshock, and revised mainshock magnitude-dependent space-time windows for declustering CEUS and CENA seismicity are suggested. These suggestions narrow the epicentral radius within which post-mainshock earthquakes are discarded as aftershocks yet substantially extend the duration of assumed aftershocks near the epicenter.

1 Introduction

1.1. USGS Seismicity-Based Background Source Model

Known faults are the primary sources of anticipated shaking over decadal timescales in most of western North America, yet few CENA faults meet the criteria to be included in the NSHM: demonstrated Quaternary activity, defined dip and length for magnitude calculation, slip rate or recurrence interval data, and results vetted in a peer-reviewed publication. Instead, for most of CENA, hazard assessments hinge on the historical/instrumental earthquake catalog.

This seismicity-based background source model [after *Frankel et al.*, 1996] is defined on a $0.1^\circ \times 0.1^\circ$ grid, where the frequency-magnitude distribution of catalog events is fit with a Gutenberg-Richter relation:

$$\log_{10}(N_{\geq M}) = A - bM, \text{ or } N_{\geq M} = A \times 10^{-bM} \quad (1)$$

In equation 1, $N_{\geq M}$ is the total number of events with magnitude equal to or greater than M . The NSHM assumes a value of 1.0 for b in the CEUS and solves for the best-fitting A -value in each cell. This map is termed the “A-grid”, and it specifically implies that $A \geq 0$ events are expected each year (including $A/10 \geq 1$, $A/1000 \geq 3$, ...) in each cell. The A -grid is then smoothed, and seismicity rates in each cell are computed accordingly. Away from the handful of defined faults—Cheraw, Meers, several sites near New Madrid and in the Wabash Valley, Charleston, and Charlevoix—this sampling is the dominant seismic source component in most of CENA.

Aftershock rates are transient and therefore introduce time dependence to earthquake rates, while Gutenberg-Richter statistics are valid for time-stationary Poisson processes. This observation was the underlying motivation of *Gardner and Knopoff* [1974], who showed that clustered catalogs are non-Poisson but declustered catalogs should be. More simply, declustering should leave time-independent rates that will be referred to as “background” herein, such that:

$$\text{Total Seismicity Rate}(t) = \text{Background Rate} + \text{Aftershock Rate}(t) \quad (2)$$

Retaining aftershocks in seismicity catalogs creates spuriously high A -values near past events, elevating projected earthquake rates. Appropriately removing aftershock clusters is therefore critical to avoiding biases in NSHM hazard assessments for CENA.

In the current NSHM approach—favored for its simplicity [*Mueller*, 2018]—all events within a certain distance from and time following a mainshock are flagged as aftershocks and deleted prior to calculating NSHM A -grids. The dimensions of this time/distance window increase with mainshock magnitude and follow relations developed for 62 southern California sequences from 1932 to 1971 by *Gardner and Knopoff* [1974] (hereafter, GK74).

Notably, the same time-distance boxes are used to decluster the NSHM catalog for West Coast plate boundaries, tectonically active parts of the Intermountain West, and cratonic CENA, despite the profound differences among these seismotectonic settings. For instance, *Stein and Liu* [2011] suggest that current New Madrid seismicity represents a 200-year aftershock sequence of the M7–8 1811–1812 earthquakes and state that intraplate aftershocks can last 1000 years or more. By contrast, even for M8.0 events, GK74 proposes a duration of 2.7 years.

Aftershocks of the 2014 M_w6.02 Napa, California earthquake illustrate typical California behavior. GK74 predicts aftershocks over an epicentral distance of ~53 km for ~1.5 years ([Figure 1A](#)). To test this prediction, the number of earthquakes in discrete time-distance windows can be counted, rescaled to a reference magnitude (here, M_w≥2.5) either using Gutenberg-Richter relations ([Figure 1B](#)) or simply setting a minimum magnitude for aftershocks. Earthquake counts within a given time-radius box are then normalized to a common area and duration to yield earthquake rate density (#events area⁻¹ year⁻¹). Here, a reference duration of 1 year is chosen for simplicity and, because it will be shown below that aftershocks are generally confined to a 25 km radius of the epicenter (area=1964 km²), a reference area of 2,000 km² is assigned. The very high rates of

seismicity observed within ~25 km of the epicenter indeed peter out near 1.5 years (**Figure 1C**), although rates appear largely unaffected in the outer half of the GK74 radius.

1.2. Omori Decay

Aftershock sequences do not cease suddenly but rather aftershock rates decay with time (**Figure 1D**), generally following the Omori [1896] relation:

$$R(t)=K/(t+c)^p \quad (3)$$

Constants K and p represent overall aftershock productivity and its time dependence, respectively. A small scalar, $c = 0.05$ days, is added to t to avoid singularity as t approaches 0; for the 1-year and longer durations of primary interest here, c has little impact.

Combining the Gutenberg-Richter relation of Equation 1 with Omori decay (Equation 3) gives the time- and magnitude-dependent rate R of aftershocks following a mainshock of magnitude M_{main} [Reasenberg and Jones, 1989]:

$$\begin{aligned} R_{\geq M}(t) &= 10^{a+b(M_{\text{main}}-M)} / (t+c)^p \rightarrow \\ \log_{10}(R_{\geq M}(t)) &= a + b(M_{\text{Main}} - M) - p \log_{10}(t+c) \end{aligned} \quad (4)$$

Here, b is again the Gutenberg-Richter b -value, p again describes how aftershock rates decay with time, and a quantifies aftershock productivity but differs from the Gutenberg-Richter A -value. Accordingly,

$$K|_M = 10^{a+b(M_{\text{main}}-M)} \quad (5)$$

Napa aftershocks illustrate Omori Decay reasonably well (**Figure 1D**). Daily rates wane approximately log-linearly over the timespan from less than 1 day to more than 1000 days post-mainshock. As a result, the total number of post-mainshock earthquakes climbs steeply over the first few weeks but levels out asymptotically to a gentler rate within two months or so (**Figure 1E**). The best-fit Omori parameters— $p=1.00$, $a=-2.67$, and $b=0.93$ —Napa typify California sequences: *Reasenberg and Jones* [1989] derived median values (± 1 s.d.) for “generic California” sequences of $p=1.07$ (0.85 – 1.3), $a=-1.75$ (-2.39 – -1.15). A value of 0.7–1.1 is common for b , both in California sequences and globally.

The long-term earthquake rate density is also readily estimated from pre-mainshock seismicity (**Figure 1A**). In the decade preceding the mainshock, the average earthquake rate density within the 53-km GK74 radius was $\sim 18 M_w \geq 2.5$ / year, as fit by Gutenberg-Richter relations. (Indeed, there were 186 $M_w \geq 2.5$ events during this decade.) Rescaled to the 2000 km² reference area, this rate is ~ 3.6 /year. To delineate the duration of increased post-mainshock seismicity and the radius affected, this estimated background rate is shown as the pink contour in **Figure 1C**. Except for a particularly active area near 40 km radius, post-mainshock rates only exceed background rates within 25 km of the epicenter and only for ~ 1 –2 years. Finally, the Omori Decay curve intersects the long-term rate at a grossly similar 0.9 years (**Figure 1D**), roughly consistent with the GK74 estimate of 1.5 years.

1.3. Previous CENA Aftershock Studies

Reasenberg and Jones [1989] also derived their typical Omori parameters for California earthquake sequences. Previous studies of multiple CENA aftershock sequences find that a and p are broadly consistent with generic California sequences. *Ebel et al.* [2009; see also *Ebel*, 2000; 2008] reported b , p , and a for 13 cratonic earthquake sequences from around the world, four in CENA, finding mean values insignificantly different from generic California parameters. Similarly, the aftershock sequences of four M4.5–5.5 events in the St. Lawrence region, as well as the stacked aftershocks of four less productive events, fall within these broad statistical ranges of b , p , and a [*Fereidoni and Atkinson*, 2014].

Table 1. Previous multi-event studies of CENA aftershock decay

| | # sequences | b | p | a |
|------------|-------------|-----------------|-----------------|------------------|
| Generic CA | 62 | 0.87 ± 0.17 | 1.07 ± 0.22 | -1.80 ± 0.58 |

| | | | | |
|-------------------------------------|-----|-----------------|-----------------|------------------|
| <i>Ebel, 2009</i> | 13* | 0.85 ± 0.24 | 1.05 ± 0.22 | -1.81 ± 0.82 |
| <i>Fereidoni and Atkinson, 2014</i> | 8# | 0.91 ± 0.20 | 1.21 ± 0.26 | -2.60 ± 0.74 |

*Ebel's dataset included 13 intraplate aftershock sequences, four from CENA.

Fereidoni and Atkinson analyzed four sequences individually and stacked an additional four less-productive sequences for analysis

There are numerous challenges in understanding CENA aftershock behavior. The studies referenced in **Table 1** find large inter-event variability, such that the p , a , and b values for any individual event are likely to fall within the large range—and therefore confidence limits—of values observed in southern California or elsewhere.

Second, previous research into CENA aftershock decay is self-contradictory. *Stein and Liu* [2009] state that aftershock duration is inversely proportional to fault loading rate, such that several CENA events may have sequences lasting centuries [*Basham and Adams*, 1983; *Ebel et al.*, 2000; *Ma and Eaton*, 2007]. If so, many CENA seismic zones could simply represent long-lived aftershock sequences from historic or unknown, prehistoric events [*Ebel*, 2008] rather than the release of long-term strain. For example, *Stein and Liu* [2009] predict that aftershocks of the ~M7.5 [*Ebel*, 2011] 1663 Charlevoix earthquake would persist for ~500 years, while the GK74 estimate for M7.5 is only 960 days (~2.6 years). This discrepancy implies that CENA sequences must differ from southern California parameters. Nevertheless, the scatter of Omori parameters for individual sequences has led statistical tests to fail to reject the null hypothesis that CENA Omori parameters are the same as their California counterparts.

Low strain rates make geodesy little help in discriminating between long-term strain accrual and transient aftershocks. Rather, GPS data have been used to argue that—if seismically active CENA regions are not currently accruing strain faster than elsewhere—past major earthquakes do not inform the likely locations of future events [e.g., *Newman et al.*, 1996]. Low tectonic earthquake rates may actually obscure aftershock behavior, since it is difficult to separate low-rate, long-duration aftershock sequences from low-rate background activity when each is stochastic, and especially as the time-dependent component approaches and becomes smaller than the steady-state background.

The present study leverages nearly 50 years of instrumentally recorded seismicity to perform a comprehensive analysis of the spatiotemporal characteristics of CENA earthquake sequences. The 145-sequence (**Figure 3**) dataset represents the largest known study of CENA clusters by a factor of ~20, and the largely automated approaches outlined below aim to provide the most exhaustive assessment of CENA aftershocks and best constrained examination of intraplate declustering parameters yet available. First, the 145 individual sequences are analyzed similarly to previous work, then sequences are merged to provide robust parameterization of the mean behavior of CENA aftershock sequences and to quantify regional differences.

2. Aftershock Sequence Analyses

2.1. Methods: Example Single-Event Workflow

The general workflow for analyzing CENA sequences is illustrated with aftershocks of the 2011 $M_w 5.65$ earthquake near Mineral, VA ([Figure 1E](#), [Figure 2](#)). GK74 predicts that aftershocks would last 0.9 years and span 48 km from the epicenter. This prediction can be tested by comparing instrumentally recorded earthquake rates near the epicenter ([Figure 2A](#)) before and since the 2011 mainshock.

a) Determine magnitude of completeness and regional b-value

The first step of the analysis determines an approximate regional magnitude of completeness m_c specific to the sequence in question and to the period intended to represent the long-term background rate. The frequency-magnitude distribution ([Figure 2B](#)) of all events spanning the background and aftershock time windows and an epicentral radius of 100 km is interactively fit to the form of Equation 1, simultaneously defining m_c and regional b -value. In a few areas with very sparse long-term seismicity, the 100 km regional radius was increased to validate m_c and regional b .

The Central Virginia Seismic Zone, subsuming the Mineral epicenter, was moderately active prior to the mainshock. Including the 25 years leading up to 2011, the catalog appears complete to approximately $M_{we} \sim 2.18$ —or $M_L \sim 2.7$ —in the epicentral area ([Figure 2B](#)). The b -value for this subset is an unremarkable 1.06.

b) Model Omori Decay of Post-Mainshock Seismicity

Over what epicentral radius?

Omori Decay is modeled from the time-dependence of post-mainshock earthquake rates near the epicenter, yet few previous studies of CENA Omori Decay have specified the area over which post-mainshock events are harvested as inputs to the modeling. To allow for semi-automation of the aftershock sequence modeling and for consistency, rates are determined from events within the GK74 radius (dashed gray line in [Figure 2C](#)) with magnitude m_c or greater. The GK74 radius almost always extends beyond the region affected (as shown throughout this report), so it is likely sufficient to capture all meaningful aftershock activity; favorable comparisons with previous studies also support this choice of radius.

Define earthquake rates vs. time

Rates as functions of time could be computed a few ways. As one example, *Wetmiller et al. [1984]* quantified aftershock rates of the 1982 $M_w 5.47$ Miramichi, NB earthquake by counting the number of events between timesteps $t_n = (\sqrt{2}) t_{n-1}$ and then simply dividing the counts by their respective interval durations. This approach works well for the well-populated multi-sequence stacks discussed later in this paper. It proved challenging for the long and sometimes sparse individual CENA sequences, however. Rates computed from inverse inter-event times over sliding multi-event windows were more stable for automated calculations across sequences with rates spanning several orders of magnitude.

Over what time interval?

Omori decay manifests as a log-linear relationship between rate and time over the aftershock interval. In an ideal case, post-mainshock seismicity rates would decrease log-linearly to intersect the average long-term (e.g., pre-mainshock) rate at some time, then plateau, and thereon bounce around near the long-term average (e.g., [Figure 1D](#)). The GK74 durations are almost always too short—as is shown throughout this report—but provide a first approximation. The log-linear fit is then extrapolated to where it crosses the estimated background rate. An automated approach is used here to define background rates and post-mainshock rates as a function of time and to solve for this intersection time. If this intersection indeed marks the sequence endtime, then the objectively defined rates at that time should be near the estimated background level. And in ideal cases

(e.g., without secondary sequences, with ample data to define rates, etc.) the seismicity rate should plateau after this intersection, with the plateau level near the estimated background rate. In other cases, rates reach a prominent local minimum and then begin to increase with time as a new cluster emerges; the Omori duration is interactively shortened to exclude these secondary clusters, and a robust fit should traverse this local minimum.

Mineral, VA example and model validation

The Mineral aftershock rate has declined steadily over the past ten years and is amenable to Omori Decay parameterization ([Figure 2D](#)). Fixing $c=0.05$ days, the least-squares log-linear fit is given as:

$$\log_{10}(\text{Rate}) = -0.86 \log_{10}(t+c) + 5.19$$

where Rate refers to the daily rate of $M_w \geq 2.18$ events within 48 km of the epicenter. This fit is derived for 0-2150 days (~5.9 years). During this time-distance window, the best-fit aftershock b -value = 1.24(± 0.06). Rearranging to the form of Equation 3 implies $a=-3.59(\pm 0.05)$. The decay exponent $p = 0.86(\pm 0.02)$. This 5.9-year window may raise skepticism because the GK74 duration is only 0.95 year. Decay was even more gradual during the first 0.95 year, however, best fit with $p=0.70(\pm 0.03)$; b remains 1.24(± 0.06), and $a=-3.68(\pm 0.05)$.

Uncertainties listed are 1.0 standard deviation. Uncertainty in b -value is estimated in a Monte Carlo fashion, in which the reported aftershock magnitudes are each perturbed with a uniform distribution of ± 0.25 magnitude units (a proxy for individual magnitude uncertainty) and the Gutenberg-Richter statistics are recomputed; 100 such trials are completed. Uncertainty in a and p is estimated from the log-linear regression (see MATLAB function *polyfitn*). Notably, however, sequences with few data points but nice, log-linear behavior are assigned lower uncertainties by *polyfitn* than is warranted.

Using a local network, site-specific duration magnitude M_D^* , and more complete catalog (to $M_D^* - 0.4$, $M_{we} 0.56$), *Wu et al.* [2015] fit the first ~130 days of decay to the form of Equation 2, reporting significantly different Omori parameter values. In fact, their estimate of $p=-1.09(\pm 0.06)$ suggested that aftershock rates from the Mineral earthquake decay indistinguishably from generic California events. Aftershock rate evolution is demonstrably different between the Napa and Mineral sequences, however ([Figure 1E](#)): Mineral accrued aftershocks at a steadier rate (lower p), while Napa rates flatten earlier (higher p). Importantly, *Wu et al.* [2015] used their M_D^* scale and $c=2.99$ days: When M_D^* is rescaled to M_{we} using Mueller's [2018] relation and c is fixed at 0.05 days, the best-fit Omori parameters for the 130-day dataset are $p=0.85$, $b=1.04$, $a=-2.21$, similar to those derived here and very different from generic California behavior.

To validate the algorithm developed here a second way, *Wu et al.*'s 130-day M_D^* catalog was analyzed using the same $c=2.99$ days and $m_c=-0.4$ ([Figure S2.1](#)). The automated fit returns $p=1.14\pm 0.01$, essentially reproducing *Wu et al.*'s findings.

c) Calculate long-term earthquake rate density

Expected rate of non-aftershock seismicity during the aftershock window

In the previous step, an estimate of background earthquake rate density was used as one of several guides in selecting the duration over which to model Omori decay. The estimated background rate itself does not influence the derived Omori parameters; it only guides the selection of the time-window over which to model Omori Decay. The only quantitative use of background rate estimates will be to examine spatiotemporal details of aftershock behavior, first in an illustrative fashion for single events and later in the analysis of stacked sequences. The arguments laid out in this paper do not hinge on these background rate estimates, so shortcomings of the approach will not vitiate its findings.

With an estimate of m_c specific to the epicentral area in the decades surrounding the mainshock in hand, the number of events in a so-called background time/radius window with magnitude m_c or greater can easily be counted. This tally is readily converted to a number of events at and above some reference magnitude, in some timeframe, and over some area using Equation 1, the b -value, and the area and duration of the background window.

$$(Background) \text{Rate Density}_{Mc} = N_{Mc} / (\text{AreaBackground} \cdot \text{DurationBackground}) \quad (6)$$

with units of (events/year) km⁻². The terms “rate density” or imprecisely “rate” will be used here. N_{Mc} is the tally of observed events m_c or greater. Area and Duration refer to the spatial area and temporal duration of the window used to define the background rates, detailed a few paragraphs below.

Background seismicity rates appear as the dashed red reference level on [Figure 2D](#). This line represents the long-term daily rate of events m_c and greater expected within the aftershock radius. Ideally, post-mainshock rates would decay to this level and then plateau there for years to decades. This rate of background events expected within the aftershock zone is given as:

$$\begin{aligned} (\text{Daily long-term}) \text{Rate}_{mc} &= \text{Rate Density}_{mc} \cdot \text{Area}_{\text{Aftershocks}} / 365.25 \text{ days/year} \\ &= N_{mc} (\text{Area}_{\text{Aftershocks}} / \text{AreaBackground}) (1 \text{ year} / \text{DurationBackground}) / 365.25 \end{aligned} \quad (7)$$

By default, the epicentral radius used to define the aftershock window is the GK74 radius, so $\text{Area}_{\text{Aftershocks}}$ is by default $\pi(\text{GK74 radius})^2$.

Rescaling background rate densities for comparison among events

To facilitate comparison among sequences that may have different duration, m_c , and area, rate densities are scaled to a common magnitude ($M_{we}2.5$), area (a ~25 km radius, 2000 km²), and duration (1 year). Doing so returns to units of number of events. These values are arbitrary, chosen to roughly express an annual number of felt events, if $M_{we} 2.5$ ($M_L \sim 3.2$ [[Mueller, 2018](#)]) might be felt and aftershocks chiefly occur with a ~25 km epicentral radius.

$$\text{Rate Density}_{M2.5} = (\text{Rate Density}_{Mc}) \times 10^{-b(2.5-Mc)} \quad (8)$$

$$\text{Standardized Event Count} = (\text{Rate Density}_{M2.5}) \times 2000 \text{ km}^2 \times 1 \text{ year} \quad (9)$$

Selecting the time and area to estimate background rate density

Just as area and duration area are specified for each aftershock sequence, they must be chosen to calculate background rate. The GK74 radius again provides a logical lengthscale, and the area used to calculate the background rate density defaults to events within the GK74 radius of the epicenter.

Selecting the time window considered as background has required more care. The window should be long enough to approximate average rates within a few tens of km (e.g., one GK74 radius) of the epicenter but should avoid obvious mainshock-aftershock sequences: 10 years is a typical minimum, though longer windows are chosen when possible. An additional consideration is that seismic monitoring has come a long way since 1974! Older portions of the catalog have higher m_c and therefore resolve fewer details of spatiotemporal patterns. However, if the aftershock rate is negligible after many years, then the stationary long-term rate density can be calculated from an interval well after the mainshock: The interval beginning 10 years after the mainshock and lasting until the end of 2021 is the default choice for events prior to 2002 (since 2002 events allow 10 years of possible aftershock activity and 10 years to determine the “background” rate). For events after 2002, such as Mineral, the background window immediately precedes the mainshock and goes back 10–30 years, depending on the site-specific m_c over time and the occurrence of locally anomalous clusters not representative of the long-term average. Since the background rate ultimately exerts no first-order control on the derived p values, the chosen background duration—although selected with some subjective care—does not warrant too much fretting.

Mineral, VA example

The Central Virginia Seismic Zone hosted 22 $M_{we} \geq 2.18$ events within the 48-km GK74 radius of the Mineral epicenter from 1980 to the 2011 mainshock. This tally translates to 0.7 events/year, $1.9 \times 10^{-3}/\text{day}$, which is taken as the long-term, time-independent (i.e., non-aftershock) seismicity rate in both the background time-window, during the aftershock window (red line in [Figure 2D](#)), and beyond. When the total seismicity rate has decayed back to this level, one may consider the aftershock sequence finished, at least rhetorically. For

reference, the Omori Decay curve is projected to intersect the empirical background rate after ~35 years. It is obvious from seismicity rates that the ~1 year duration suggested by GK74 does not capture the end of Mineral aftershocks. Nevertheless, it also appears from the first 10.3 years of aftershock rate data that activity will become negligible in another few decades, rather than centuries.

d) Quantify empirical aftershock rate density

The estimates of background seismicity rates are used to sharpen images of the temporal and radial distribution of aftershocks. Specifically,

$$\text{Total Seismicity Rate Density } (t,r) - \text{Background Rate Density} \approx \text{Aftershock Rate Density } (t,r) \quad (10)$$

In [Figure 1C](#), total rate density is computed from event counts in small time-radius windows, while the background rate density contour is shown to delineate the time-radius areas with anomalous activity.

Subtracting the background rate density from total rate density ([Figure 2E](#)) illuminates where (in radius), when, and how much rates are elevated. The units are again a standardized count, now the number of excess events per year in a 2000 km² area. Areas with very different background rates can now be compared directly, since the analysis has now turned to the number of extra events plausibly dependent on the mainshock. Also, it may be possible to isolate very low aftershock rates, even aftershock rates that are lower than background (i.e., comprise less than half of the total activity).

Excess seismicity following Mineral has a different spatiotemporal shape than the GK74 window (gray dashed box in [Figure 2E](#)). Apart from a handful of events near 30 km epicentral distance, excess activity is not detected beyond ~20 km, and nearly all of the extra events are within 10 km ([Figure 2E](#)), and anomalous rates persist near the epicenter more than 10 years later ([Figure 2A,E](#)). Detailed Coulomb stress transfer modeling, earthquake relocation, and delineation of specific structures are not aims of this paper, and *Wu et al. [2015]* have already completed this work for the Mineral earthquake. Rather, a completely standardized workflow has been established for CENA aftershock sequence investigation, and a largely automated set of algorithms has been validated against previous, more targeted studies. The approach detailed above will now be applied to 144 other CENA mainshocks, M_{we}3.65–5.84 from 1974–2020.

2.2. Catalog and Magnitude Scaling

The NSHM non-declustered 1974–2016 catalog with non-earthquake sources removed [*Mueller, 2018*] served as the primary catalog from which mainshocks and associated sequences were selected. For this catalog, *Mueller [2018]* rescaled all magnitudes to consistent M_{we} using relations that depend on magnitude type and differ for events in the northeast United States (NEUS), southeastern and central United States east of -100° (SEUS, CUS) and the Great Plains west of -100° to the Rocky Mountain front (GP), as well as for magnitudes determined by the Geological Survey of Canada (GSC) for certain time periods.

M_w, M_{wr}, M_{ww}: ~10% of events, including most mainshocks

M_L, M_D: ~75% of events:

$$M_{we} = 0.806 M_L + 0.633 \text{ (NEUS)}$$

$$0.762 M_L + 0.869 \text{ (SEUS, CUS)}$$

$$M_L - 0.316 \text{ (GP)}$$

$$M_L - 0.526 \text{ (GSC before 1997); } M_L - 0.718 \text{ (GSC after 1997)}$$

m_b, M_N: ~15% of events:

$$M_{we} = m_b - 0.434 \text{ (NEUS);}$$

$$m_b - 0.316 \text{ (SEUS, CUS, GP)}$$

$$m_b - 0.626 \text{ (GSC after 1997)}$$

For example, a typical empirical magnitude of completeness determined from background seismicity is $M_{we} \sim 2.24$, which corresponds to $m_b 2.67$ or $M_L 2.44$ in the NEUS, $m_b 2.56$ or $M_L 2.57$ in the SEUS/CUS, $M_L 2.56$ in the GP, and $M_L 2.77$ or $M_N/m_b 2.87$ in southeastern Canada.

The 1974–2016 NSHM M_{we} catalog was extended through the end of 2021 using the USGS ComCat catalog with non-earthquake sources removed and converting magnitudes uniformly to M_{we} following the equations above.

The merged 1974–2021 catalog was then scrutinized for candidate mainshocks. Events were limited to east of the Rocky Mountain front (defined loosely: [Figure 3](#)) and restricted to the comparatively well instrumented areas south of $\sim 52^\circ\text{N}$ latitude. Because well-operational parameters—which are often altered in response to seismicity [e.g., [Yeck et al., 2016](#)]—introduce complex time-dependence to injection-induced seismicity, known areas and time periods of potentially induced seismicity are excluded: in particular 21st-century events in central/northern Oklahoma and southern Kansas; Timpson and Dallas/Fort Worth, Texas; and Guy-Greenbrier, Arkansas. Finally, individual events that are obvious direct aftershocks of larger events are not considered. Nevertheless, retaining moderate-magnitude events near New Madrid, for example, does not imply that ongoing seismicity cannot represent—in whole or part—aftershocks of the 1811–1812 sequence [e.g., [Stein and Liu, 2009](#)]. Rather, to the extent that the rates of aftershocks from the 1811–1812 aftershock rates are constant across the ~ 10 -year windows used for each sequence, it is still possible to isolate the time-dependent rate perturbations following moderate-magnitude events from the combined tectonic and long-duration aftershock background. Complete mainshock metadata, aftershock sequence data, and analyses for all 145 sequences are available at <https://github.com/WillLevandowski/AftershockSequences>

The 145 mainshocks are not meant to be an authoritative or comprehensive set, but they are intended to be representative of mainshocks in the central and eastern United States and southeastern Canada, at least those $M_w 3.61$ – 5.84 . For this reason, “mainshocks” with no aftershocks are retained, as are sparse “sequences” of one or just a few scattered post-mainshock events. These deficient sequences will be stacked with others in a later section.

Of the 145 sequences examined, Omori Decay is adequately resolved to be modeled in 51. Another 40 have no aftershocks (i.e., no events within the GK74 radius and within a few years of the mainshock) but are retained to ensure that meta-analyses presented below better represent all CENA mainshocks and not only aftershock-productive ones. The remaining 55 sequences have some post-mainshock activity yet too few events; a minimum of five aftershocks was demanded so that Omori Decay parameters and other model parameters would be suitably overdetermined. These sequences are grouped geographically and merged for analysis as multi-event stacks [e.g., [Davis and Frohlich, 1991](#)]. The standardized single-sequence analysis templates of identical form to Figure 2 are auto-generated for all 145 mainshocks and provided in the Supporting Information. The larger, more recent, illustrative, and peculiar sequences are discussed in the following section, then the results of the individual sequences are compiled, and finally meta-analyses of the 145 sequences are conducted.

3. CENA Aftershock Sequences

Aftershock sequences of the remaining six M_5+ events are presented here in reverse chronological order. Then, a handful of other notable sequences are grouped geographically for discussion. All 145 analyses are presented in the form of Figure 2 in the Supporting Information, available at: <https://github.com/WillLevandowski/AftershockSequences>

3.1. Aftershock Sequences of M_5+ Mainshocks

a) 2020 $M_w 5.1$ Sparta, NC (Appalachia)

The most recent event analyzed, the Sparta event occurred in an area of sparse background seismicity. Over the 1.3 years since the mainshock (until the time of writing), nearly 50 $M_w 2.2$ and greater events cataloged

in ComCat cluster within 5–10 km of the epicenter ([Figure 4](#)). This lengthscale is similar to the average rupture length for M5 earthquakes [e.g., *Wells and Coppersmith*, 1994], possibly reflecting stress-transfer peaks at rupture termini, stress concentration at tips of pre-existing cracks, or up-dip slip transfer to and partitioning on pre-existing faults. Temporally, post-mainshock seismicity depicts a well-resolved Omori Decay pattern. Aftershock parameters are typical of CENA sequences studied here, with significantly lower p (0.89 ± 0.04) than generic California sequences, and a projected duration of a few decades rather than the ~0.5 years predicted by GK74. High b -values (~1.8) characterize both regional seismicity over the past decade(s) and the aftershock window.

b) 2010 M_w5.04 Val de Bois, QC (Western Quebec Seismic Zone)

The Val de Bois sequence has previously been studied by *Fereidoni and Atkinson* [2014] who found similar parameter values ($p=1.41\pm0.17$, $b=1.23$, $a=-3.43$) to those presented here ($p = 1.18\pm0.04$, $b=1.25\pm0.07$, $a=-3.24\pm0.05$). Beyond the first few hours, the sequence indeed has a well behaved and uncharacteristically steep decay rate ([Figure 5](#)) more akin to generic California patterns than to the Mineral or Sparta events. Seismicity rates only remained elevated for a few months, and the GK74 duration is a close approximation of the time at which rates drop back to pre-mainshock levels (0.43 years). Most of this activity is concentrated within 15 km of the epicenter.

The Val de Bois sequence illustrates the convergence of three features that, together, strongly suggest a well-constrained end of anomalous activity. The first proxy is that the fit to Omori Decay data from minutes after the mainshock through ~100 days crosses the estimated background rate at ~0.4 years (~150 days). Second, the earthquake rate data (black circles) near 100 days are, indeed, at or near background levels. Third, the rate data plateau after ~100 days, and that plateau is at approximately the estimated background rate. Taken together these factors substantiate the estimated background seismicity rate, and the three factors all indicate an end of anomalous activity at 0.4–0.5 years.

c) 2008 M_w5.23 Mt. Carmel, IL (Wabash Seismic Zone)

After more than 15 quiescent years, this earthquake revived the Wabash Valley Seismic Zone and set off a moderate-duration (by CENA standards) sequence. Although most activity is clustered within 10 km and 0.5 years of the mainshock ([Figure 6](#)), the very low pre-mainshock background rate implies that the handful of events through several years and out to ~40 km are anomalous. Log-linear decay has proceeded along a slope of $p\sim0.99$. This slope falls in the middle of previous solutions of $p=0.78$ [*Ebel* 2008; 2009], $p=1.0$ [*Yang et al.*, 2009], and $p=1.15$ [*Hamburger et al.*, 2014] ([Table 2](#)).

The estimated endtime of the Carmel sequence varies across several proxies. Seismicity very near the epicenter ends by 0.5 years after the mainshock, which would be consistent with GK74 estimates. However, the Omori Decay fit does not return to background for ~4.5 years. Similarly, earthquake rates within ~40 km of the epicenter reach a nadir after ~3 years before rising again, though this nadir is still well above the estimated background rate. Finally, the observed rates may only be returning to the estimated background at present, nearly 15 years after the mainshock.

Table 2. Comparison of previous Omori Decay analyses, Mw5.23 2008 Mt. Carmel, IL

| Source | M_c | b | p | a |
|--|-------|-----------------|-----------------|------------------|
| Ebel, 2008; 2009 | 1.5 | 0.56 | 0.78 | -1.20 |
| Yang <i>et al.</i> , 2009 $n=C/(k+t)^p$ C=19; k=0.2 | 1.0 | 0.6 | 1.0 | N/A |
| Hamburger <i>et al.</i> , 2014 | 1.0 | 0.58 | 1.152 | -0.66 |
| This study | 2.28 | 0.69 ± 0.03 | 0.99 ± 0.03 | -1.58 ± 0.04 |

d) 1988 M_w5.84 Saguenay, QC (Saguenay Graben/Quebec City Seismic Zone)

The Saguenay doublet is the largest event, let alone event complex, investigated here. The NSHM catalog includes a M_w5.80 just prior to and 12 km from the larger M_w5.84 shock. For modeling purposes, the start time of this sequence was set to the origin time of the M_w5.80 ~45 seconds prior to the M5.84 largest shock. Activity concentrates within the first ~5 months (~0.4 year) and 20 km of the epicenters ([Figure 7](#)), and seismicity is otherwise sparse in the region. Citing low aftershock numbers despite a portable seismic network deployment [*Du Berger et al.*, 1991], *Fereidoni and Atkinson* [2014] elected not to model Saguenay aftershock decay as a standalone dataset; its data was instead stacked with three other St. Lawrence region sequences.

Here, a satisfactory fit is achieved to the few months of aftershocks with a slope of $p=1.07\pm 0.03$. This slope parallels generic California sequences more closely than most other CENA sequences studied here and is similar to *Fereidoni and Atkinson*'s [2014] $p=0.97$ derived for the four-sequence stack that included Saguenay.

e) 1982 M_w5.47 Miramichi, NB (Atlantic Provinces)

The January 9, 1982 earthquake shook a region of known but moderate seismic activity. At M_w5.47, it was likely the largest event in the New England/Northern Appalachian/Atlantic Provinces region for nearly 40 years, since 1944 Cornwall/Massena ON/NY. A joint Canadian/American team responded with a seismometer deployment January 10–22 that was followed by two ~1-week-long surveys April 2–7 and June 17–23 [see *Cranswick et al.*, 1982]. Semi-permanent stations operated by the Canadian government and Weston Observatory of Boston College also recorded dozens of magnitude ~2+ aftershocks. Finally, the mainshock was one of the first events in eastern North American large enough to be recorded on digital seismometers worldwide.

This sequence is lively, long-lived, and complex ([Figure 8](#)). A M_w5.14 event 2.3 days after the mainshock, and M_w4.1 at 81 days each spawned a handful of second-generation aftershocks that create distinct spikes in post-mainshock rates. Note that the magnitudes listed here are M_w or M_{we} from the NSHM catalog and differ slightly from other catalogs. *Wetmiller et al.* [1984] report M_b5.7 for the January 9 mainshock, M_b 5.4 for the January 11 aftershock, and M_b5.0 for the March 31 aftershock. Similarly, epicentral locations used in this study are taken from the NSHM catalog, which collocates most of the aftershocks at -66.60° longitude, 47.00°N latitude. This collocation causes the strip of activity at ~10 km epicentral distance in [Figure 7E](#). Possibly imprecise locations notwithstanding, nearly all aftershocks again occur within ~15 km of the epicenter rather than occupying the full 45-km GK74 radius.

The Miramichi aftershock sequence has been previously studied ([Figure 8F](#)). First, *Wetmiller et al.* [1984] presented analyses of four different space/time subsets of aftershocks. Three were taken from near the mainshock and divided according to the occurrence of primary aftershocks, with durations 0.2 days, 2.2 days, and 228 days. The fourth selected events from a 198-day window from near one of the more distal aftershocks. The b -values of all four sets are all indistinguishable from the regional standard of 0.8, thus not indicative of swarm-like behavior. All four subsets decay roughly as $p = 0.8$, or rate $\propto t^{0.8}$, which *Wetmiller et al.* [1984] recognize as “somewhat lower than values of 1.0 or greater that have been reported for other aftershock sequences in Alaska and Japan (Utsu, 1962; Mogi, 1962; Page, 1968)”. Subsequently, *Ebel et al.* [2000] added unpublished data to derive a similar $b=0.81$ but a higher Omori Decay exponent, $p=1.01$. *Fereidoni and*

Atkinson [2014] used the first 1000 days of aftershocks from the Canadian composite seismicity catalog [Fereidoni *et al.*, 2012] and Wetmiller *et al.*'s $b=0.80$, finding intermediate $p=0.89$ and an estimate of $a=-1.75$.

In the eight years prior to the mainshock, five $M_w 2.27$ or greater earthquakes occurred within the 45-km GK74 radius of the epicenter. All four studies in [Table 3](#) demonstrate that post-mainshock rates did not return to this level within the 0.75-year GK74 estimate. All four studies estimate that overall earthquake rates will or did return to the average $\sim 0.6 M_w 2.27$ events/year after several years to a few decades (8–48 years).

The present analysis benefits from 40 years of available aftershock data—between 12 and 100 times the duration of previous studies—yet reaches similar results: The best-fit Omori Decay rate $p=0.86\pm 0.04$ falls in the middle of the pack. Moreover, with these additional decades of data, one can observe that rates did indeed approach pre-mainshock levels around 20 years post-mainshock and appear to have remained near this level for the past ~ 20 years. A moderate increase in activity ~ 32 years after the mainshock may be a distinct cluster and thus indicate that the 1982 aftershock sequence has concluded.

Alternative Omori Decay models with different m_c , and models in which background rates are defined by post-mainshock rates (20–39.96 years or 30–39.96 years) give $0.7 < p < 0.94$. In conclusion, Miramichi aftershocks lasted or will last for a few decades, not several months to a year as predicted by GK74, yet not many centuries or millenia as proposed for some intraplate aftershock sequences [e.g. Stein and Liu, 2009].

Table 3. Comparison of previous Omori decay analyses, $M_w 5.47$ 1982 Miramichi, NB

| Source | Time window | M_c | b | p | a |
|--------------------------------|---------------------|--------------------------|-----------------|-----------------|------------------|
| Wetmiller <i>et al.</i> , 1984 | 1–228 days, divided | $-\infty$ (~ 2.0) | 0.8 | 0.8 | N/A |
| Ebel, 2009 | | 1.7 | 0.81 | 1.03 | -1.83* |
| Fereidoni and Atkinson, 2014 | 0.01–1000 days | 2.5 | 0.8 | 0.89 ± 0.10 | -1.75 |
| This study (M_w) | 0 –14591 days | 2.27 | 0.90 ± 0.02 | 0.86 ± 0.04 | -2.01 ± 0.09 |

* Ebel 2022, written communication

f) 1980 $M_w 5.04$ Mt. Sterling, KY

This substantially older event illustrates the use of post-mainshock seismicity to determine “background” rates ([Figure 9](#)). Doing so allows comparatively cavalier m_c (2.01), which has the benefit of retaining as many events as possible from this rather sparse sequence. Despite only having 11 events in the aftershock window, the decay of this sequence paints an internally consistent picture with steady rate decline on a slope $p=0.86$. The time at which rates return to background levels is poorly constrained because of the lack of events between 1 and 8 years post-mainshock.

3.2. Results: Other Notable Sequences and Seismic Zones

a) Charlevoix Seismic Zone

1979 $M_w 4.75$ Malbaie, QC (Charlevoix Seismic Zone)

This event was examined by Fereidoni and Atkinson [2014], who noted an insufficient number of aftershocks and instead grouped this event with three others for meta-analysis. The behavior of the sequence is indeed poorly constrained because of a hiatus in recorded seismicity between a few days and almost one year, but an acceptable fit to the first ~ 1 year of data is obtained ([Figure 10](#)). Omori Decay proceeds along a slope $p=0.92\pm 0.05$, and seismicity rates return to the estimated long-term average in ~ 0.75 years.

1997 $M_w 4.26$ Malbaie, QC (Charlevoix Seismic Zone)

This earthquake occurred in one of the seismically busiest parts of CENA ([Figure 11](#)). The background rates can therefore be reliably estimated. Sufficient catalog time is available after the sequence to use 10–25

years post-mainshock seismicity to define the background. Moreover, the area is well instrumented, creating a complete catalog to at least M_w 1.67.

Aside from bursts of activity \sim 50 and \sim 180 days after the mainshock, rates decline log-linearly for just over a year, at which time they reach a nadir. The decay follows a slope of $p=0.83\pm0.02$. Post-mainshock activity rates remain above the estimated background for at least \sim 0.5 years.

2005 M_w 4.57 Charlevoix, QC (Charlevoix Seismic Zone)

This sequence ([Figure 12](#)) shares several characteristics with the slightly larger 2010 Val de Bois sequence. Both occurred in active seismic zones, and their aftershocks are superimposed on high rate-densities. Both also produce well recorded bursts of small-magnitude aftershocks within just a few km of the epicenter that disappear within a year. While Val de Bois exhibited steep decay akin to California sequences ($p\sim1.18$), however, the best-fit p for this sequence is 0.80 ± 0.05 .

b) Quebec City/western Quebec/Ontario and Lower St. Lawrence/Atlantic Provinces

1997 M_w 4.47 Cape Rouge, QC (Quebec City Seismic Zone)

This sequence responded rapidly, releasing eight aftershocks in the first day and a dozen in the first three ([Figure 13](#)). Seismicity then disappeared quickly ($p=1.03\pm0.03$). This fit is determined from the first \sim 1.5 years of rate estimates, which is dubious given the hiatus between 2.5 and 482 days. Nevertheless, Omori fits to the first 2.5 days are less steep ($p=0.86$) and therefore overpredict even the very low rates observed over the following 2 years. In fact, the rates of seismicity are roughly constant from \sim 2 to 20 years following the mainshock. For this sequence, the interval 10–20 years post-mainshock is used to estimate background.

1990 M_w 4.56 Mont Laurier, QC (Western Quebec Seismic Zone)

Unlike the other sequences examined so far, results presented here ([Figure 14](#)) differ somewhat from those of *Fereidoni and Atkinson [2014]* (dashed black line in [Figure 14D](#)). Our a and b estimates are quite similar, yet their $p=1.47\pm0.22$ is significantly higher than the $p=1.05\pm0.07$ depicted by the solid black line in [Figure 14D](#). Notably, their Figure 2C—log-rate vs log-time—reveals that $p=1.47$ systematically overshoots early data and underpredicts later rates. In other words: It is too steep. There are a few possible causes for the discrepancy. *Fereidoni and Atkinson [2014]* use a minimum magnitude 0.0 [citing *LaMontagne et al., 1994*]; here $m_c=1.57$. They also use a time interval 1.375 to 405 days after the mainshock, though rate decay does not appear any steeper in this window than at other times.

Empirically, Mont Laurier seismicity rates decay to long-term averages over somewhat less than a year. A handful of small-magnitude events and apparent aftershocks cloud the picture beginning \sim 0.75 years after the mainshock. Omori parameters are derived from the initial 60 days of data to steer clear of this secondary burst. This slope intersects the estimated long-term rate after 0.6 years. This duration is inconsistent with a p value that is even steeper than generic California sequences, for which the expected duration is only 0.23 years.

2013 M_w 4.49 Lac Barnes, QC (Western Quebec/Ontario)

As with most sequences discussed so far, aftershocks of the Lac Barnes earthquake huddle near the epicenter ([Figure 15](#)). Within the first year, 16 events were located within 5 km of the mainshock, and a few additional events out to \sim 3 years continue a log-linear rate decay with slope $p=1.01\pm0.02$. The sequence contains six M_w 2.61 or greater aftershocks that lead to a lower b -value (0.45 ± 0.02) for the sequence than the typical $b=0.83\pm0.03$ generally observed in the epicentral regional.

2000 M_w 4.59 Kipawa, QC (Western Quebec/Ontario): An example of poorly resolved Omori Decay

Fereidoni and Atkinson [2014] did not model this meager sequence, citing low aftershock numbers, but rather merged it with three others for analysis, finding $p=0.97$ for the meta-sequence. As a second challenge, the

Kipawa area experienced moderate levels of seismicity for the 20 years preceding and the 7 years following the mainshock but has little cataloged seismicity since then ([Figure 16](#)). Earthquakes occurred within the 35.8-km GK74 radius ~30 minutes, then 93, 127, 136, 144, 318, and 770 days after the mainshock.

Kipawa is the largest mainshock for which the mostly automated procedure does not work well. The automated approach produces a rather poor fit and a very low estimate of $p=0.65\pm0.11$. Manually setting the first five time-bins to 0–10 days, 10–130 days, 130–300 days, 300–700 days, and 700–1500 days results in an apparent monotonic decrease in rate over the first year or so. This decay is also steeper, $p=1.01\pm0.07$, than the very slow model generated from default time-bins, and it parallels *Fereidoni and Atkinson's* [2014] model for the meta-sequence that included Kipawa.

1999 M_w 4.39 Cote Nord (Lower St. Lawrence Seismic Zone)

The 1999 Lower St. Lawrence sequence illustrates several of the methods applied here ([Figure 17](#)). It struck a highly active region, introducing the challenge of separating aftershock activity from background. There is also sufficient time after the sequence waned to use post-mainshock seismicity to define the background rate. These determinations are particularly robust and intuitive: It can easily be seen that the post-mainshock seismicity rate returns to the estimated background rate at ~1 year, plateaus near this level, and has remained stable near this inferred time-independent rate for more than a decade.

This sequence's Omori Decay is steep by CENA standards: $p=1.06\pm0.01$. Both *Fereidoni and Atkinson* [2014] and *LaMontagne et al.* [2004] also find comparatively high $p = 1.29$ and 1.34 , respectively ([Table 4](#)). Nevertheless, it is patent that earthquake rates had not reached their years-long plateau by the 0.19-year GK74-estimated duration. Rather, even this steeply decaying sequence empirically lasted four times as long, ~0.9 years. As with most CENA events, aftershocks are only registered within ~15 km of the epicenter instead of the 35-km radius suggested by GK74.

Table 4. Comparison of Omori Decay analyses, M_w 4.39 1999 Cote Nord, Lower St. Lawrence

| Source | M_c | b | p | a |
|--|-------|----------------|-----------------|------------------|
| <i>LaMontagne et al.</i> , 2004 ($c=0.03$ days) | 0.9 | 0.97 ± 0.17 | 1.34 | -2.60 |
| <i>Fereidoni and Atkinson</i> , 2014 | 0.9 | 0.98 | 1.29 ± 0.16 | -2.60 |
| This study (M_w) ($c=0.01$ days) | 1.37 | 1.05 ± 0.5 | 1.06 ± 0.01 | -2.57 ± 0.02 |

c) New England

2002 M_w 4.97 Au Sable Forks, NY (New England)

The Au Sable Forks, NY earthquake occurred in a moderately active region of northern New York state. A burst of activity within ~10 km of the epicenter waned in a bit over a year ([Figure 18](#)), but seismicity rates remained above the very low long-term average for several years ($p = 0.91\pm0.01$). Some 3 years after the mainshock, activity rates decreased below pre-mainshock levels, so the interval from 7.5–15 years can be used to estimate background rates, with the advantage that a low m_c can be chosen without spuriously increasing the apparent aftershock activity (assuming completeness magnitude generally decreases with time). *Ebel* [2008;2009] used a similar minimum magnitude 1.5 and found $p = 0.78$ ([Table 5](#)), lower than modeled here and implying greater differences from generic California decay.

Table 5. Comparison with previous Omori Decay analyses: Au Sable Forks and Goodnow, NY

| Source | M_c | b | p | a |
|--|-------|-----------------|-----------------|------------------|
| <i>Au Sable Forks, Ebel, 2009</i> | 1.5 | 0.60 | 0.78 | -1.55 |
| <i>Au Sable Forks, This study (M_w)</i> | 1.37 | 0.61 ± 0.03 | 0.91 ± 0.01 | -1.94 ± 0.03 |

| | | | | |
|-------------------------------|------|-----------------|-----------------|------------------|
| Goodnow, Ebel, 2009 | 1.5 | 0.85 | 0.74 | -2.50 |
| Goodnow, This study (M_w) | 2.41 | 1.29 ± 0.11 | 0.89 ± 0.03 | -2.80 ± 0.04 |

1983 $M_w4.83$ Goodnow, NY (New England)

About 80 km from Au Sable Forks and 18 years earlier, this similar-magnitude event produced a similarly slow decay ([Figure 19](#)). Seismicity persisted for ~2 years, giving way to a hiatus from 2–10 years. For $m_c=2.41$, two background rate estimates give similar values: three events occurred in the 9 years before, and three occurred between 10 and 20 years after the mainshock. The present study finds $p = 0.89 \pm 0.03$, which is again modestly higher than Ebel's [2000] $p=0.74$, though both are significantly lower than the generic California $p=1.07$.

d) Midcontinent: Ohio and Kentucky

1988 $M_w4.17$ Owingsville, KY

The Mt. Sterling sequence abated, seismicity in central Kentucky was quiet for several years until this sequence ([Figure 20](#)). Apart from these small sequences, seismicity is sporadic in the region. Therefore, the estimated background rate is not robust, and the time at which rates return to background does not indicate the end of the sequence (here, it is an overestimate).

The Omori Decay model does not directly depend on this estimated return to background, however. Log-linear decay appears steady over several years, following a slope of $p=0.95 \pm 0.02$. This sequence is not alone in its low activity: The 1980 M5.04 Mt. Sterling, KY was followed by only a handful of aftershocks as well.

2001 $M_w4.3$ Northeast Ohio (Midcontinent)

A handful of aftershocks occurred within hours of this event, followed by a hiatus of a few months, when a secondary sequence kicked off just ~2 km from the mainshock epicenter ([Figure 21](#)). The most reliable Omori Decay fit can be achieved by omitting the rates during this secondary increase. For $m_c1.57$, $p=0.92 \pm 0.06$; an alternative model with $m_c1.37$ and resulting $p=0.99 \pm 0.05$ is shown as a dashed line in Figure 25. (The background rate is calculated from post-mainshock seismicity, so reducing m_c should cause the aftershock sequence to appear to finish earlier, if anything.) In either case, the sequence lasts for several years—not the 0.17 years predicted by GK74—but only impacts a ~10-km radius.

e) Eastern Tennessee / Appalachia

2003 $M_w4.59$ Ft. Payne, AL (Eastern Tennessee Seismic Zone)

Even though the expected GK74 duration for the Ft. Payne earthquake is only 0.24 years, post-mainshock activity rates did not return to pre-mainshock levels for about 4 years, decreasing as $p=0.93 \pm 0.02$ ([Figure 22](#)). Anomalous rate density is most pronounced within 1 year and 10 km of the origin, but elevated activity is noted throughout the 36-km epicentral zone for more than five years. Both the aftershock sequence and regional seismicity display higher b -values than many other CENA settings analyzed here; the reason for these high values is unknown.

2018 $M_w4.40$ Decatur, TN (Eastern Tennessee Seismic Zone)

The Decatur earthquake occurred in the central part of the Eastern Tennessee Seismic Zone, an area with plentiful background activity. The epicentral zone is characterized by high b -values. Anomalous activity relative to the 10 years prior to the mainshock concentrates within the first 5 months (0.4 years) and a few km of the epicenter ([Figure 23](#)). Seismicity rates return to estimated background levels after 0.42 years along a slope $p=0.89 \pm 0.02$ that is notably similar to the other decent standalone sequence from the Eastern Tennessee Seismic Zone—2014 M4.59 Ft. Payne, AL ($p=0.93 \pm 0.02$).

f) New Madrid and surrounding areas

1976 $M_w4.62$ Marked Tree, AR (New Madrid Seismic Zone)

The proportion of modern New Madrid area seismicity that represents aftershocks of the 1811-1812 M~7 events is debated [e.g., Stein and Liu, 2009; Page and Hough, 2014; Boyd et al., 2014]. Over intervals of years to a decade or two, however, the rates of any centuries-long aftershock sequences should be roughly constant. Therefore, the impacts of moderate-magnitude events should be separable from longer-term phenomena, even amid active backgrounds such as New Madrid. The Val de Bois event discussed above, for example, occurred in a rather active region, yet its influence on overall earthquake rates is readily extracted.

The 1976 Marked Tree earthquake was followed by a rate increase within 10 km of the epicenter for just under a year, with some additional seismicity—moderately dense even by New Madrid standards—throughout the 37-km GK74 radius ([Figure 24](#)). Between 1.25 and 3 years, however, these overall rates decline to estimated background levels, and post-mainshock rates hit a local minimum at ~2 years. Omori Decay proceeds log-linearly from minutes after the event through this nadir at 2 years as $p=0.81\pm0.04$. This interval of consistent decay exceeds the 0.25-year estimate for generic California sequences by nearly an order of magnitude. Moreover, this event—one of the oldest analyzed here and in the busiest region—illustrates that viable aftershock sequence parameters can be extracted from old, moderate-magnitude events whose sequences may be superimposed on larger, longer-duration phenomena.

2005 $M_w4.22$ Manila, AR (New Madrid Seismic Zone)

Amid a busy background, anomalous activity is most pronounced within 10 km and 1 year of the mainshock ([Figure 25](#)). Seismicity rates return to estimated background levels in just over a year. This decay is typical for CENA— $p=0.86\pm0.02$ —but remains significantly lower than the generic California model. As such, it is not surprising that the 1.1-year empirical duration is 7 times the GK74 prediction. The b -values for both regional seismicity and the aftershock sequence, 1.68 and 1.66, are high by CENA standards.

1987 $M_w4.28$ Cairo, IL (New Madrid Seismic Zone)

This event in the greater New Madrid region was followed a moderate but resolvable increase in seismicity rates within ~30 km of the epicenter that endured for approximately one year ([Figure 26](#)). Seismicity rates dropped over that year along a slope of $p=0.81\pm0.07$ to the average rate observed between 10 and 20 years after the mainshock. Rates then hovered near this level from 1–4 years post-mainshock before entering 5-year lull. The estimated GK74 duration of the sequence, 0.16 years, is not sufficient to capture the aftershock sequence, which lasts several times longer.

1990 $M_w4.28$ Chaffee, MO (WNW of New Madrid Seismic Zone)

Chaffee lies ~60 km north of New Madrid, just WNW of the area of most concentrated seismicity. As shown on its sequence one-pager ([Figure 27](#)), dense activity begins beyond ~40 km. By contrast, there are few events near this epicenter (i.e., within the GK74 radius, 32.6 km), averaging 0.6 $M_w2.39$ or greater per year from 2000 to 2020. This rate is exceeded for about a year following the mainshock; projecting the Omori Decay fit probably overestimates this sequence's duration at 2.7 years. Whether 1 or 2.7 years, the duration is much longer than the 2 months (0.16 year) from GK74. Because the range of aftershock magnitudes is small, the aftershock sequence b -value is very high. Therefore, a becomes exceptionally negative.

Enola, AR: 1982 $M_w4.38$ & 2001 $M_w4.34$ (SW of New Madrid Seismic Zone)

This seismic zone has experienced three bursts of seismicity since the beginning of the catalog in 1974, yet it is otherwise seismically silent ([Figure 28](#)). Between the 1974 beginning of the catalog used here and three days prior to the 1982 event, no earthquakes were recorded in the epicentral zone. Five foreshocks preceded the

1982 sequence, which produced 129 M_w 2.24 and greater events through 1990. After a single event in 1992, no activity was detected until the May 2001 M_w 4.34 earthquake. Its aftershocks events continued through 2006, then a two-year hiatus preceded the onset of induced seismicity in the Guy-Greenbrier area.

With no modeling at all, it is obvious that the 1982 sequence lasted ~10 years (the final event is at 10.13 years). The GK74 estimate is 0.19 years. That stated, seismicity rates decrease log-linearly for the first 90 days after the mainshock, then increase (perhaps a second-generation aftershock sequence), fall near 2 years, increase again, and finally bottom out after 10 years. Therefore, the most reliable Omori Decay fit is to the first 90 days. Amazingly, extrapolating this 90-day trend faithfully predicts the local minimum rate near 2 years and even the final nadir near 10-14 years! Moreover, the minimum rate (near 14 years) is indeed very close to the estimated long-term average, suggesting that the long-lived compound sequence was indeed finished.

With no modeling at all, it is obvious that the 2001 sequence lasted ~5.5 years: The final event occurred at 5.45 years. The GK74 estimate is 0.18 years. Additionally, the Omori Decay curve does intersect the estimated background rate near 6 years, a few years before the onset of induced seismicity near Guy-Greenbrier, AR.

With no modeling at all, it is obvious that the generic California parameters do not reproduce observations. Nevertheless, both sequences are amenable to Omori Decay fits. Both decay as $p=0.88$: 1982 $p=0.88\pm0.04$, 2001 $p=0.88\pm0.01$. Both display b values between 1.1 and 1.24, modestly higher than is typical.

These sequences are illustrative of CENA aftershock behavior. Because no events are recorded apart from the aftershock sequences, a least upper bound is easily placed on the duration of the sequences. Importantly, however, the lack of seismicity between 1992 and 2001 implies that the 1982 sequence was dead as a doornail after 10 years. Similar conclusions are reached from the hiatus between aftershocks of the 2001 event and the onset of Guy-Greenbrier activity. Plainly, these CENA aftershock sequences do not last only months as predicted from California observations. Plainly, these CENA aftershock sequences do not last centuries or millennia either. They unquestionably endure over a timescale of years.

g) Deficient Aftershock Sequences on the Great Plains

Reviewing the sequences discussed so far, one might notice that none lies west of -95° longitude. That dearth is not an error or an omission: All 21 aftershock sequences on the Plains ($M_{we}3.68$ – $M_{we}4.51$) from Saskatchewan to Texas are duds.

The 21 sequences are stacked, creating an equivalent $M_{we}4.95$ in terms of moment release. Omori Decay of this stacked sequence ([Figure 29](#)) proceeds log-linearly over about a year: It also takes a bit over one year for seismicity rates to decline to pre-mainshock levels, and there is a nadir in activity between 300 and 500 days ([Figure 29D](#)). This duration is about three times the GK74 estimate for the summed moment release, and the associated slope— $p=0.84\pm0.02$ —is significantly gentler than the generic California values currently used to decluster catalogs in this region and across CENA.

3.3. Results: Regional Variations in a and p

Aftershock productivity appears to vary across CENA: Overall, approximately half of the sequences examined produced sufficient activity to be recorded and modeled, while the Great Plains are devoid of usable individual aftershock sequences, and all seven of the mainshocks in the Charlevoix Seismic Zone generated passable sequences. Three metrics are used here to quantify aftershock productivity ([Figure 30](#)). The Omori parameter a ([Figure 30A](#)) offers the advantage that it is independent of magnitude (here, the Pearson correlation coefficient between M_{main} and a is -0.15), yet the subjective choice of m_c and the vagaries b -values exert strong influences on the derived a . By contrast, K ([Figure 30B](#)) subsumes tradeoff between a and the chosen m_c (Equation 5) but shows a strong empirical correlation with mainshock magnitude. To account for the trend of increasing K with increasing M_{main} , the empirical K are least-squares-fit as $1.06 M_{\text{Main}}^2 - 7.90 M_{\text{Main}} + 15.90$, and deviations from this regression are taken to represent anomalously high or low aftershock productivity relative to other CENA events of comparable magnitude ([Figure 30C](#)). Events such as Saguenay and Mt. Sterling (KY) have remarkably low productivity, while Mineral and Sparta produced comparatively more aftershocks. The primary regional-scale signal is anomalously high productivity apparent in the Lower St. Lawrence and other Atlantic regions; the cause of this high productivity is not known, and the rest of southeastern Canada does not differ substantially from the CEUS.

The rate of aftershock decay, specifically the average exponent p , also differs significantly among the CENA seismic zones examined here ([Figure 31](#); [Table 6](#)). Activity wanes faster ($p \gtrsim 1.00$) in southeastern Canada, excepting Charlevoix, than in the northeastern United States ($p \approx 0.90$). This trend may continue west/southwestward, with slightly slower decay in New Madrid ($p=0.82$) and on the Great Plains ($p=0.84$), although feeble sequences on the Plains and the challenge of extracting aftershock rates from the dense seismicity in New Madrid invite incredulity.

| Zone | mean $p \pm 1$ std of mean | # | Comments |
|--|-------------------------------|---|--|
| Lower St. Lawrence | 1.02±0.03 | 4 | 4/9 sequences examined were sufficient. |
| Charlevoix | 0.84±0.02 | 7 | All 7 sequences sufficient. The three most reliable Charlevoix sequences (1997 Malbaie, 2005 Charlevoix, 2012 Mt. Grand Fonds) average $p=0.79 \pm 0.03$. |
| Quebec City to Montreal | 1.02±0.01 | 6 | 6/11 sequences sufficient. The stack of 5 stragglers is not worthwhile. |
| Western Quebec/Ontario | 1.03±0.03 | 7 | 6/13 individual events. Six individual sequences, 1 seven-sequence stack of the others. |
| New York / New England / Mid-Atlantic / Central Virginia | 0.89±0.01 | 5 | 5/18 sequences viable. Stacks of remaining sequences yield lower p (0.75–0.82) than any of the five well resolved individual sequences. |
| Midcontinent / NE Ohio / Kentucky | 0.90±0.02 | 5 | 5/12 individual sequences sufficient. Also includes 8-sequence Midcontinent stack. |
| Eastern Tennessee / Appalachia | 0.91±0.01 | 5 | 4/11 individual sequences sufficient. Also includes 8-sequence stack. |
| Wabash/Southern Illinois | 0.91±0.04 | 4 | 3/10 individual sequences, one 7-sequence stack. |
| Enola, Arkansas | 0.88±0.00 | 2 | Both well resolved, $p=0.88$. |
| New Madrid | 0.82±0.01 | 9 | 9/11 individual sequences. |
| Great Plains | 0.84±0.02 | 1 | One stack of 21 sequences. No individual sequence was sufficient for modeling Omori Decay. |

Table 6: Average p values in CENA seismic zones.

4. Meta-analyses

Most previous CENA aftershock studies have failed to find statistically significant differences between individual CENA sequences and a generic California model, partially because of large uncertainties in the parameters for individual sequences and partially because of large differences between individual sequences. For instance, *Ebel* [2009] reported p values for four CENA sequences ($p=0.74, 0.78, 0.78, 1.01$) with an average/standard deviation of 0.83 ± 0.12 . *Fereidoni and Atkinson* [2014] also examined four individual sequences, plus one four-sequence stack, but found substantially higher $p=1.21\pm0.26$. Notably, neither set of observations is significantly different from the 62 California sequences investigated by *Reasenberg and Jones* [1989] $p=1.07\pm0.22$, or from the mean thereof ($p=1.07\pm0.03$) at 95% confidence.

4.1. Omori Decay of Stacked Sequences

To overcome challenges posed by the large uncertainties of any one sequence, *Davis and Frohlich* [1991] merged multiple sequences—summing the mainshocks’ moment releases to create a single meta-event—by simply aligning the mainshocks at $t=0$ and using all aftershocks to define the Omori parameters of this meta-sequence. Following this approach, all 145 CENA sequences are combined into one large meta-sequence for analysis, they are subdivided into four ~ 0.5 magnitude-unit bins ($<M_{we}4.0$, $n=82$; $M_{we}4.0\text{--}4.5$, $n=45$; $M_{we}4.5\text{--}5.0$, $n=12$; $M_{we}5.0\text{--}5.84$, $n=7$) and processed as four smaller meta-sequences, and they are grouped spatially to explore regional differences further.

For the Omori Decay fits, time steps are objectively defined. Time windows $[0, t_1, \dots t_n \dots t_{max}]$ are defined as $t_n = \sqrt{2} * t_{n-1}$ [e.g., Wetmiller et al., 1984]. The seed time t_1 is set to the origin time of the fifth aftershock relative to the mainshock, such that there are 5 aftershocks in the first window. The number of events in each time-bin is counted, empty bins are split between the preceding and subsequent windows (increasing their durations but not aftershock counts), and the counts are simply divided by the respective bin durations to derive interval rates of aftershocks. Finally, the Omori Decay parameters are fit to the log-rates vs. time.

The 145 sequences are next binned by mainshock magnitude to check for systematic differences in aftershock behavior, in particular p , with increasing magnitude. Larger events tend to have better developed aftershock sequences, and the larger difference between M_{Main} and m_c typically allows more reliable sequence parameterization. In any single analysis a common m_c is used for all sequences, and Omori parameters are derived for multiple m_c ($M_{we}1.57, 1.97, 2.17, 2.33, 2.50, 2.75$, and 3.00) for each group to examine the impact of the chosen common m_c . (The main impacts are on b -value, which in turn affects a ; patterns in the decay rate p are conserved across the seven m_c choices.)

Omori parameters for the meta-sequences are consistently different from generic California sequences ([Figure 32](#)). Results discussed here are for $m_c=2.5$, and results with other minimum magnitudes are tabulated in [Table 7](#). All 145 CENA mainshocks sum to an equivalent $M_w6.06$. Their meta-sequence is initially less productive than California counterparts (dashed cyan line), but CENA decay is much slower ($p=0.84\pm0.01$), so CENA aftershock rates exceed California rates from ~ 1.5 days post-mainshock onward. Post-mainshock earthquake rates decline to pre-mainshock levels in a bit over a year (421 days), while the generic California Omori Decay curve returns to background in ~ 140 days, about one-third as long. For the seven M_w5 and greater events, CENA rates overtake the generic California model later, around 100 days, but seismicity rates are not projected to return to background for some 30 years.

There is substantial tradeoff between b -value and a ([Table 7](#)). The best-fit parameters are $a=-2.31$ and $b=1.05$, yet b depends in turn on the arbitrarily chosen m_c . Setting $b=0.91$, the California average, yields best-fit $a = -1.59$, which is very similar to the generic California $a=-1.67$. Because of the interdependence of a , b , and m_c , discussion focuses on p and overall earthquake rates rather than a or b themselves. This pattern of lower initial productivity but substantially slower decay is conserved across all magnitude ranges, and there is no monotonic trend in p with magnitude.

| Magnitude Range | # Sequences | $M_{\text{equivalent}}$ | M_{min} | #Aftershocks (first 2 years) | Radius | Duration | p | a | b |
|---------------------------|-------------|-------------------------|------------------|------------------------------|--------|------------------------|-----------------|------------------|-----------------|
| 3.65 – 5.84 | 145 | 6.03 | 2.5 | 465 | 25 km | 375 days | 0.85 ± 0.01 | -2.85 ± 0.01 | 1.20 ± 0.02 |
| 5.00 – 5.84 | 7 | 5.99 | 2.5 | 143 | 25 km | 11453 days* | 0.88 ± 0.02 | -2.06 ± 0.03 | 0.88 ± 0.02 |
| 5.00 – 5.84 w/o Miramichi | 6 | 5.95 | 2.5 | 73 | 25 km | 5579 days ⁺ | 0.90 ± 0.02 | -2.47 ± 0.03 | 0.96 ± 0.05 |
| 4.50 – 4.99 | 13 | 5.42 | 2.5 | 61 | 25 km | 623 days | 0.95 ± 0.02 | -3.10 ± 0.04 | 1.28 ± 0.08 |
| 4.00 – 4.49 | 46 | 5.31 | 2.5 | 111 | 25 km | 261 days | 0.90 ± 0.02 | -3.15 ± 0.03 | 1.43 ± 0.05 |
| 3.65 – 3.99 | 82 | 5.02 | 2.5 | 139 | 25 km | 177 days | 0.68 ± 0.04 | -3.33 ± 0.05 | 1.55 ± 0.06 |
| | | | | | | | | | |
| 3.65 – 5.84 | 145 | 6.03 | 1.97 | 1085 | 25 km | 325 days | 0.81 ± 0.01 | -2.54 ± 0.01 | 1.04 ± 0.01 |
| 5.00 – 5.84 | 7 | 5.99 | 1.97 | 296 | 25 km | 19147 days* | 0.84 ± 0.01 | -2.32 ± 0.02 | 0.89 ± 0.01 |
| 5.00 – 5.84 w/o Miramichi | 6 | 5.95 | 1.97 | 192 | 25 km | 8819 days ⁺ | 0.88 ± 0.02 | -2.94 ± 0.02 | 1.03 ± 0.03 |
| 4.50 – 4.99 | 13 | 5.42 | 1.97 | 98 | 25 km | 173 days | 0.94 ± 0.02 | -3.13 ± 0.03 | 1.14 ± 0.04 |
| 4.00 – 4.49 | 46 | 5.31 | 1.97 | 184 | 25 km | 175 days | 0.88 ± 0.01 | -2.59 ± 0.02 | 1.09 ± 0.03 |
| 3.65 – 3.99 | 82 | 5.02 | 1.97 | 455 | 25 km | 118 days | 0.72 ± 0.02 | -3.08 ± 0.02 | 1.35 ± 0.02 |
| | | | | | | | | | |
| 3.65 – 5.84 | 145 | 6.03 | 1.57 | 1432 | 25 km | 328 days | 0.80 ± 0.01 | -2.39 ± 0.01 | 0.94 ± 0.01 |
| 5.00 – 5.84 | 7 | 5.99 | 1.57 | 352 | 25 km | 15179 days* | 0.86 ± 0.01 | -1.94 ± 0.02 | 0.75 ± 0.01 |
| 4.50 – 4.99 | 13 | 5.42 | 1.57 | 209 | 25 km | 209 days | 0.93 ± 0.02 | -2.87 ± 0.02 | 0.96 ± 0.03 |
| 4.00 – 4.49 | 46 | 5.31 | 1.57 | 226 | 25 km | 166 days | 0.88 ± 0.01 | -2.35 ± 0.02 | 0.92 ± 0.02 |
| 3.65 – 3.99 | 82 | 5.02 | 1.57 | 679 | 25 km | 129 days | 0.70 ± 0.02 | -2.79 ± 0.03 | 1.14 ± 0.01 |
| | | | | | | | | | |
| 3.65 – 5.84 | 145 | 6.03 | 3.0 | 124 | 25 km | 414 days | 0.90 ± 0.02 | -1.74 ± 0.02 | 0.86 ± 0.03 |
| 5.00 – 5.84 | 7 | 5.99 | 3.0 | 43 | 25 km | 7830 days* | 0.93 ± 0.03 | -1.25 ± 0.04 | 0.61 ± 0.03 |
| 4.50 – 4.99 | 13 | 5.42 | 3.0 | 11 | 25 km | 247 days | 1.13 ± 0.19 | -1.90 ± 0.25 | 0.88 ± 0.14 |
| 4.00 – 4.49 | 46 | 5.31 | 3.0 | 42 | 25 km | 471 days | 0.93 ± 0.03 | -3.08 ± 0.03 | 1.55 ± 0.14 |
| 3.65 – 3.99 | 82 | 5.02 | 3.0 | 26 | 25 km | 246 days | 0.85 ± 0.05 | -3.27 ± 0.07 | 1.77 ± 0.24 |
| | | | | | | | | | |
| 3.65 – 5.84 | 145 | 6.03 | 2.75 | 265 | 25 km | 553 days | 0.83 ± 0.01 | -2.07 ± 0.02 | 0.98 ± 0.02 |
| 5.00 – 5.84 | 7 | 5.99 | 2.75 | 82 | 25 km | 10218 days* | 0.88 ± 0.03 | -1.38 ± 0.02 | 0.66 ± 0.02 |
| 4.50 – 4.99 | 13 | 5.42 | 2.75 | 29 | 25 km | 686 days | 0.94 ± 0.04 | -2.57 ± 0.07 | 1.14 ± 0.13 |
| 4.00 – 4.49 | 46 | 5.31 | 2.75 | 78 | 25 km | 413 days | 0.89 ± 0.02 | -3.24 ± 0.04 | 1.54 ± 0.09 |
| 3.65 – 3.99 | 82 | 5.02 | 2.75 | 67 | 25 km | 232 days | 0.76 ± 0.02 | -3.20 ± 0.03 | 1.63 ± 0.10 |
| | | | | | | | | | |
| 3.65 – 5.84 | 145 | 6.03 | 2.33 | 699 | 25 km | 397 days | 0.81 ± 0.01 | -2.45 ± 0.01 | 1.07 ± 0.02 |
| 5.00 – 5.84 | 7 | 5.99 | 2.33 | 214 | 25 km | 24878 days* | 0.81 ± 0.02 | -1.78 ± 0.02 | 0.79 ± 0.02 |
| 4.50 – 4.99 | 13 | 5.42 | 2.33 | 80 | 25 km | 512 days | 0.94 ± 0.02 | -3.20 ± 0.03 | 1.27 ± 0.06 |
| 4.00 – 4.49 | 46 | 5.31 | 2.33 | 136 | 25 km | 961 days | 0.91 ± 0.02 | -2.94 ± 0.03 | 1.29 ± 0.04 |
| 3.65 – 3.99 | 82 | 5.02 | 2.33 | 231 | 25 km | 150 days | 0.68 ± 0.02 | -3.27 ± 0.04 | 1.50 ± 0.04 |
| | | | | | | | | | |
| 3.65 – 5.84 | 145 | 6.03 | 2.17 | 933 | 25 km | 304 days | 0.82 ± 0.01 | -2.50 ± 0.01 | 1.07 ± 0.01 |
| 5.00 – 5.84 | 7 | 5.99 | 2.17 | 270 | 25 km | 20437 days* | 0.83 ± 0.02 | -1.87 ± 0.02 | 0.81 ± 0.02 |
| 4.50 – 4.99 | 13 | 5.42 | 2.17 | 91 | 25 km | 218 days | 0.96 ± 0.02 | -3.25 ± 0.03 | 1.24 ± 0.05 |
| 4.00 – 4.49 | 46 | 5.31 | 2.17 | 170 | 25 km | 243 days | 0.89 ± 0.01 | -2.66 ± 0.02 | 1.16 ± 0.03 |
| 3.65 – 3.99 | 82 | 5.02 | 2.17 | 358 | 25 km | 109 days | 0.72 ± 0.03 | -3.16 ± 0.03 | 1.44 ± 0.03 |
| | | | | | | | | | |
| 3.65 – 5.84 | 145 | 6.03 | 2.5 | 479 | 25 km | 426 days | 0.84 ± 0.01 | -1.59 ± 0.01 | Fixed 0.91 |
| 5.00 – 5.84 | 7 | 5.99 | 2.5 | 144 | 25 km | 9516 days* | 0.89 ± 0.02 | -1.97 ± 0.02 | Fixed 0.91 |
| 4.50 – 4.99 | 13 | 5.42 | 2.5 | 61 | 25 km | 623 days | 0.95 ± 0.02 | -1.78 ± 0.04 | Fixed 0.91 |
| 4.00 – 4.49 | 46 | 5.31 | 2.5 | 111 | 25 km | 261 days | 0.90 ± 0.02 | -1.48 ± 0.03 | Fixed 0.91 |
| 3.65 – 3.99 | 82 | 5.02 | 2.5 | 139 | 25 km | 177 days | 0.68 ± 0.03 | -1.51 ± 0.05 | Fixed 0.91 |

Table 7: Omori Decay parameters for multi-sequence stacks. Events are modeled as one stack and separated into magnitude bins. Values of m_c are systematically varied to investigate dependence of results on this subjective choice, and a set of models has b fixed at the California average 0.91.

*The anomalous Miramichi sequence is retained in these models, unlike in [Figures 33–35](#).

[†]Miramichi is excluded to examine its influence. Removing Miramichi reduces the apparent durations of M5+ stacked sequences by 50% or more and increases p by 0.02 to 0.04.

To investigate spatial differences further ([Figure 33](#)), the seven largest events from the CEUS ($M \geq 4.83$), seven largest from Charlevoix ($M \geq 3.71$), and seven largest—excluding Miramichi—from the rest of southeastern Canada ($M \geq 4.39$) are stacked and analyzed as three separate meta-sequences. Consistent with the results from individual sequences studied previously by others [e.g., *Fereidoni and Atkinson, 2014; Ebel et al., 2009*] and those presented here, southeastern Canadian aftershocks ($p=1.11 \pm 0.02$) decay parallel to generic California sequences. By contrast, the CEUS meta-sequence decays more slowly ($p=0.86 \pm 0.02$), and Charlevoix-stack aftershocks behave more like the CEUS ($p=0.93 \pm 0.03$).

4.2. The Shape of Aftershock Sequences: Average Spatiotemporal Behavior

Previous sections described the process of estimating earthquake rate density perturbations and normalizing these post-mainshock rate increases to a reference minimum magnitude, area, and time. These normalized rate densities provide a second quantitative way to merge multiple sequences: tabulating the rate-density anomalies in the same predetermined radius-time bins for all events and averaging the values in these bins across many events. These stacked heat maps are generated for magnitude bins ~ 0.5 units wide ($< M_{we} 4.0$, $n=82$; $M_{we} 4.0–4.5$, $n=46$; $M_{we} 4.5–5.0$, $n=12$; $M_{we} 5.0–5.84$, $n=7$). In this analysis, “background” seismicity rates are estimated from only 15 km epicentral radius. This choice is an attempt to be conservative in light of the fact that most aftershocks occur in previously active locations [Page and van der Elst, 2020], including the same faults/fault systems that host mainshocks, and therefore limiting the background zone to 15 km epicentral radius results in generally higher normalized background rate density estimates than using the entire GK74 radius.

[Figure 34](#) illustrates the average spatiotemporal behavior of CENA sequences: Aftershock activity is insignificant beyond ~ 25 km epicentral radius, but earthquake rates within ~ 10 km of the epicenter remain elevated for several years for all magnitude ranges. Thus, the aftershock window is not rectangular in radius vs. time space, as parameterized in GK74 relations, but rather vaguely right-triangular or boot-shaped in that more distal aftershocks (e.g., 15 km and greater epicentral radius) disappear sooner than aftershocks within a few km of the mainshock. As an alternative to a single radius-time box or a radius-time triangle (which would be more complicated to implement in NSHM model runs), a two-phase parameterization with an initial radius of 15–25 km and duration less than 1 year, followed by a tighter radius for a few years offers a simple approximation of this boot shape.

4.3. Magnitude Dependence of Aftershock Duration and Radius

In the previous two subsections, it is clear that empirical sequence duration increases with mainshock magnitude: Rates remain elevated relative to pre-mainshock levels for longer after larger events. With the goal of providing quantitative rules of thumb to relate mainshock magnitude to aftershock duration, two metrics are introduced. The more intuitive is the occurrence of the first nadir or local minimum in post-mainshock rate density for the stacked heat maps. This lull occurs at roughly 5 years for the $M < 4$ stack and 7, 9, and 11 years for $M 4–4.5$, $M 4.5–5.0$, and $M \geq 5.0$, or

$$t_{\text{post-mainshock nadir}} \approx (M_{\text{Main}} \times 4 \text{ years/magnitude unit}) - 10 \text{ years}$$

For instance, following a M4.75, rates bottom out around 9 years. Daring to extrapolate this simple relation to higher magnitudes, Cramer and Boyd's [2014] M7.7 estimate for the largest 1812 New Madrid event only corresponds to a ~20-year aftershock sequence, rather than the thousands of years posited by Stein and Liu [2009].

Alternatively, the rate densities have been scaled to represent the annual excess rate of M2.5+ events within ~25 radius. This radius is similar to the aftershock zone, and M2.5 is near the felt threshold, so one may consider it a crude proxy for the annual rate of felt aftershocks. The 1.0 excess-event/year contour is used as a second metric to quantify aftershock sequence duration. Here, the 1.0 excess-event/year contour is crossed at 2.3, 4, 6, and 9.5 years for the four magnitude bins, or approximately:

$$t_1 \text{ felt aftershock/year} \approx (M_{\text{Main}} \times 4.25 \text{ years/magnitude unit}) - 14 \text{ years.}$$

Thus, CENA aftershock sequences elevate rates for a years ($3 < M < 4$) to a decade or more ($M > 5$), and these increases may lead to modestly higher rates of felt seismicity for a few years in areas 10-15 km and less from the epicenter.

4.4. Declustering parameters for CEUS events

Because of the differences between CEUS and Canadian sequences, the latter are discarded, and the magnitude-duration relations are reexamined. The 15-km maximum radius for considerable aftershock activity is even more pronounced for the CEUS subset and is conserved across all four magnitude bins (Figure 35). The post-mainshock nadirs again occur near 4.5, 7, 8 and 11 years, while the 1.0 excess-felt-event/year threshold is crossed at 3, 6, 5, and 10 years, or approximately

$$\text{CEUS only: } t_{\text{post-mainshock nadir}} \approx (M_{\text{Main}} \times 4.3 \text{ years/magnitude unit}) - 12 \text{ years.}$$

$$\text{CEUS only: } t_1 \text{ felt aftershock/year} \approx (M_{\text{Main}} \times 3.75 \text{ years/magnitude unit}) - 11 \text{ years.}$$

Using the stacked heat maps as a guide, the following time-radius boxes are suggested CEUS-specific substitutions for the GK74 parameters. Two-stage, boot-shaped windows are also suggested.

| | | | | | |
|-----------|---------|----------|-------------------|-------|------------|
| M3.65–4 | 17.5 km | 4 years | Compared to GK74: | 28 km | 0.1 years |
| M4–4.5 | 17.5 km | 6 years | | 32 km | 0.16 years |
| M4.5–5.0 | 17.5 km | 8 years | | 37 km | 0.3 years |
| M5.0–5.65 | 27.5 km | 10 years | | 44 km | 0.6 years |

Suggested two-phase windows for the CEUS aftershock sequences are:

| | | |
|-----------|------------------|------------------|
| M3.65–4 | 20 km/0.75 years | 12.5 km/4 years |
| M4–4.5 | 20 km/1.0 year | 12.5 km/6 years |
| M4.5–5.0 | 20 km/1.5 years | 12.5 km/8 years |
| M5.0–5.65 | 30 km/2 years | 17.5 km/10 years |

For CENA-wide analyses, I offer these single-window suggestions:

| | | | | | |
|-----------|---------|-----------|-------|-------|------------|
| M3.65–4 | 17.5 km | 3 years | GK74: | 28 km | 0.1 years |
| M4–4.5 | 17.5 km | 5.5 years | | 32 km | 0.16 years |
| M4.5–5.0 | 22.5 km | 6.5 years | | 37 km | 0.3 years |
| M5.0–5.65 | 30 km | 10 years | | 44 km | 0.6 years |

For the two-box alternative, I suggest these CENA declustering parameters:

| | | |
|-----------|--------------------|-------------------|
| M3.65–4 | 17.5 km/0.75 years | 10 km/3 years |
| M4–4.5 | 20 km/0.75 years | 10 km/5.5 years |
| M4.5–5.0 | 25 km/1.5 years | 12.5 km/6.5 years |
| M5.0–5.65 | 35 km/2.5 years | 12.5 km/10 years |

Additional work to examine the impact of these suggestions on the declustered seismicity catalog and to quantify their influence on NSHM hazard are needed.

5. Conclusion

This report presents results of the largest study of CENA aftershock sequences ($n=145$) to date, by a factor of nearly 20. Aftershock sequences are parameterized in terms of Omori Decay, or a log-linear decrease of seismicity rate with time following the mainshock at a slope p . Moderate-magnitude ($M_w 3.65\text{--}5.84$) CEUS sequences are found to proceed more slowly ($p=0.86$) than the California sequences ($p=1.07$) on which NSHM declustering parameters are currently based. By contrast, Canadian sequences nearly parallel their plate-boundary counterparts ($p=1.11$), except near Charlevoix, where decay is slower and CEUS-like ($p=0.93$). The area over which notable CENA aftershock activity occurs (<25 km epicentral radius, typically 10–15 km) is smaller than current estimates, however. Near epicenters, aftershocks persist for a year ($M\sim 4$) to a decade or more ($M5+$), but there is no evidence for millennial-duration sequences that would invalidate the use of appropriately declustered historical seismicity for NSHM hazard projections.

Revised declustering parameters for intraplate CENA sequences and specifically for the CEUS subset are presented. Rather than spanning ~30 km or more but lasting only a few months, aftershock windows may not need to extend more than ~20 km radially from the epicenter but should last several years at distance less than 10–15 km from the mainshock. Implementing these new declustering parameters may reduce NSHM estimates very near historical epicenters and make hazard more even across areas within a few 10s of km of historical to instrumental sequences.

Data and code availability:

Catalogs are available from the references noted and <https://github.com/WillLevandowski/AftershockSequences>. Omori Decay modeling algorithms, plotting scripts, and the 145 single-sequence analysis templates are available at <https://github.com/WillLevandowski/AftershockSequences>

Publications related to this award

Aftershock Sequences in Central/Eastern North America Last Years—Decades at Most—Not a Few Weeks, Not Millennia: Results From 149 Modern Mainshocks $M_w 3.65\text{--}5.84$. Levandowski, W. (2022) *SSA Ann. Mtg.*

Modern CENA aftershock sequences are smallish, a little lazy, and persistent. Levandowski, W. (2021) *Eastern Section SSA Ann. Mtg.*

Statistics of recent aftershock sequences in eastern North America and their implications for declustering. Levandowski, W. (2020) *SSA Ann. Mtg.*

M6.02 2014 Napa, CA

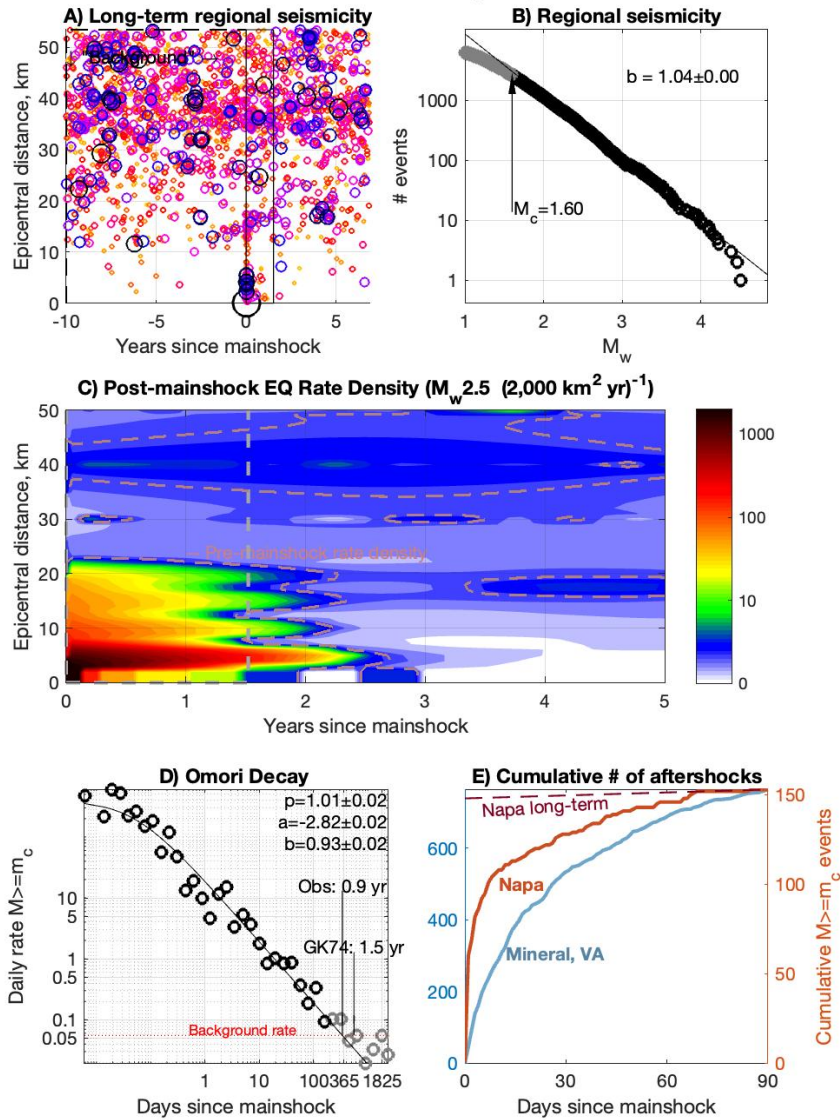


Figure 1: Aftershocks of the 2014 Napa, CA M6.0

A) Seismicity near the epicenter, 2004–2021. The GK74 time-radius window is shown as the solid dark gray line. Circles show seismicity; size and color depict magnitude.

B) Frequency-magnitude distribution of seismicity in A. Catalog appears complete to $M_{\text{we}}=1.60$.

C) Earthquake rate density following the mainshock in units of number of $M_w 2.5$ and greater events per 2000 km^2 per year. The dashed pink line shows average rate density in the 10 years before the mainshock within 50 km of the epicenter.

D) Omori Decay of Napa aftershocks Gray circles: All daily rate estimates. Black circles: Data used to derive Omori Decay parameters, which are listed at the top right. Red line: Estimated background rate. Rates decrease log-linearly with time over $\sim 1\text{--}2$ years, returning to the estimated background rate at 0.9 year (indicated as “Obs: 0.9 yr”). The GK74 duration, 1.5 years, is indicated for reference.

E) Cumulative number of events following the mainshock (red line) levels off after ~ 60 days and then parallels the long-term rate (dashed line). For comparison, aftershocks of the 2011 $M_w 5.65$ Mineral, VA earthquake accumulate more slowly.

M5.65 2011 Mineral, VA

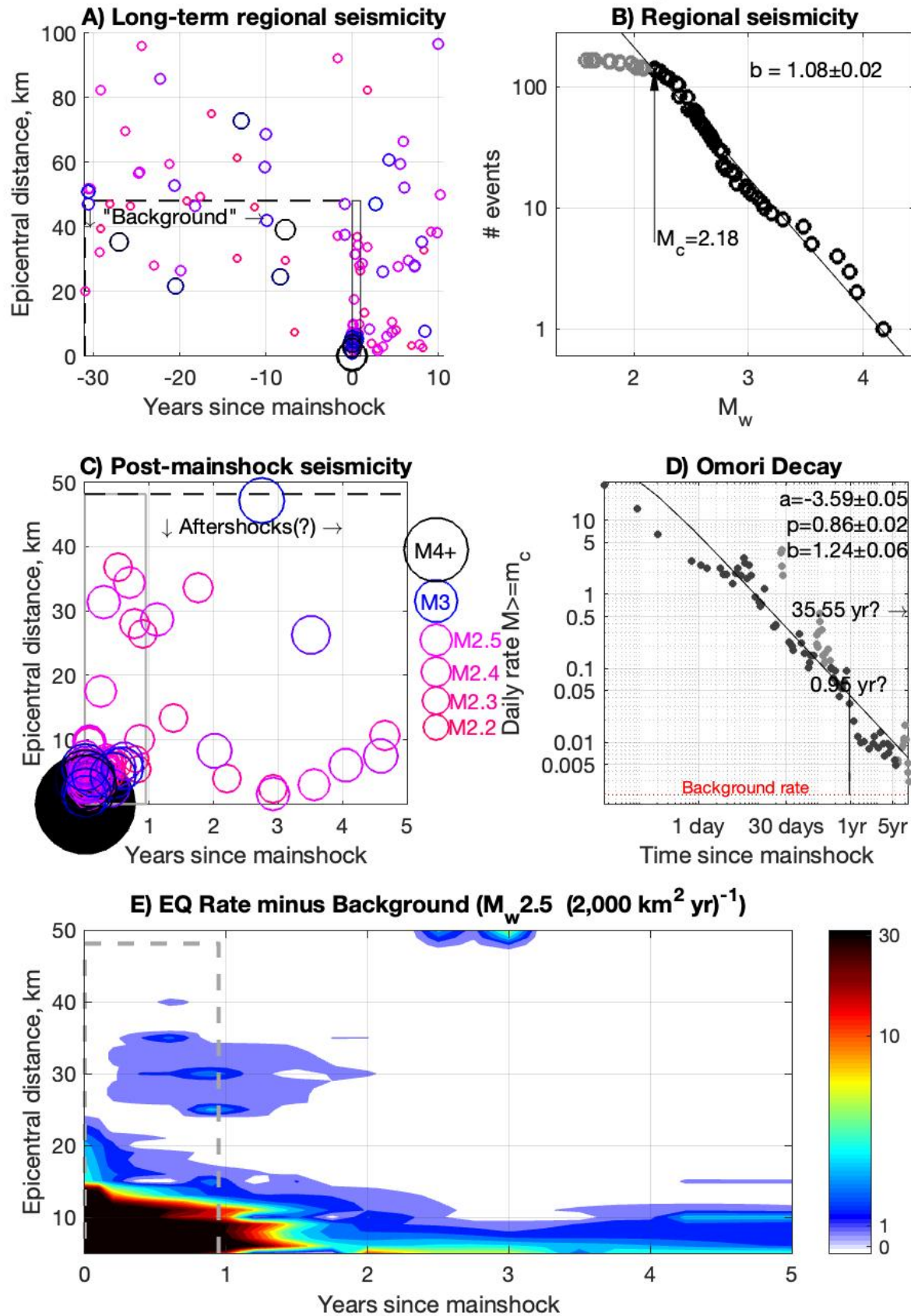


Figure 2: Aftershocks of the 2011 Mineral, VA M5.65

- A) Seismicity near the epicenter**, 1980–2021. The GK74 time-radius window is shown as the solid dark gray line. Circles show seismicity (m_c and greater); size and color depict magnitude according to the scale in **C**. The window used to calculate background earthquake rate density is indicated by the dashed line.
- B) Frequency-magnitude distribution** of seismicity in **A**. Catalog appears complete to $M_{we}2.18$.
- C) Seismicity following the mainshock** is concentrated within 1 year and 10 km of the mainshock, and seismicity persists near the epicenter for at least several years.
- D) Omori Decay of Mineral aftershocks** Rates have decreased log-linearly with time over the 10.3 years since the mainshock. Gray circles: All seismicity rate estimates. Black circles: Rates estimates used for Omori Decay fit. Best-fit Omori parameters are listed at top right. The decay is projected to intersect the estimated background rate (red dashed line) after three decades or more. The GK74 duration, 0.95 years, is indicated for reference.
- E) Excess earthquake rate density following the mainshock** in units of number of $M_w2.5$ and greater events per 2000 km^2 per year.

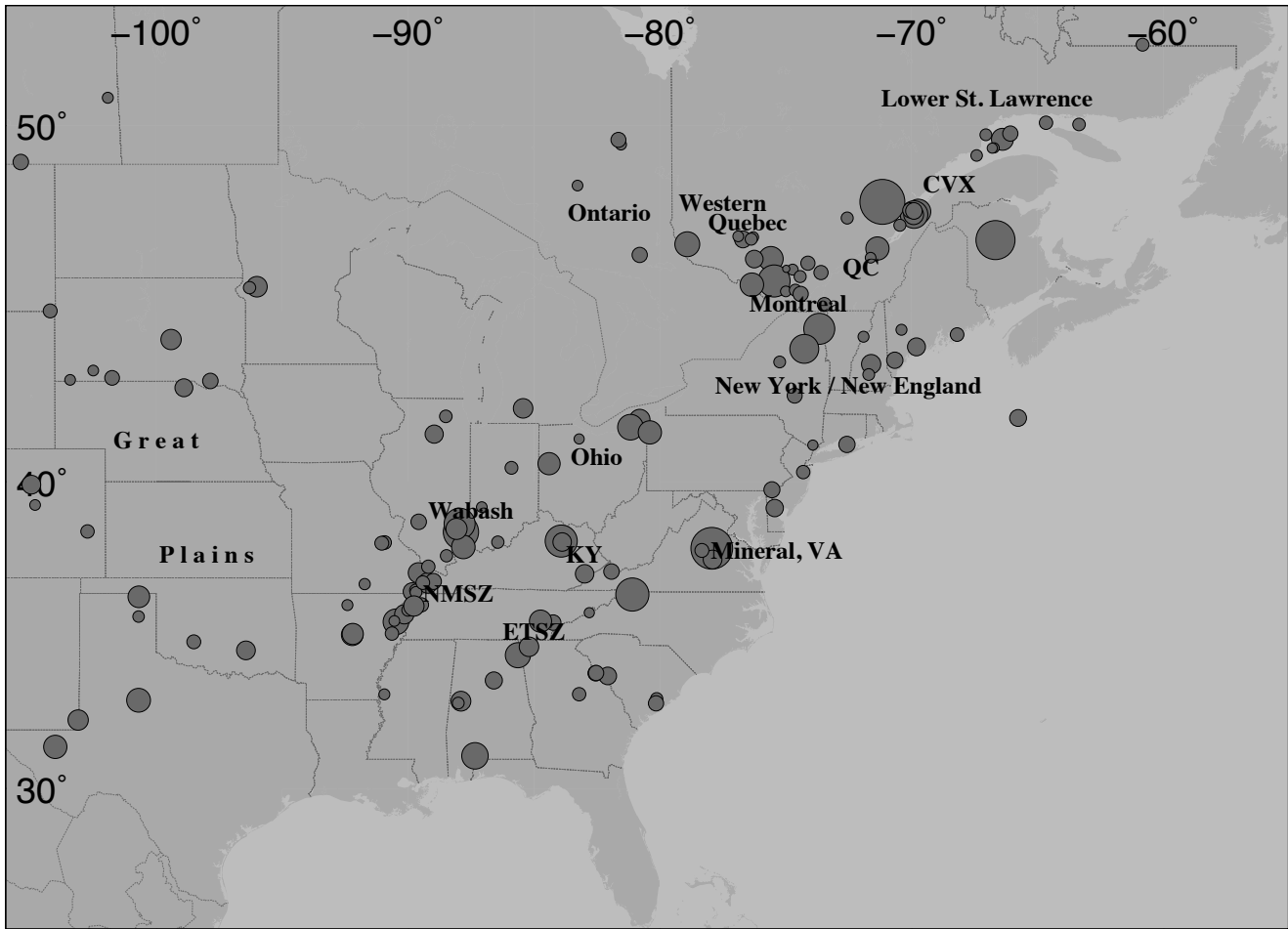


Figure 3: Mainshocks and seismic zones. CVX: Charlevoix. ETSZ: Eastern Tennessee Seismic Zone. KY: Kentucky (state). NMSZ: New Madrid Seismic Zone. QC: Quebec City.

M5.1 2020 Sparta, NC

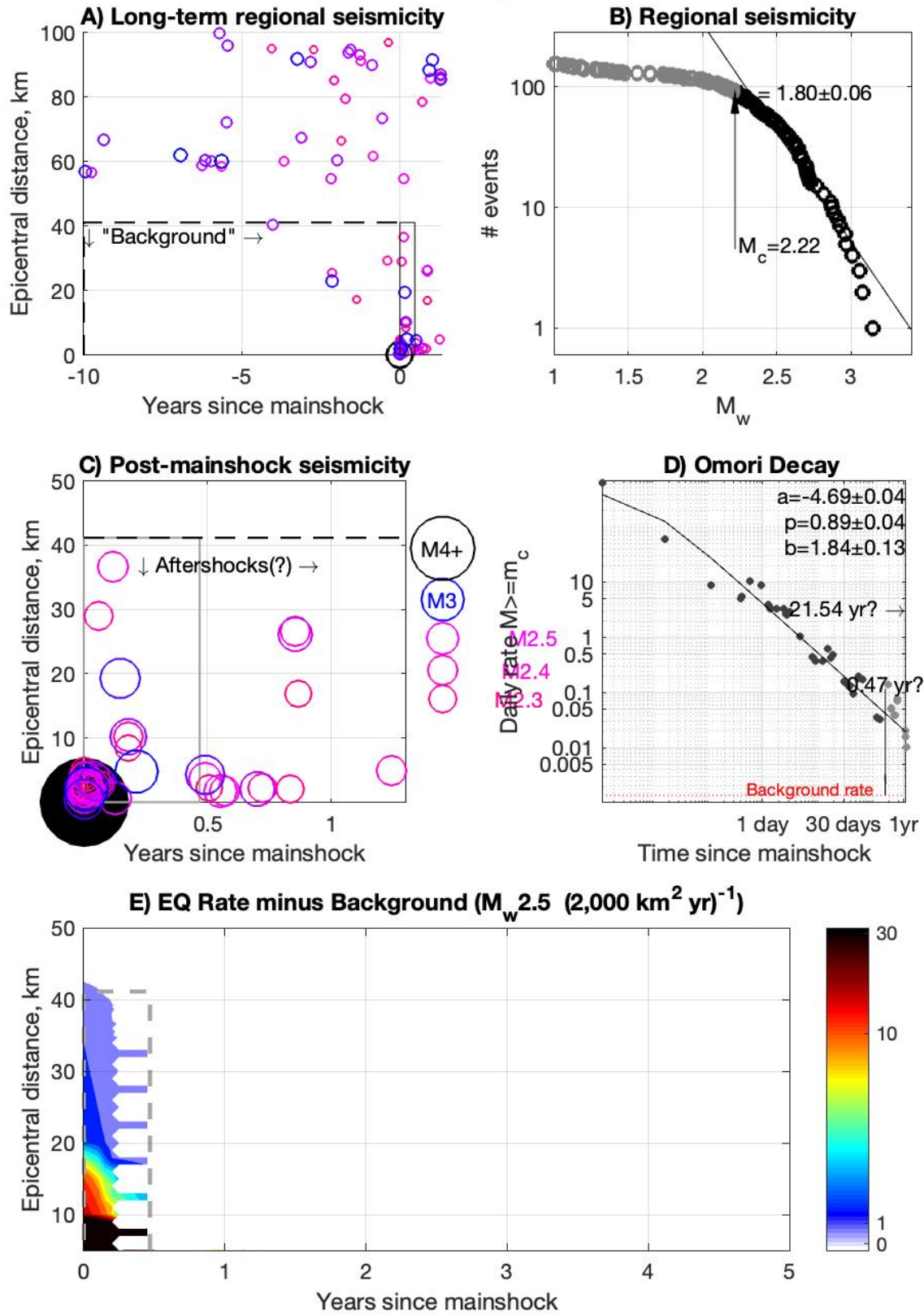


Figure 4: $M_w 5.1$ Sparta, NC, USA

M5.04 2010 Val de Bois, QC

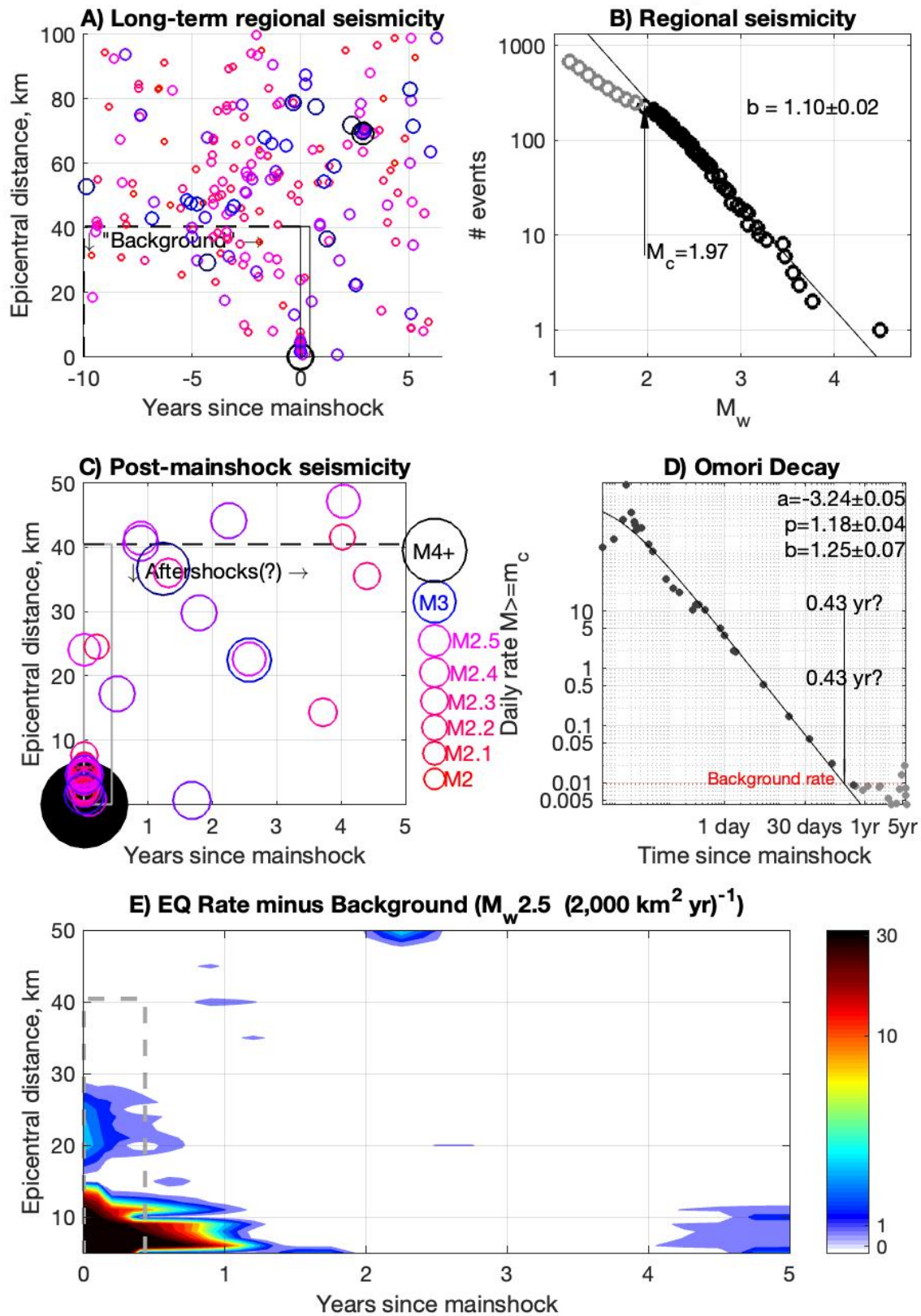


Figure 5: Val des Bois, Quebec, Canada

M5.23 2008 Mt. Carmel, IN

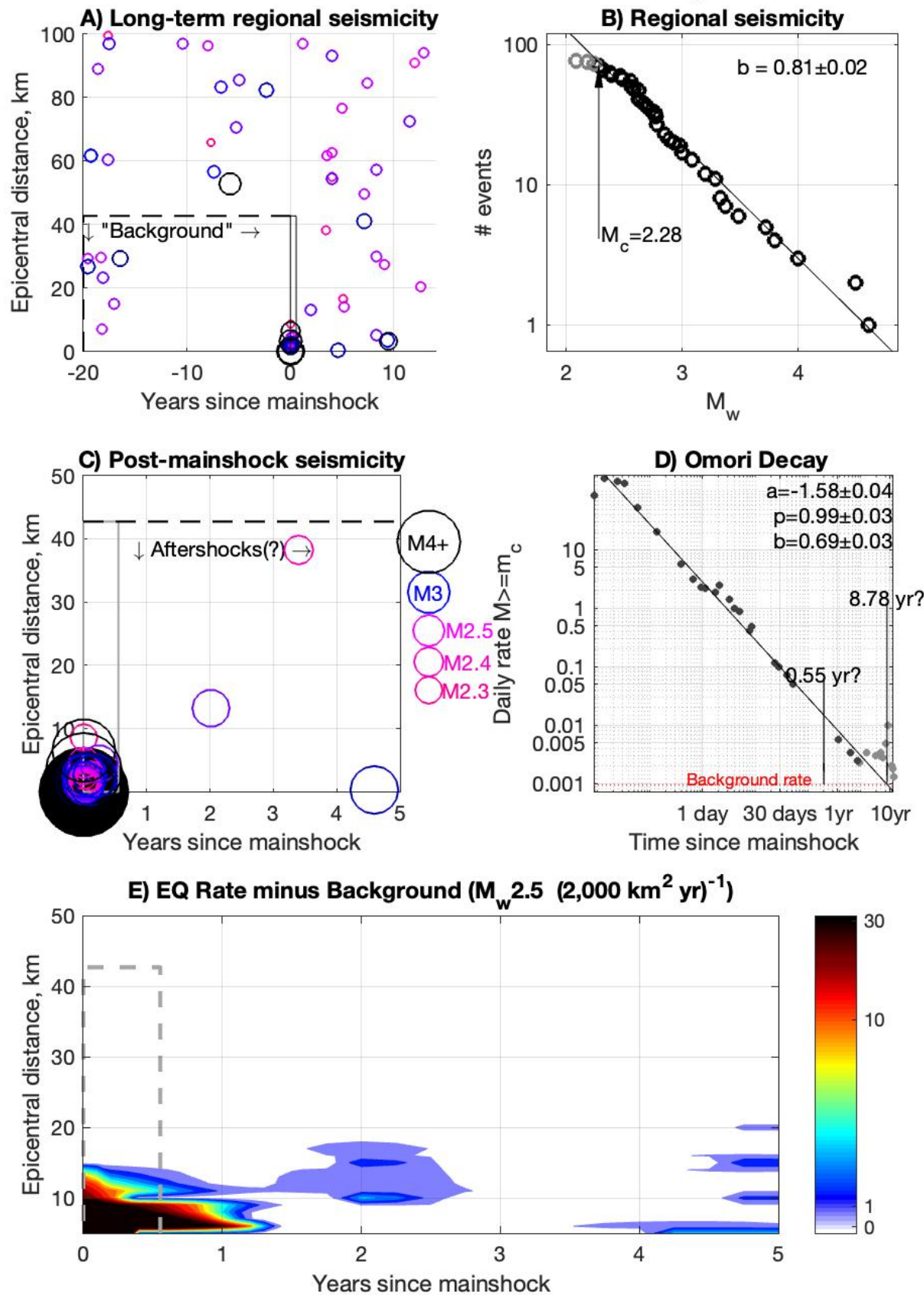


Figure 6: Mt. Carmel, IN, USA

M5.84 1988 Saguenay, QC

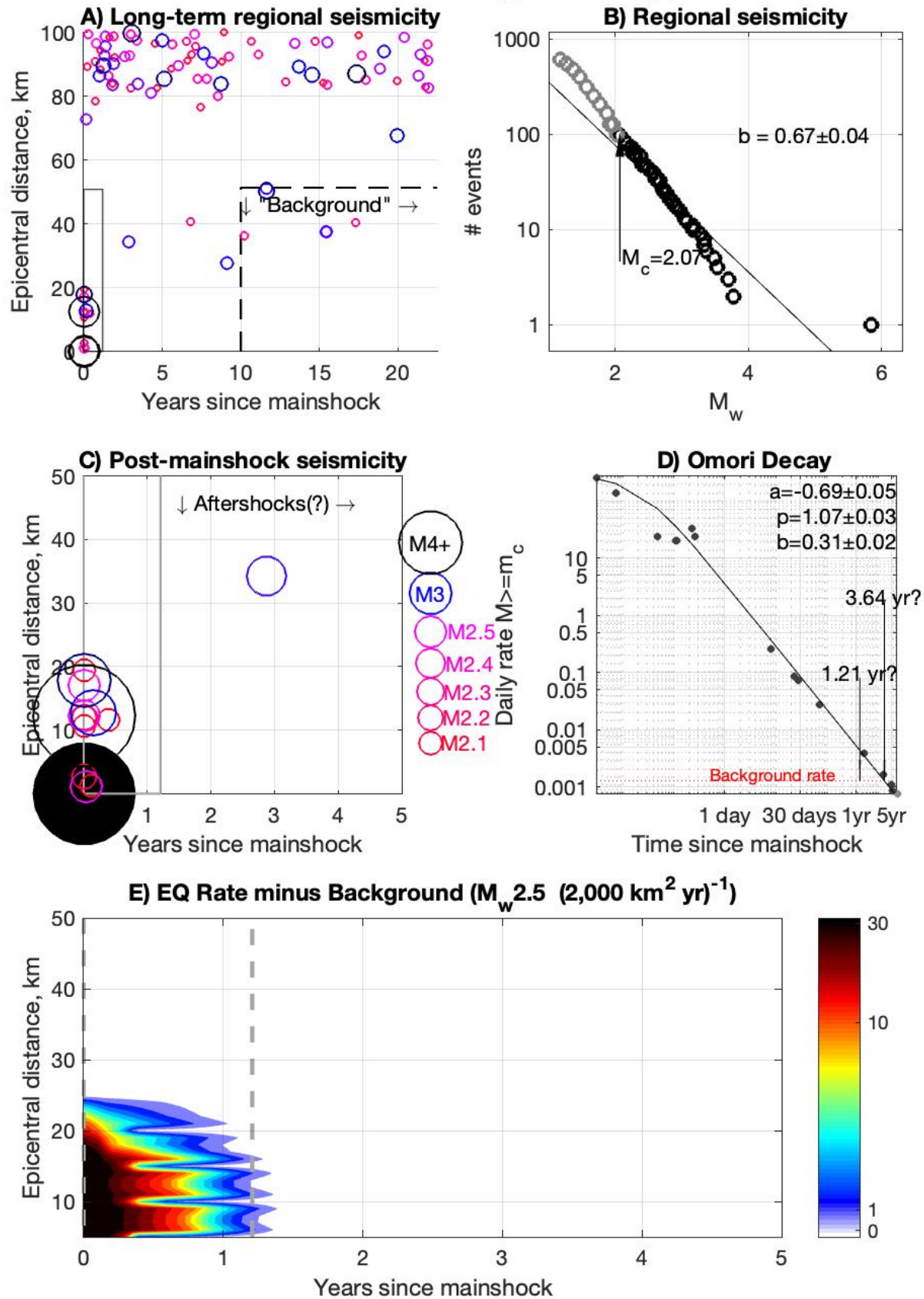
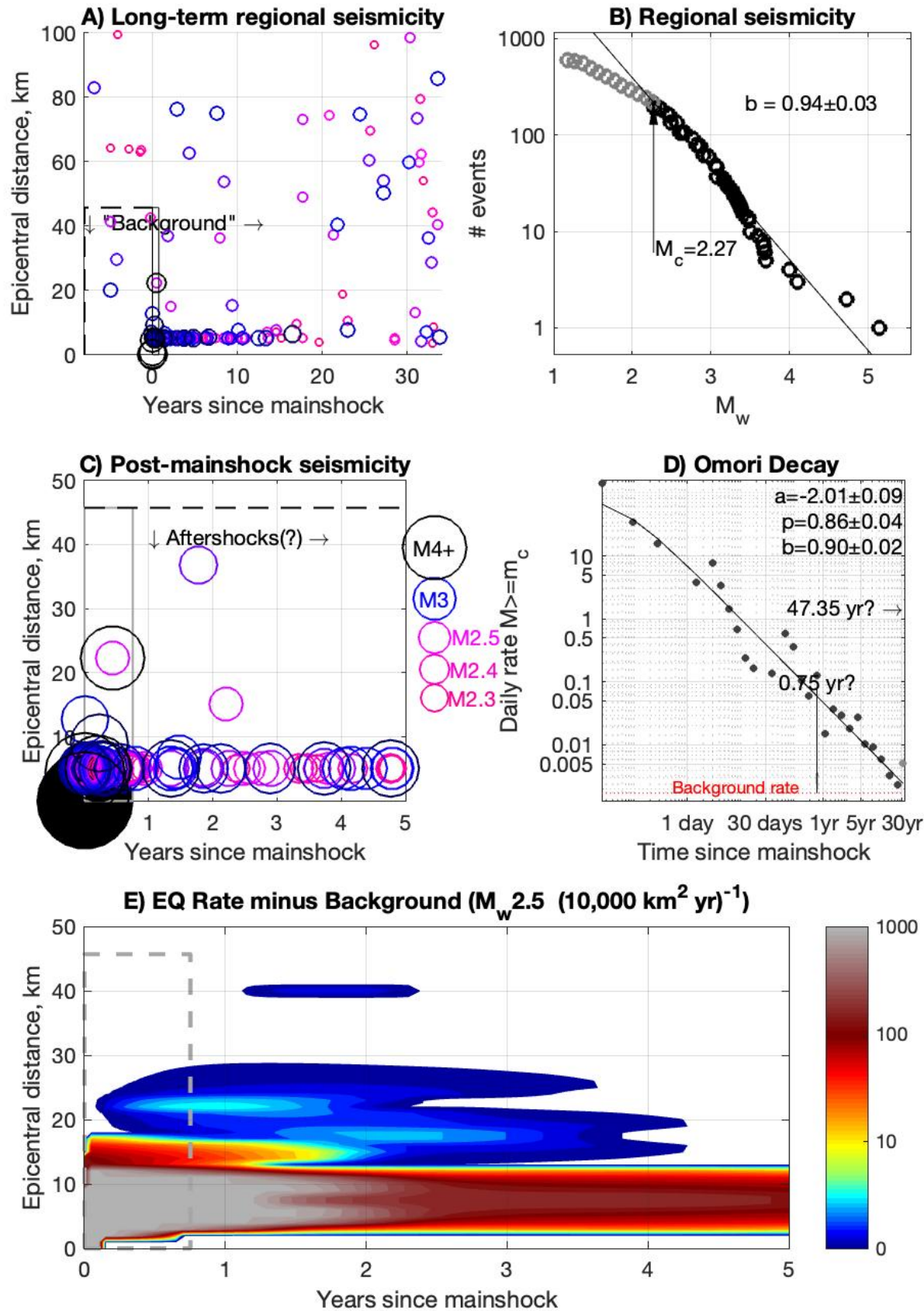


Figure 7: Saguenay, QC

M5.47 1982 Miramichi, NB



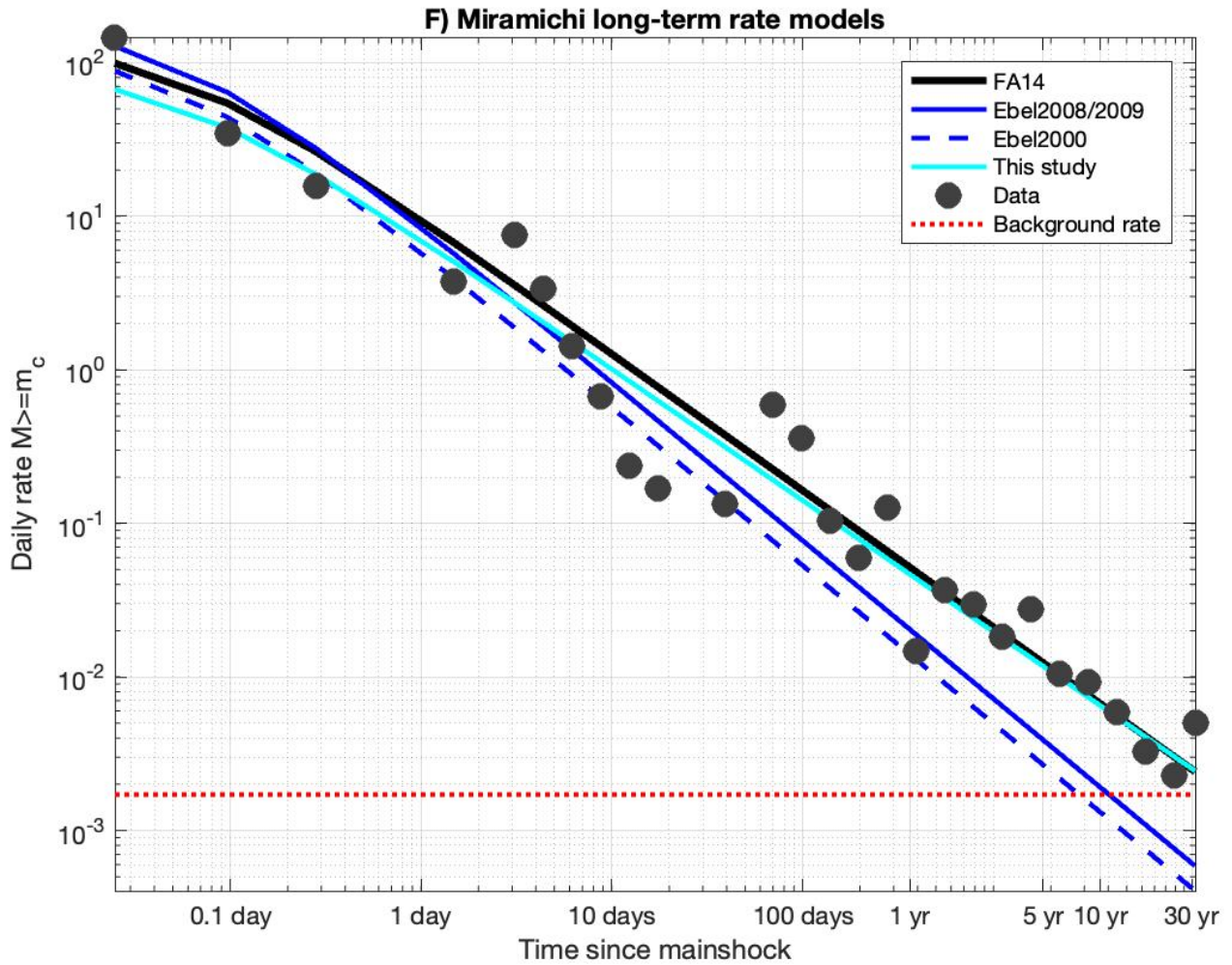


Figure 8: Miramichi, NB. A–E) Same as previous figures. F) Comparison of previous aftershock decay models with long-term rate evolution. The decades-long decay is better fit by $p=0.89$ [Fereidoni and Atkinson, 2014] (cyan line) or $p=0.86$ (this study; black line) than $p=1.03$ [Ebel, 2000; 2008; 2009] (blue lines). Although the projected decay rate does not reach the background seismicity rate for 47 years, the end of the sequence is subjectively better defined by the generally sparse activity between 18 and 30 years post-mainshock.

M5.04 1980 Mt. Sterling, KY

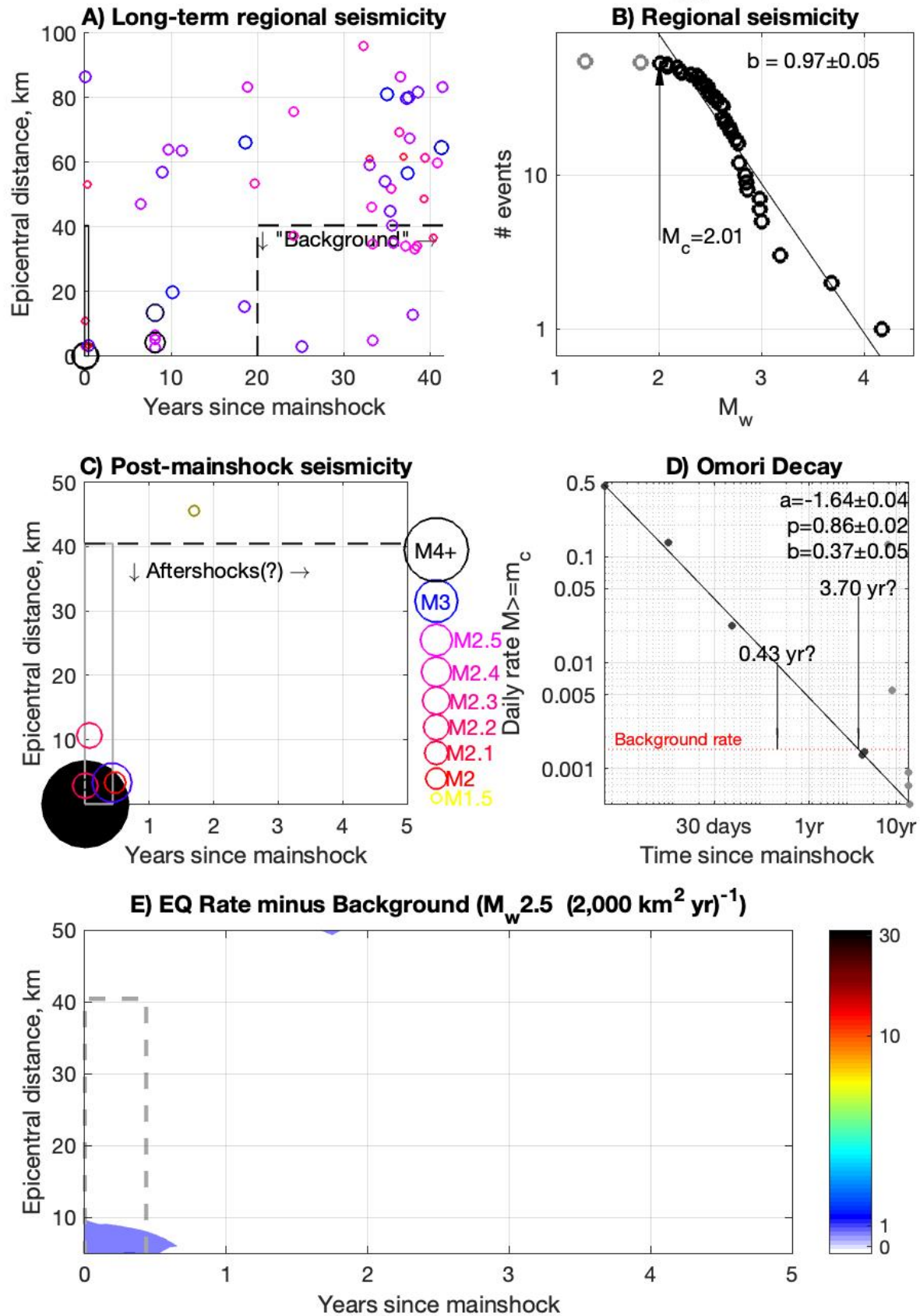


Figure 9: Mt. Sterling, KY

M4.75 1979 Malbaie, QC

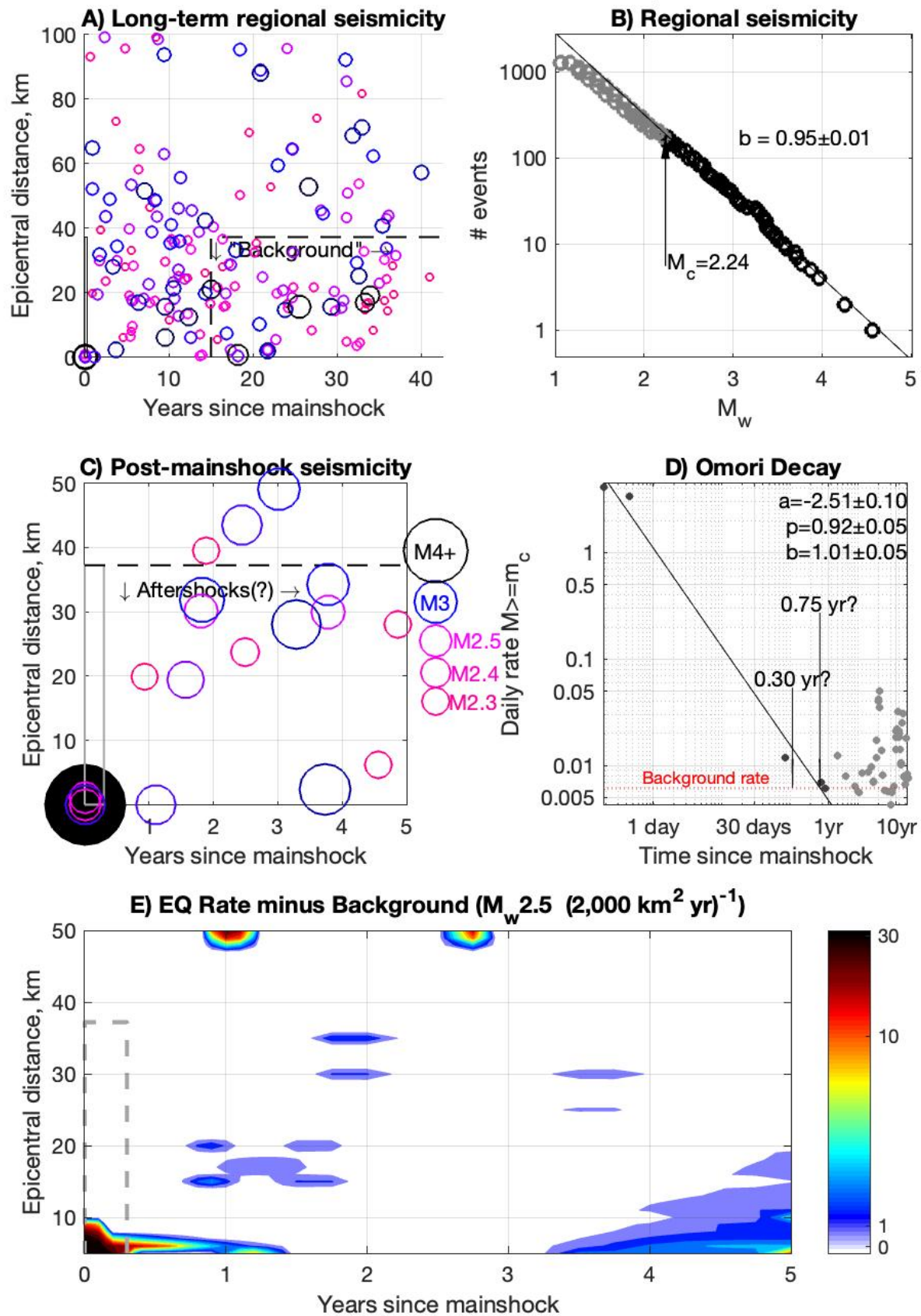


Figure 10: 1979 Malbaie, QC

M4.26 1997 Malbaie, QC

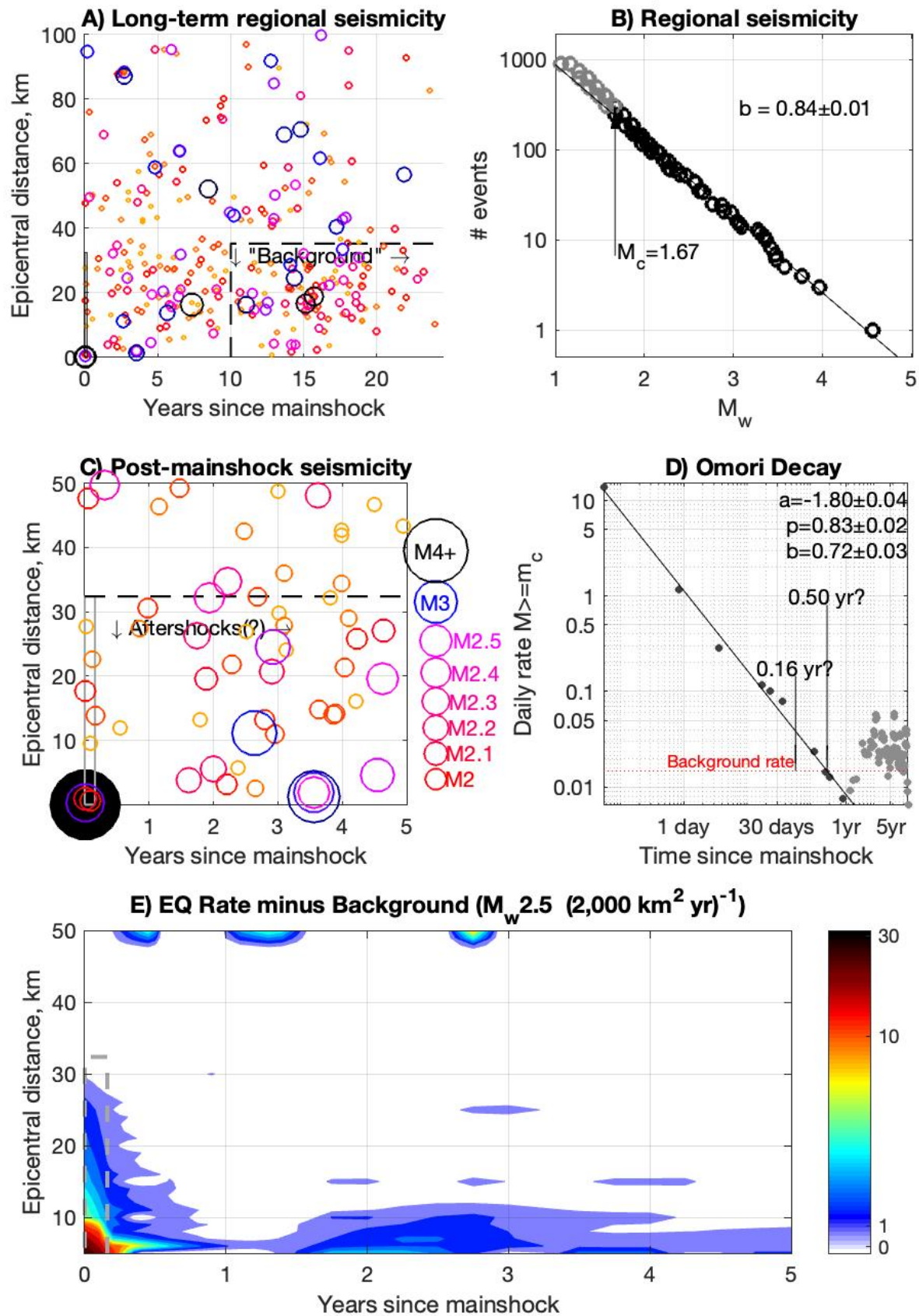


Figure 11: 1997 Malbaie, QC

M4.57 2005 Charlevoix

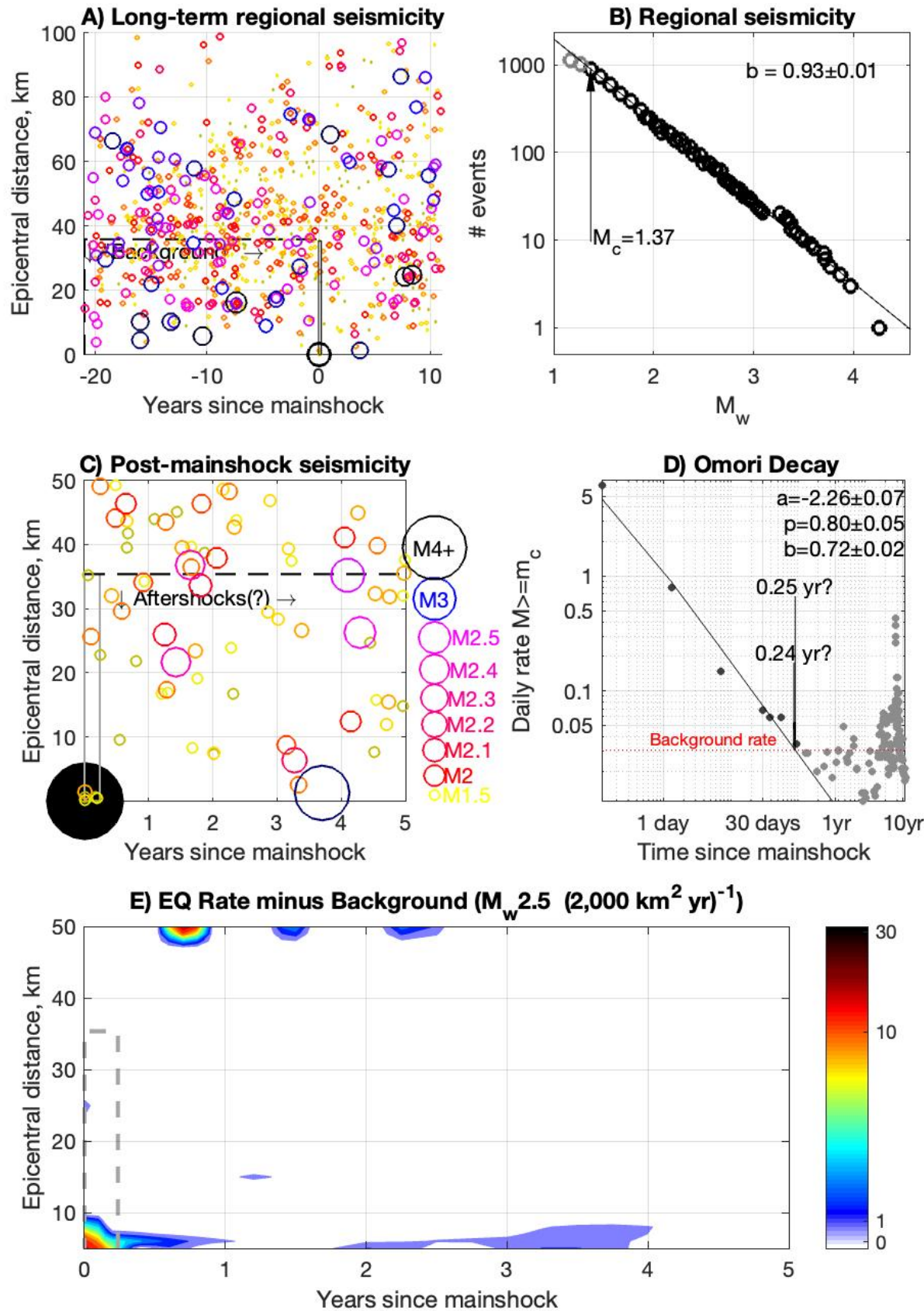


Figure 12: 2005 Charlevoix, QC

M4.47 1997 Quebec City

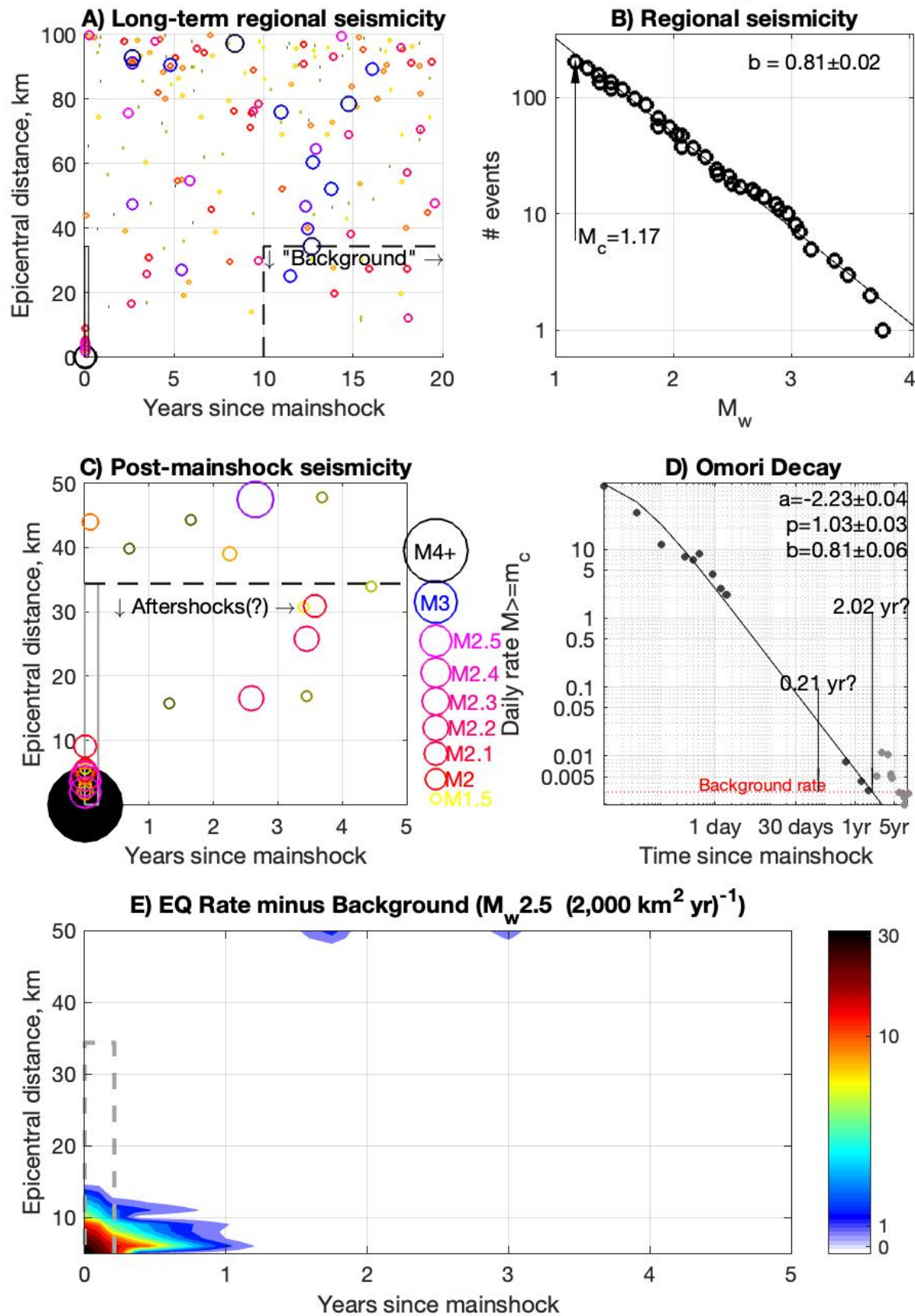


Figure 13: Cape-Rouge, Quebec City, QC

M4.56 1990 Mont-Laurier, QC

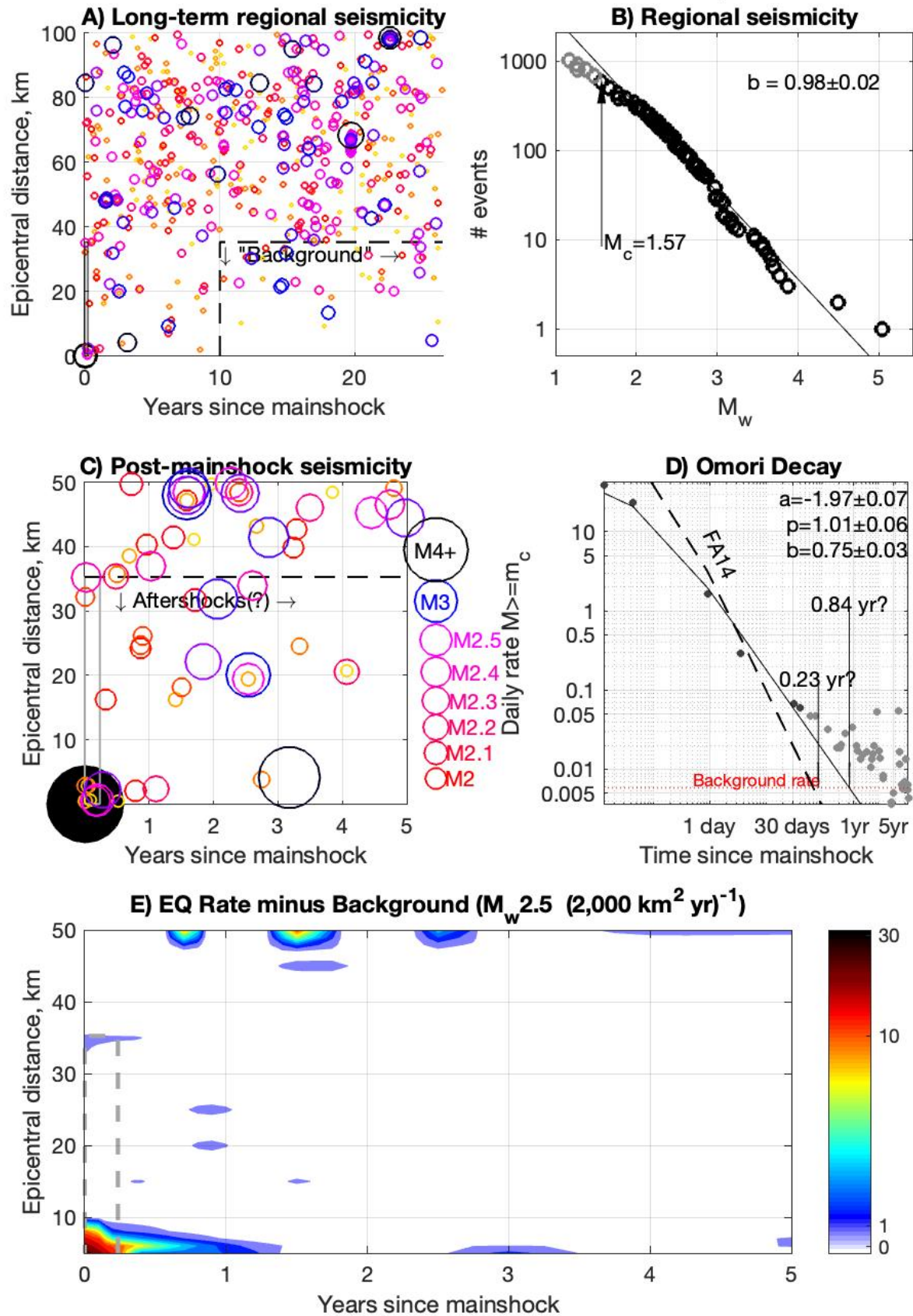


Figure 14: Mont Laurier, QC

M4.49 2013 Lac Barnes, QC

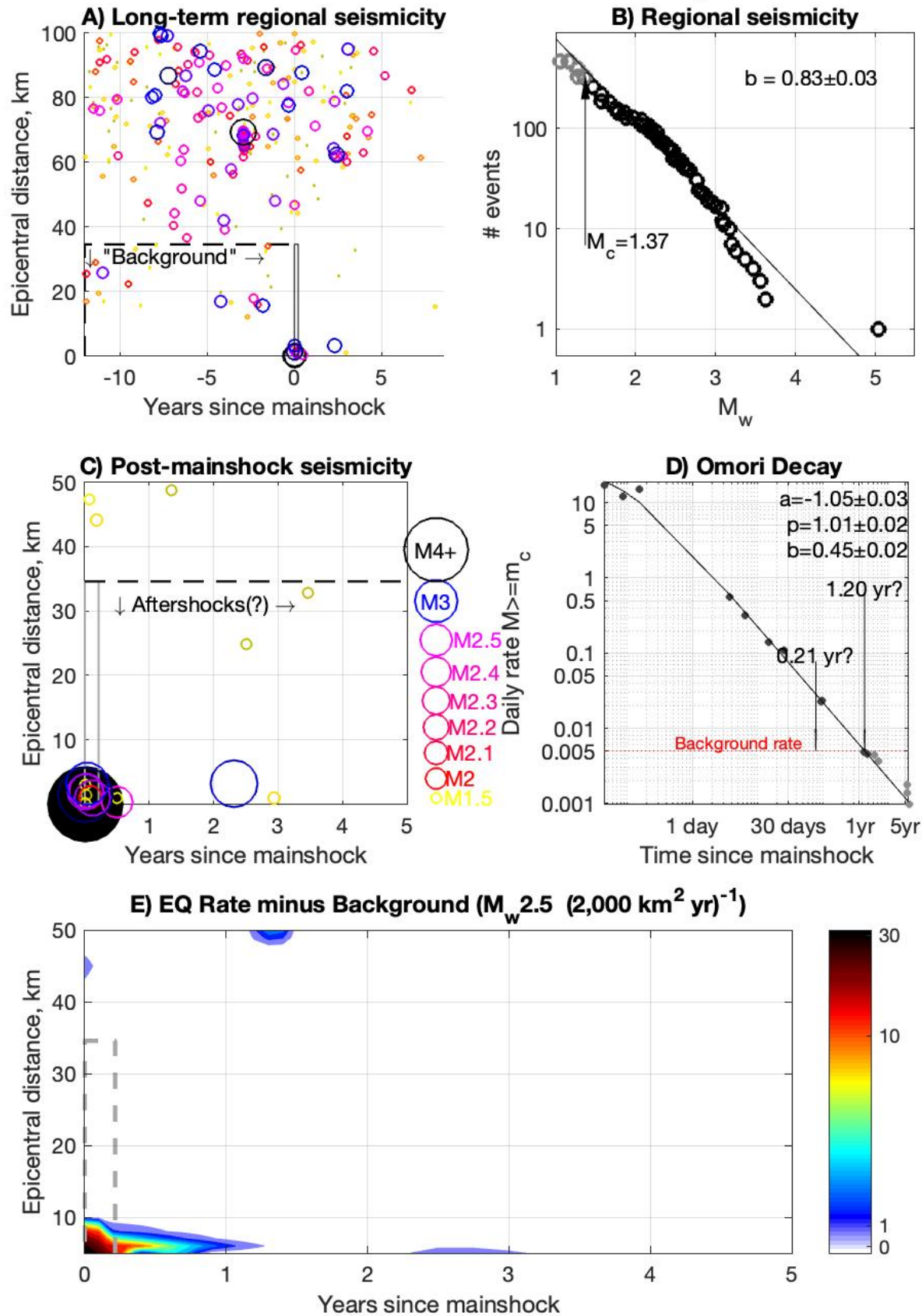


Figure 15: Lac Barnes, QC

M4.57 2000 Kipawa, QC

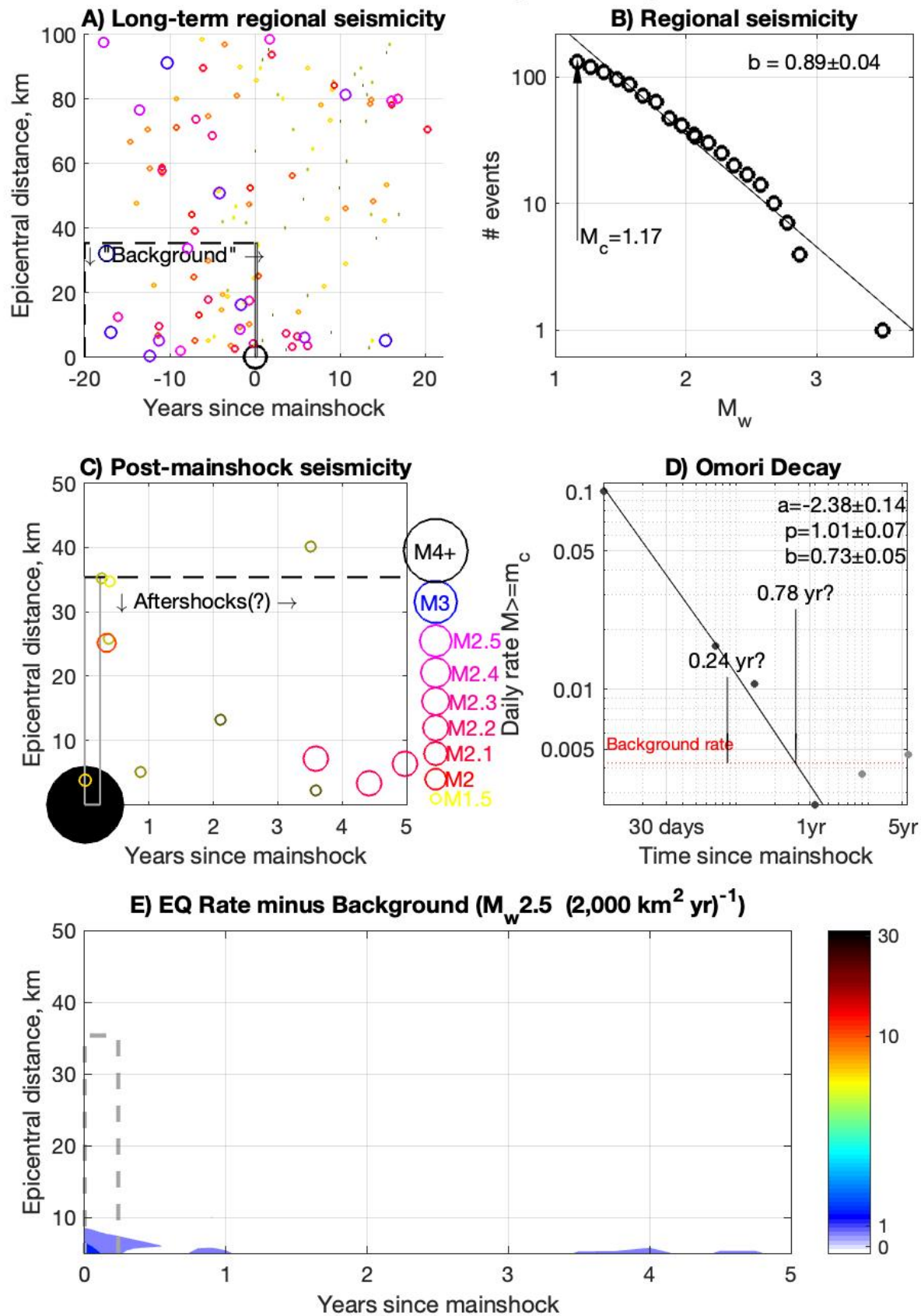


Figure 16: Kipawa, ON

M4.39 1999 Cote Nord, Lower St. Lawrence

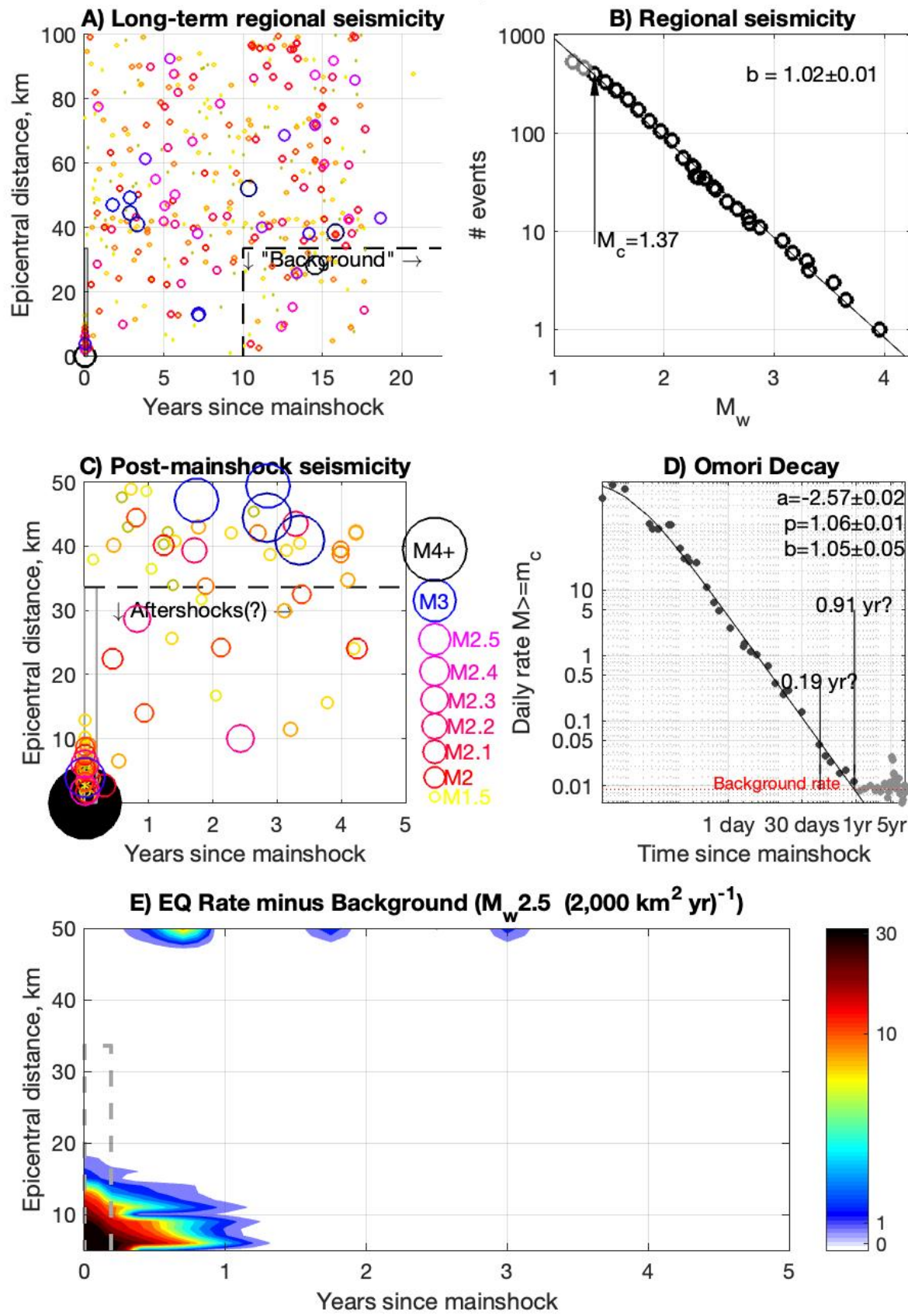


Figure 17: Côte Nord, Lower St. Lawrence seismic zone

M4.97 2002 Au Sable Forks, NY

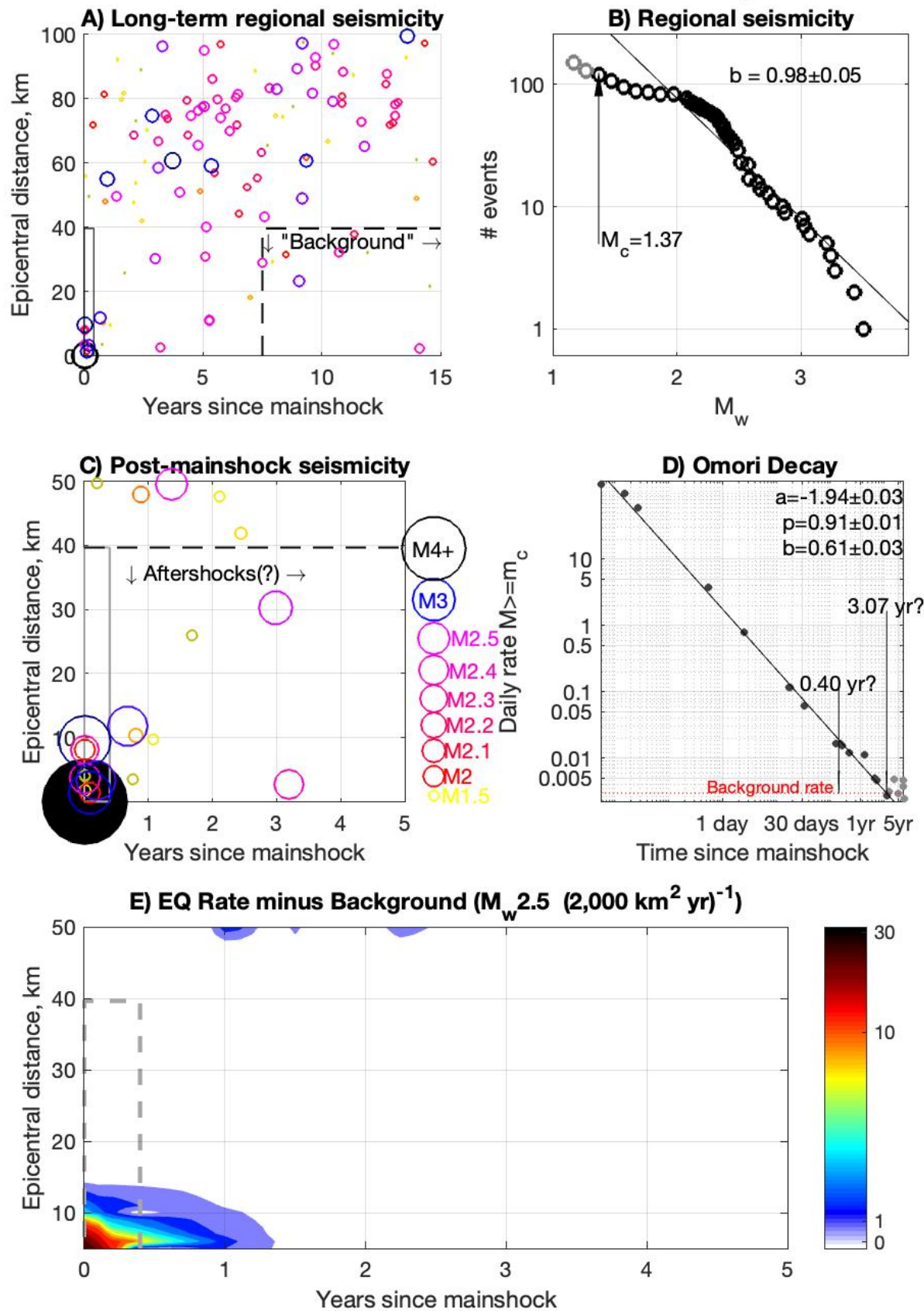


Figure 18: Au Sable Forks, NY

M4.83 1983 Goodnow, NY

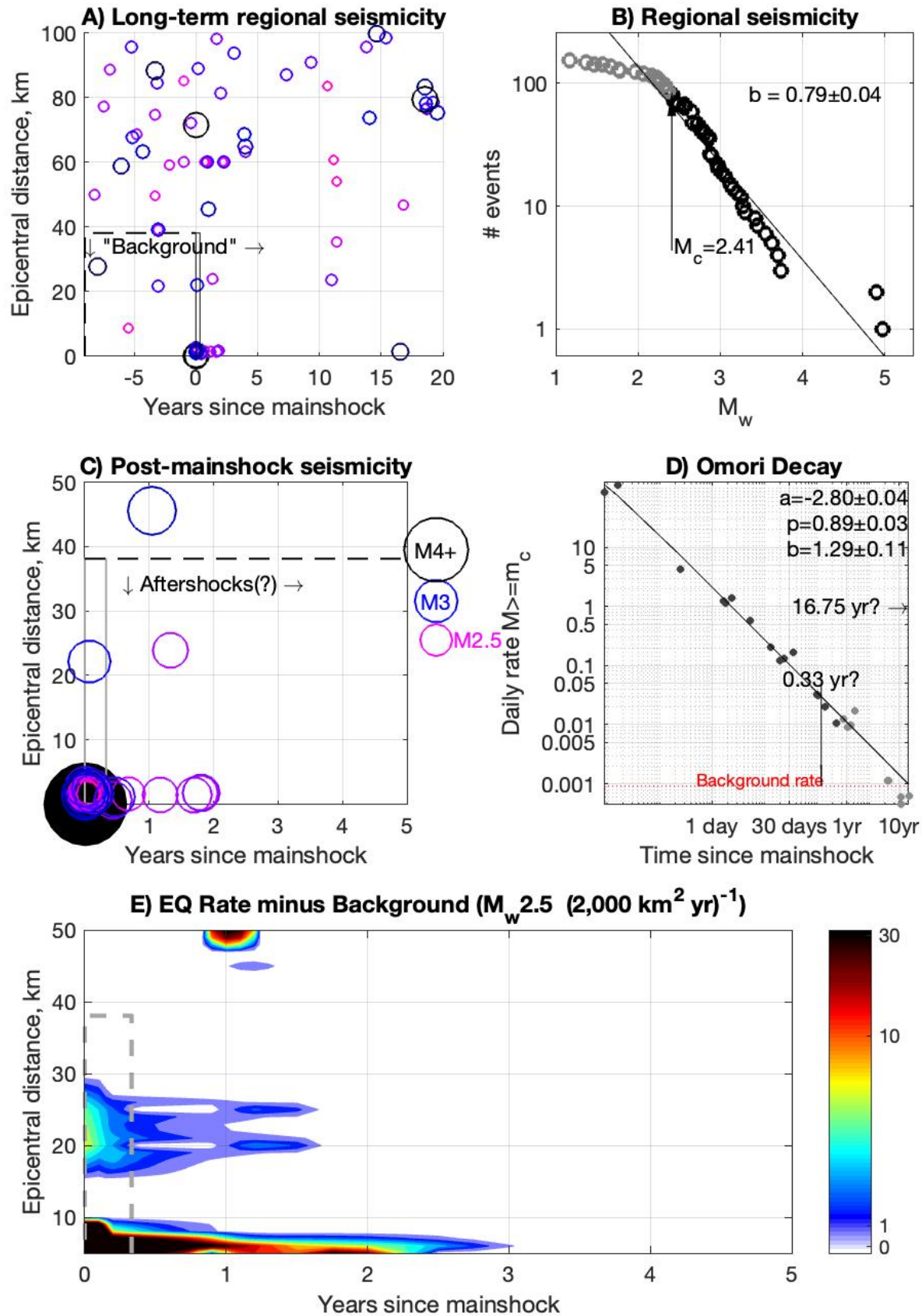


Figure 19: Goodnow, NY

M4.17 1988 Owingsville, KY

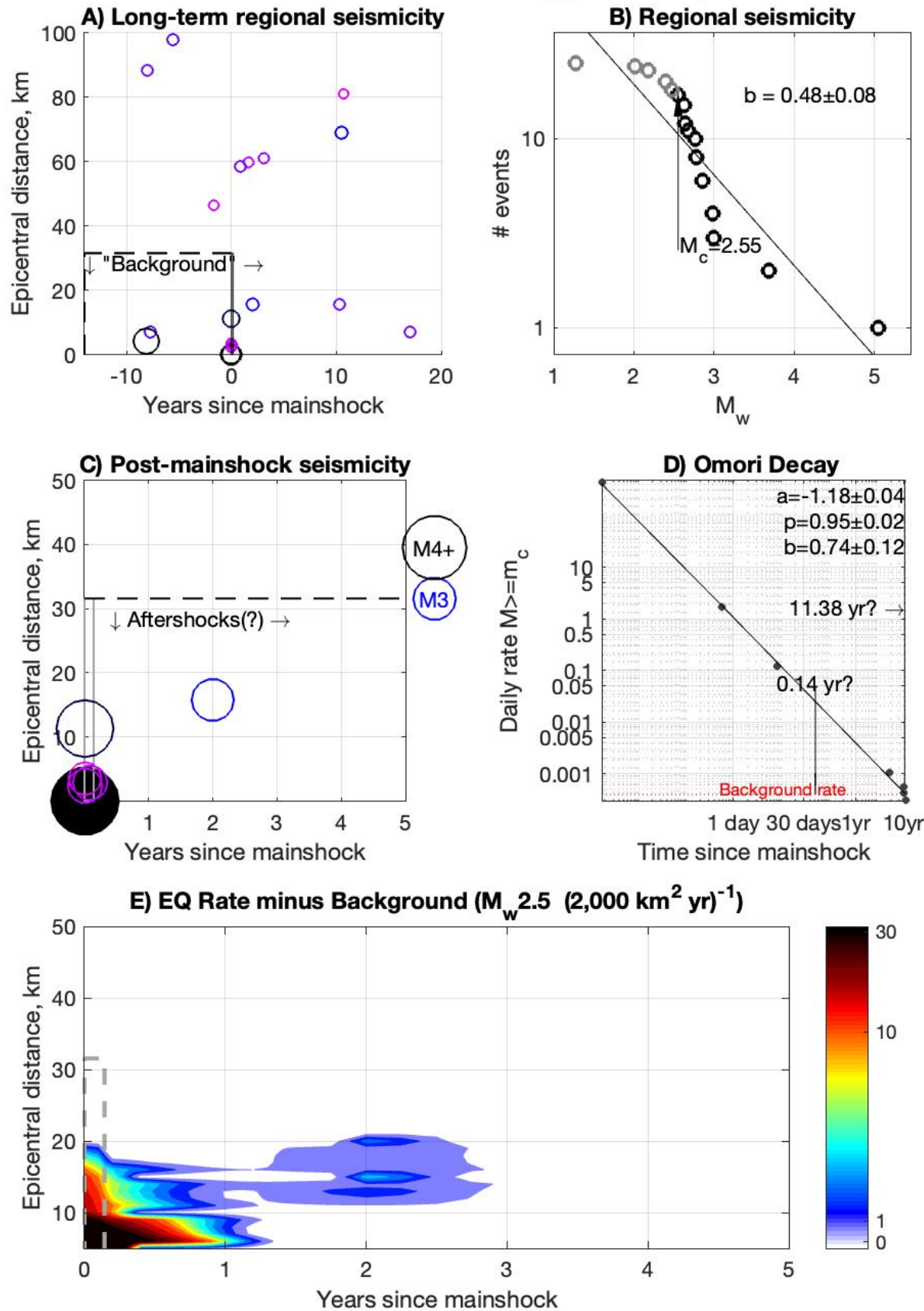


Figure 20: Owingsville, KY

M4.3 2001 Ashtabula, OH

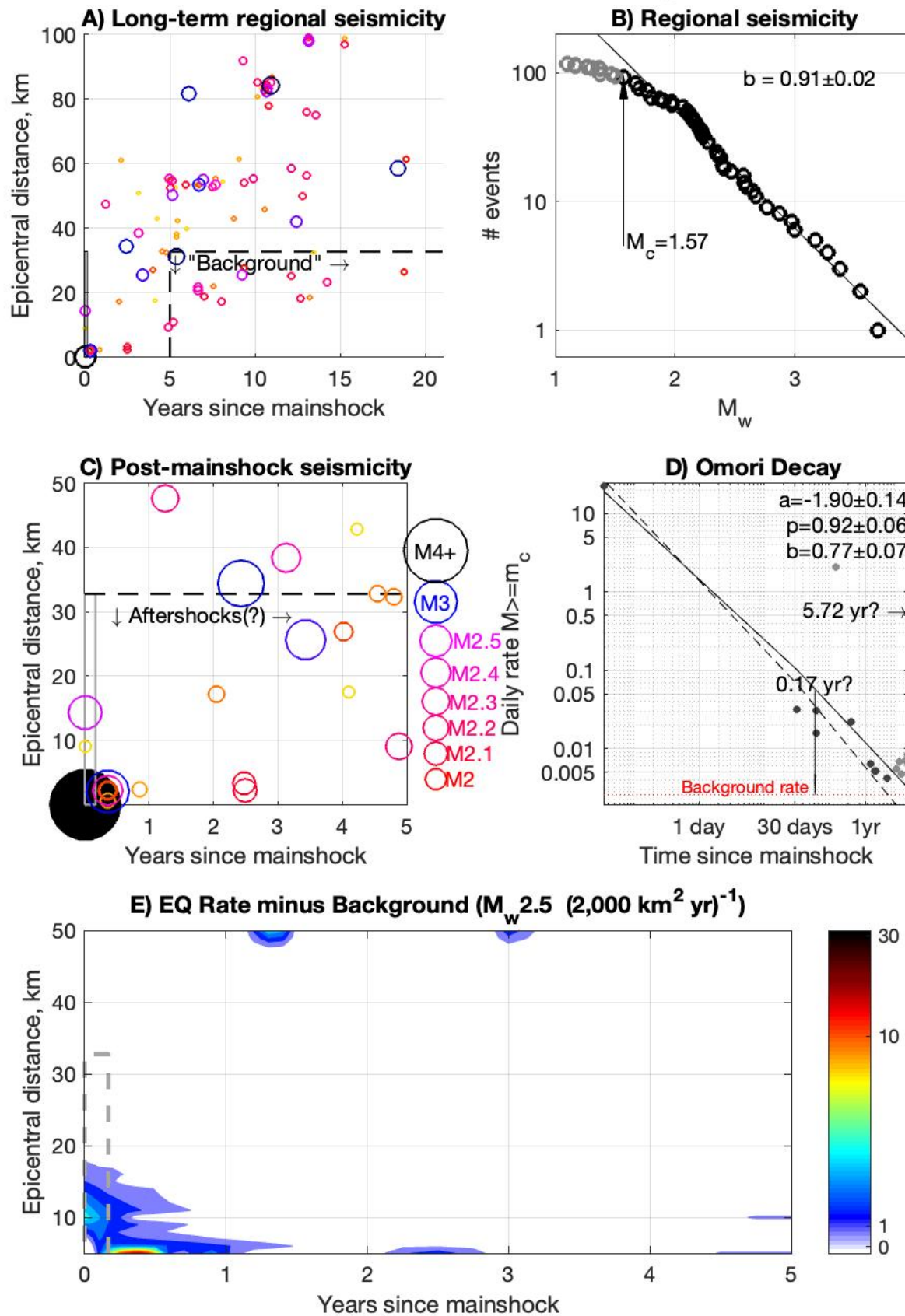


Figure 21: Ashtabula, OH. Dashed line in D) depicts an alternative model ($p=0.99$) derived for $m_c=1.37$.

M4.59 2003 Ft. Payne, AL

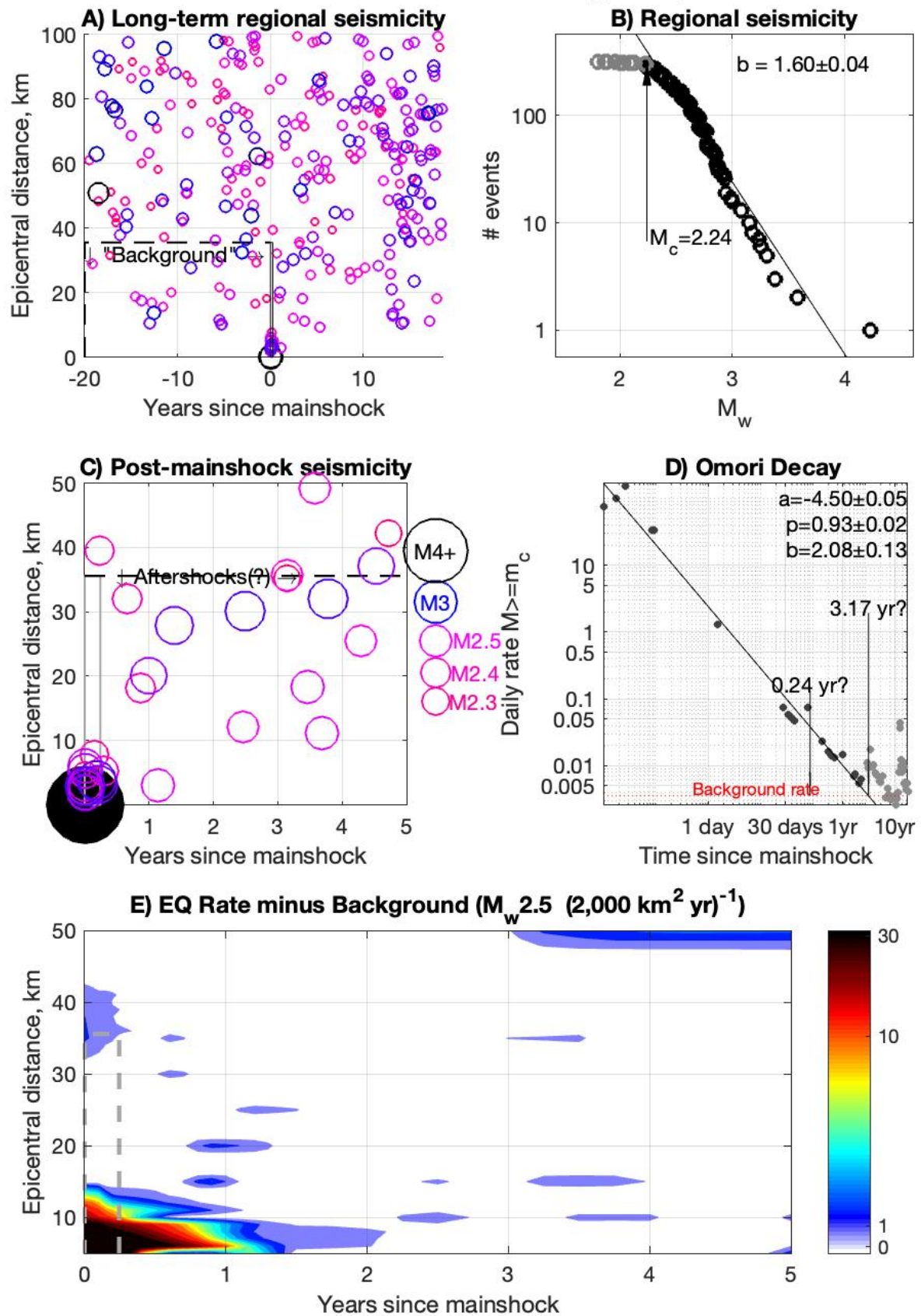


Figure 22: Fort Payne, AL, Eastern Tennessee seismic zone

M4.4 2018 Decatur, TN

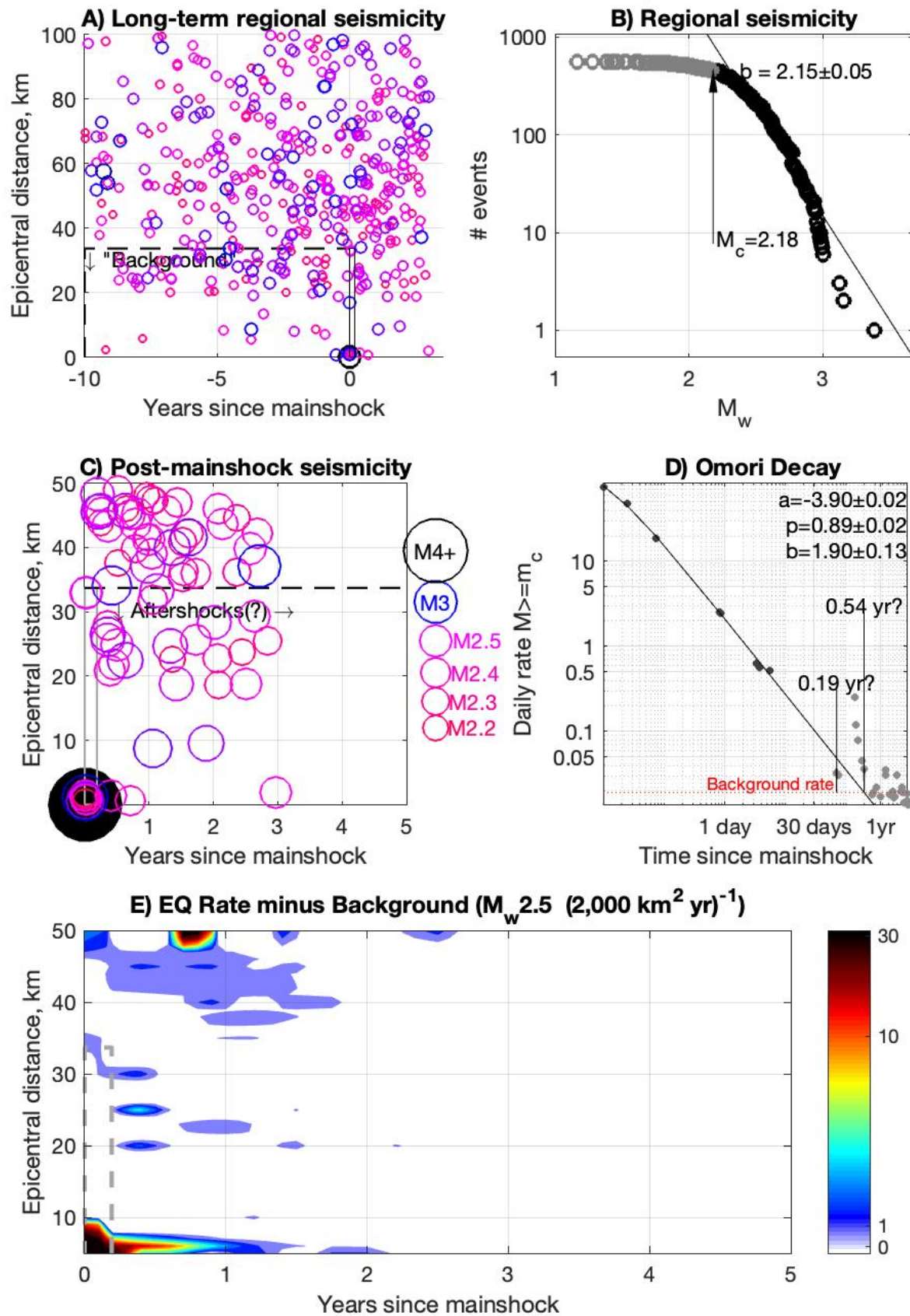


Figure 23: Decatur, TN, Eastern Tennessee seismic zone

M4.62 1976 Marked Tree, AR

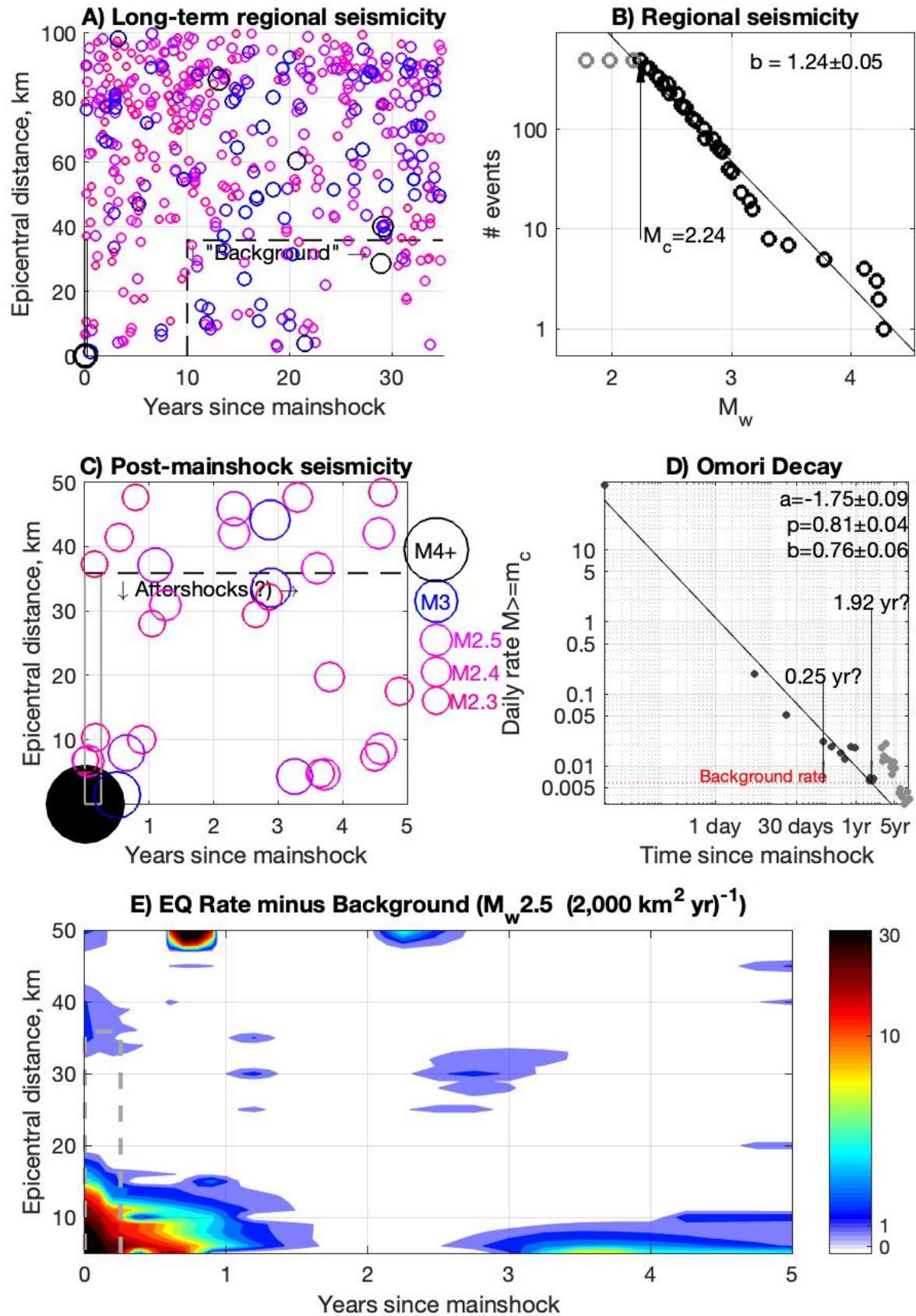


Figure 24: Marked Tree, AR, New Madrid seismic zone

M4.22 2005 Manila, AR

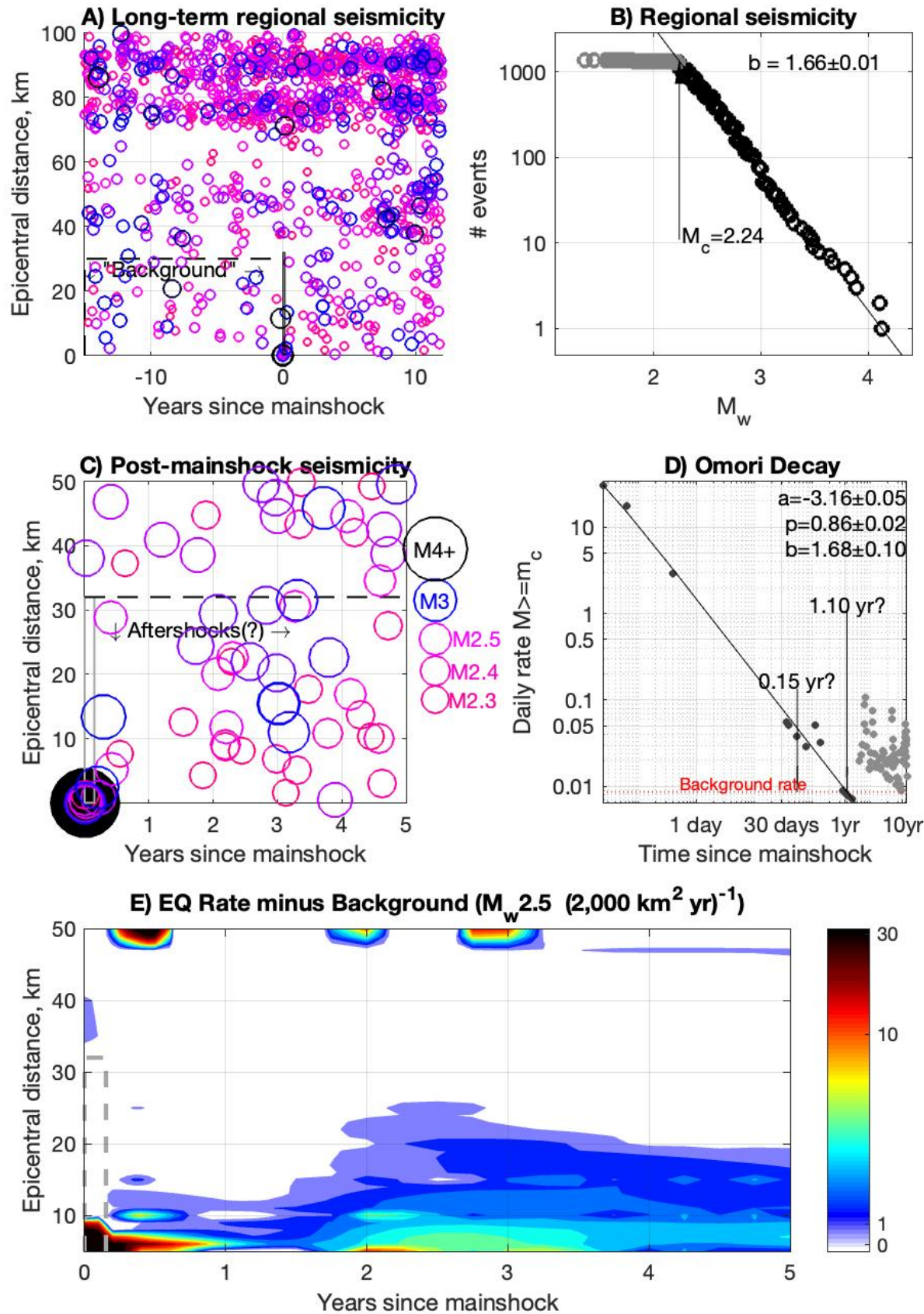


Figure 25: Manila, AR, New Madrid seismic zone

M4.28 1987 Cairo, IL

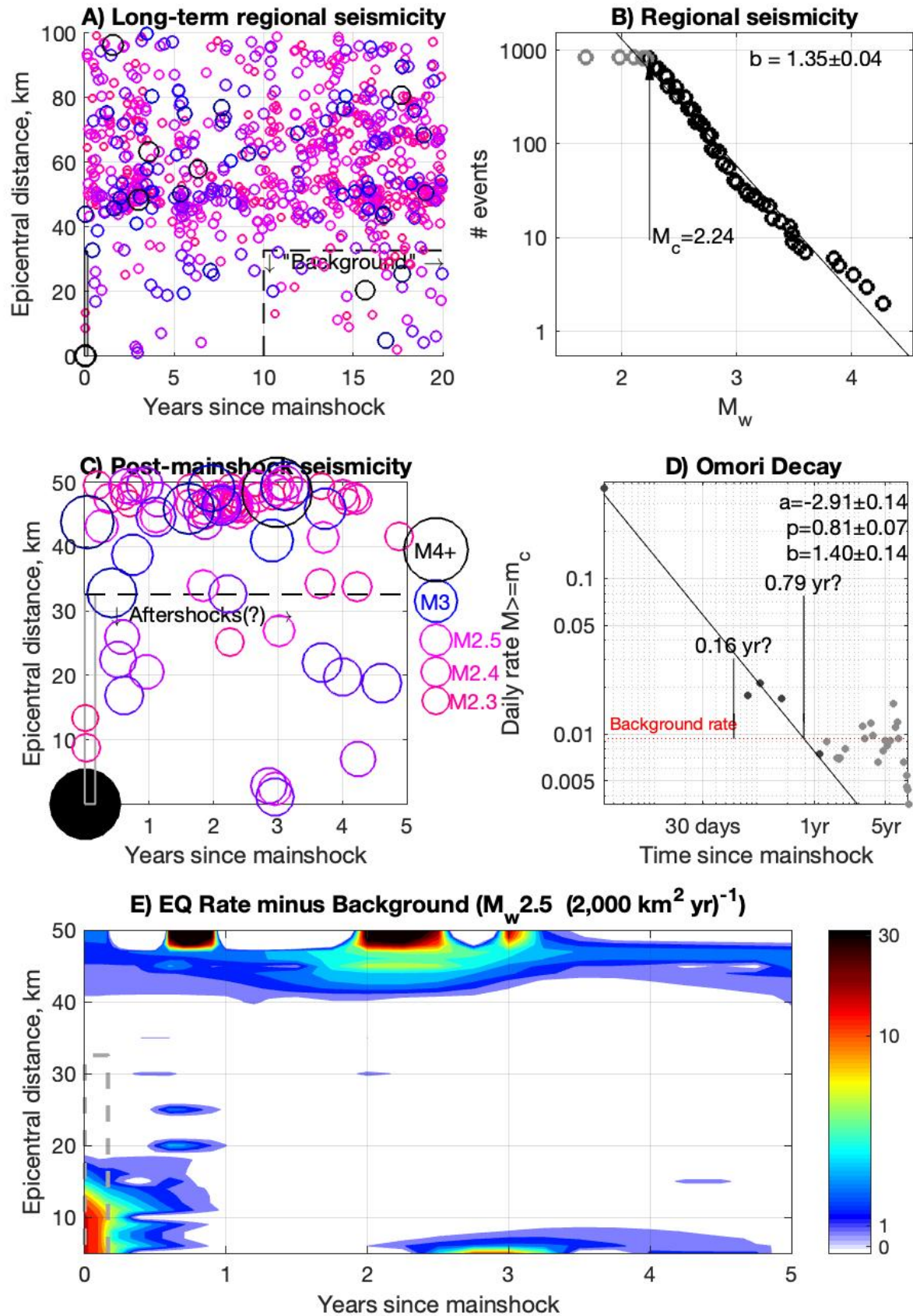


Figure 26: Cairo, IL

M4.28 1990 Chaffee, MO

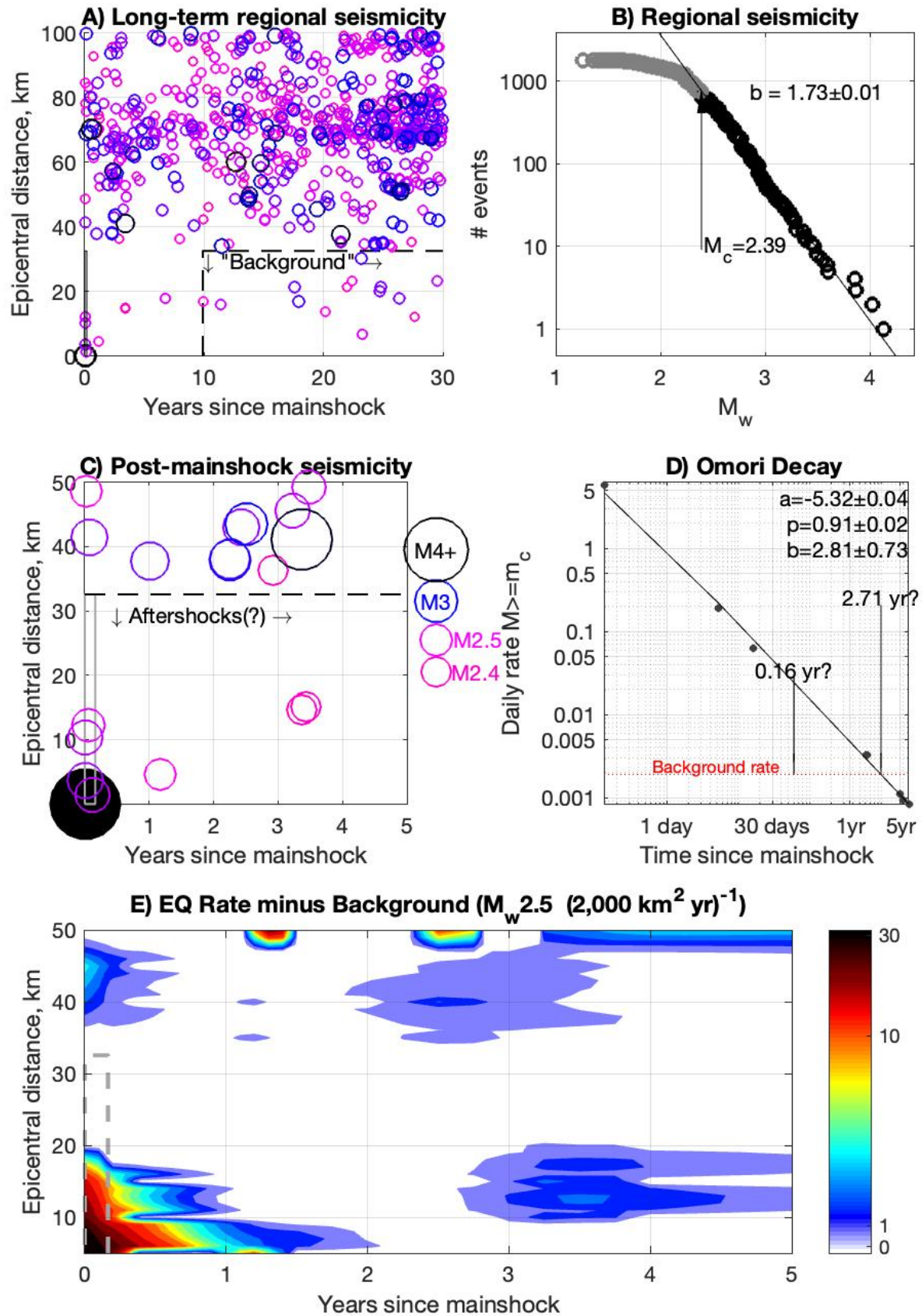
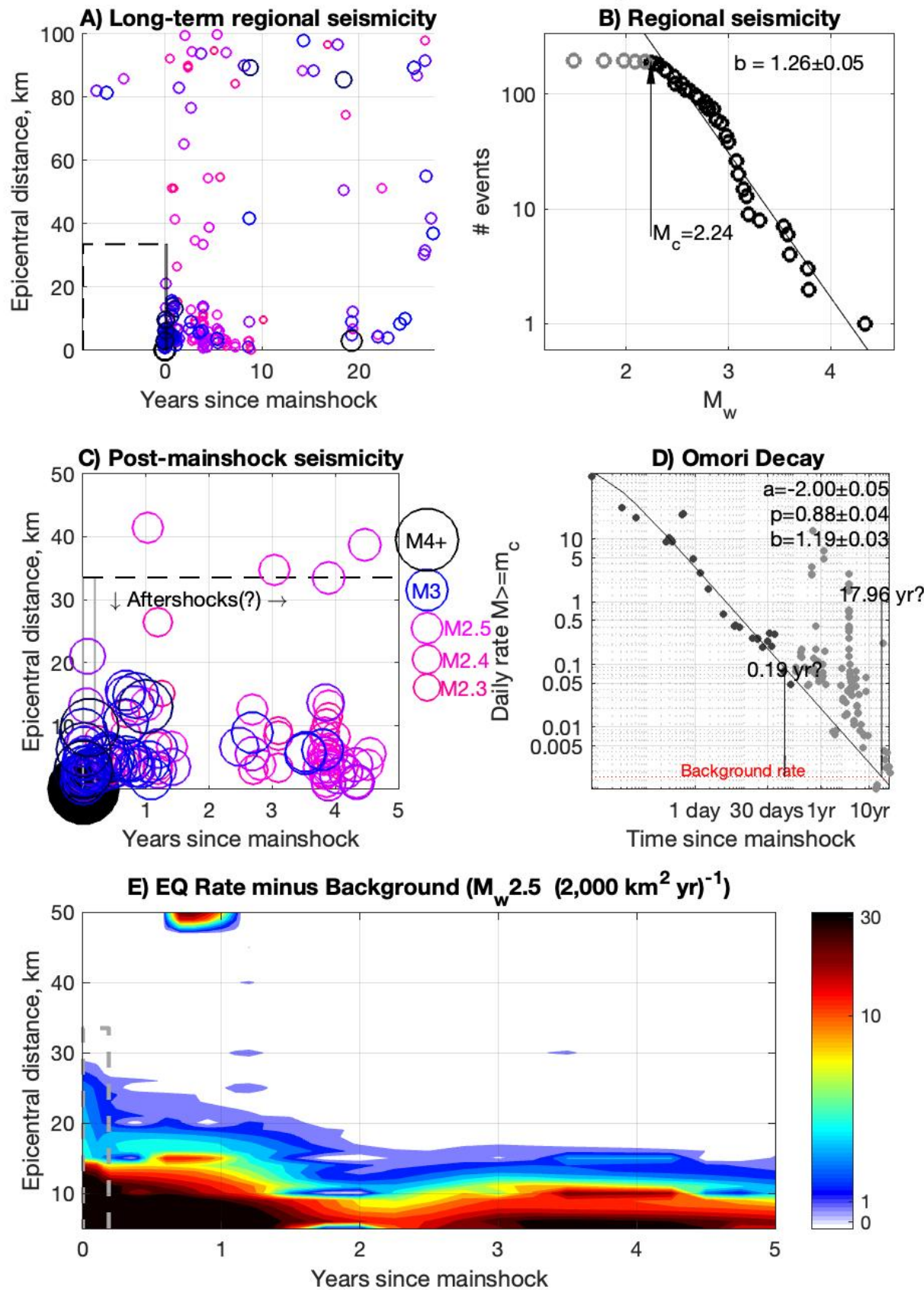


Figure 27: Chaffee, MO

M4.38 1982 Enola, AR



M4.34 2001 Enola, AR

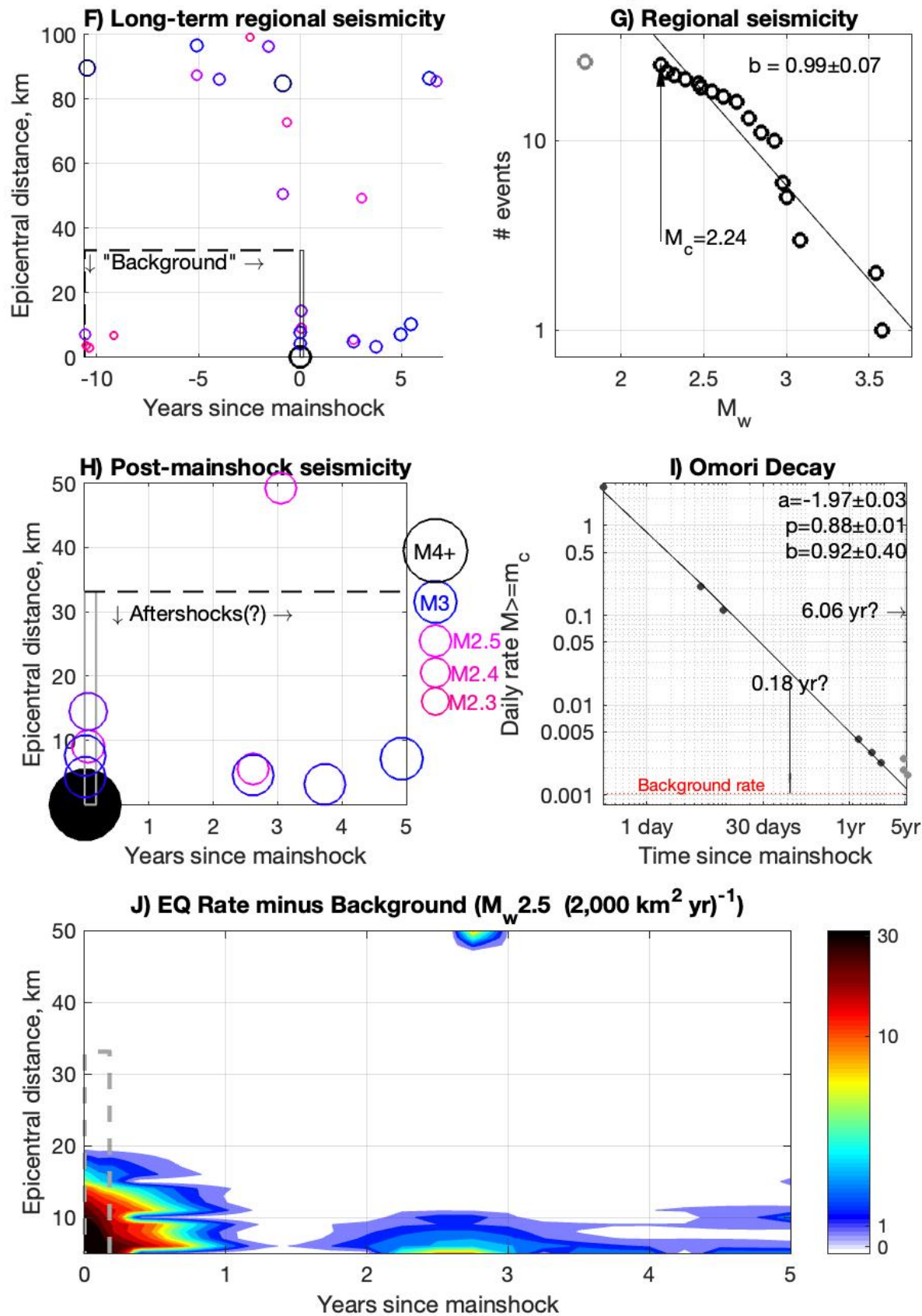


Figure 28: Enola, AR. **A–E**) 1982 sequence. **F–J**) 2001 sequence

Great Plains (n=21)

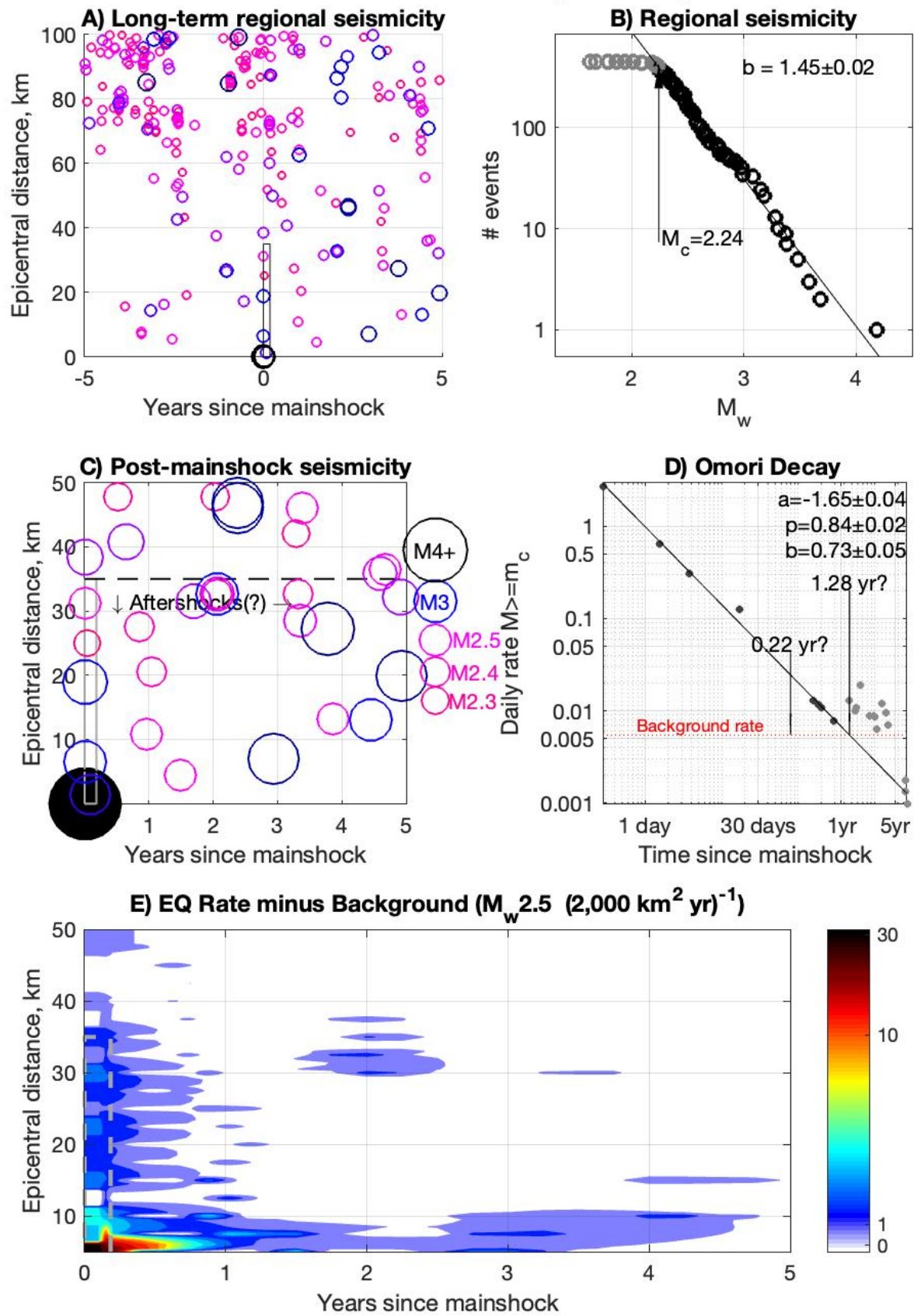


Figure 29: Stacked sequences ($n=21$) from the Great Plains, loosely defined as the area between -95° and the Rocky Mountain front and spanning Texas to Saskatchewan.

Figure 30: Metrics of sequence productivity.

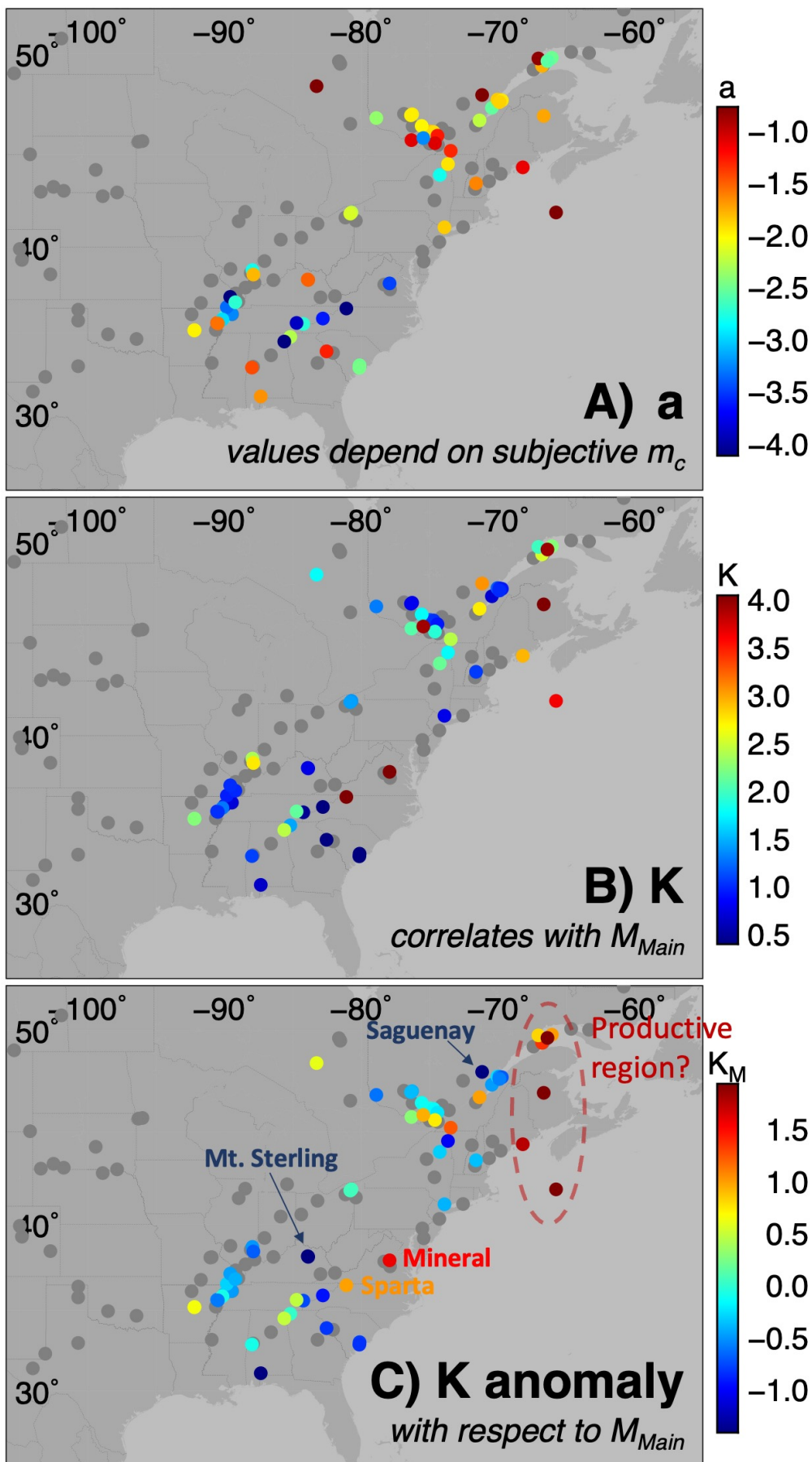
A) Omori a parameter is generally higher in SE Canada than the CEUS, yet there is substantial inverse tradeoff between the magnitude of completeness m_c and a , and m_c is typically lower in SE Canada.

B) Overall productivity $K = 10^{a+b(M_{\text{main}} - m_c)}$ subsumes both a and m_c but correlates strongly with M_{main} . Empirically, $K \approx 1.06 M_{\text{Main}}^2 - 7.90 M_{\text{Main}} + 15.90$.

C) Productivity variations with respect to M_{main} given as $K - 1.06 M_{\text{Main}}^2 + 7.90 M_{\text{Main}} - 15.90$.

For example, of the M5+ mainshocks, the Mineral, VA and Sparta, NC sequences are comparatively productive, and Mt. Sterling, KY and Saguenay, QC are lethargic.

Sequences in the Lower St. Lawrence seismic zone and elsewhere in the Atlantic appear to be anomalously lively.



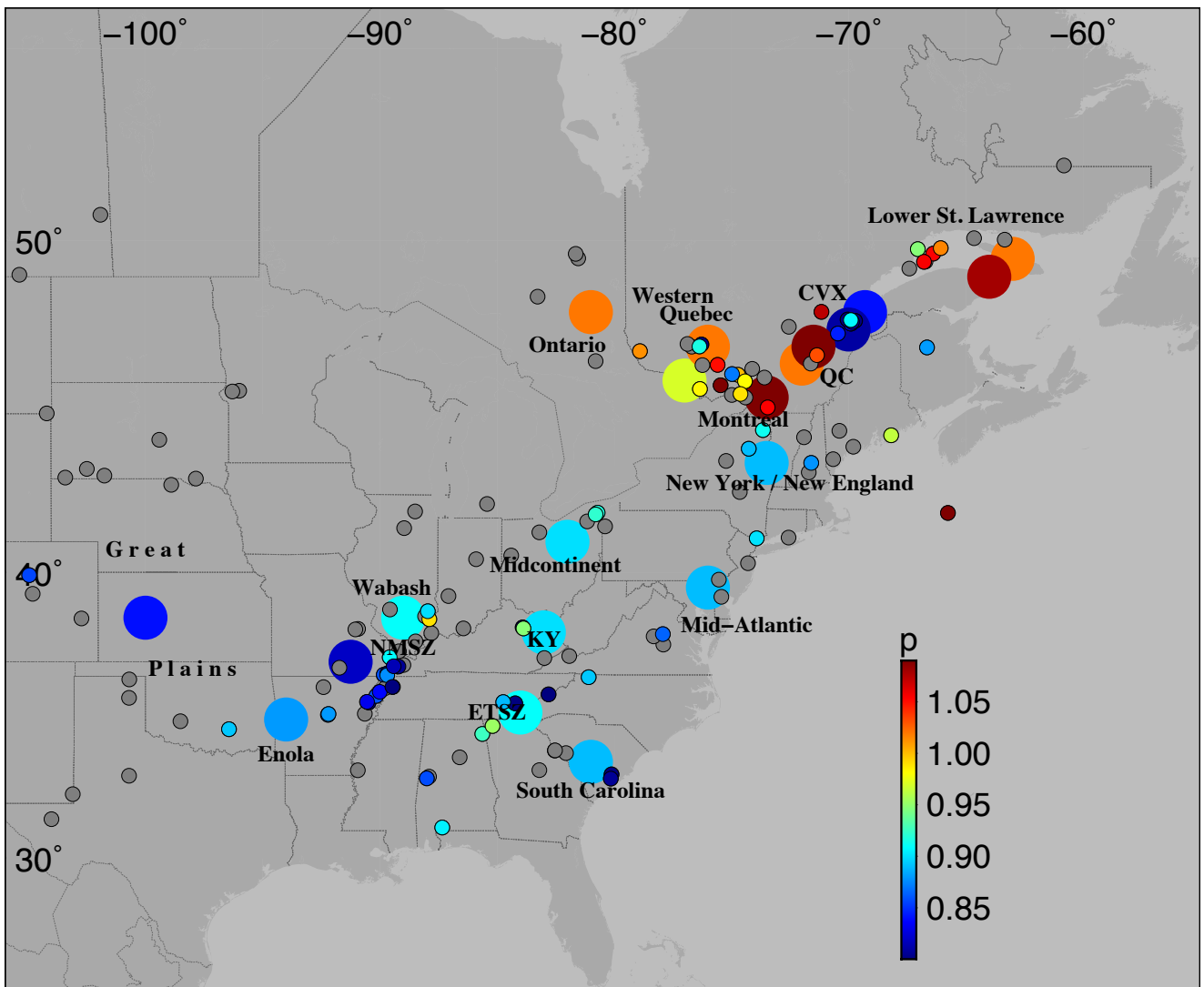


Figure 31: Aftershock decay rate p . Small circles: Individual sequences. Gray circles: Sequences with insufficient activity for Omori Decay modeling. Large circles: seismic-zone-wide average p from individual sequences and zone-wide stacks. CVX: Charlevoix. ETSZ: Eastern Tennessee seismic zone. KY: Kentucky. NMSZ: New Madrid seismic zone. QC: Quebec City.

Rapid decay— $p \gtrsim 1$ —characterizes SE Canadian sequences compared to CEUS sequences ($p \lesssim 0.9$), except near Charlevoix ($p \approx 0.9$)

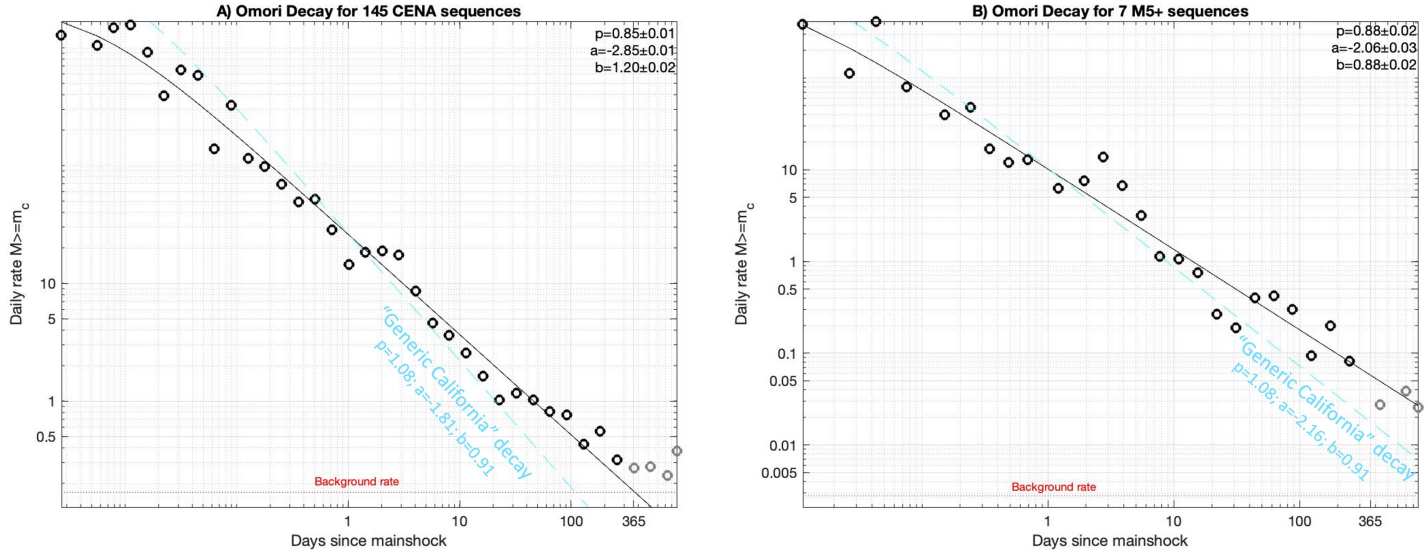


Figure 32: Omori Decay of stacked CENA sequences.

A) All 145 sequences analyzed here ($M_{\text{main}} 3.65–5.84$). **B) M5+ sequences.**

Reasenberg and Jones (1989) average model is shown in cyan, except a is adjusted so that CENA decay and generic California curve intersect at 1.0 days in order to highlight differences in decay slope p . Fits in A and B are derived from the first 365 days of rate data.

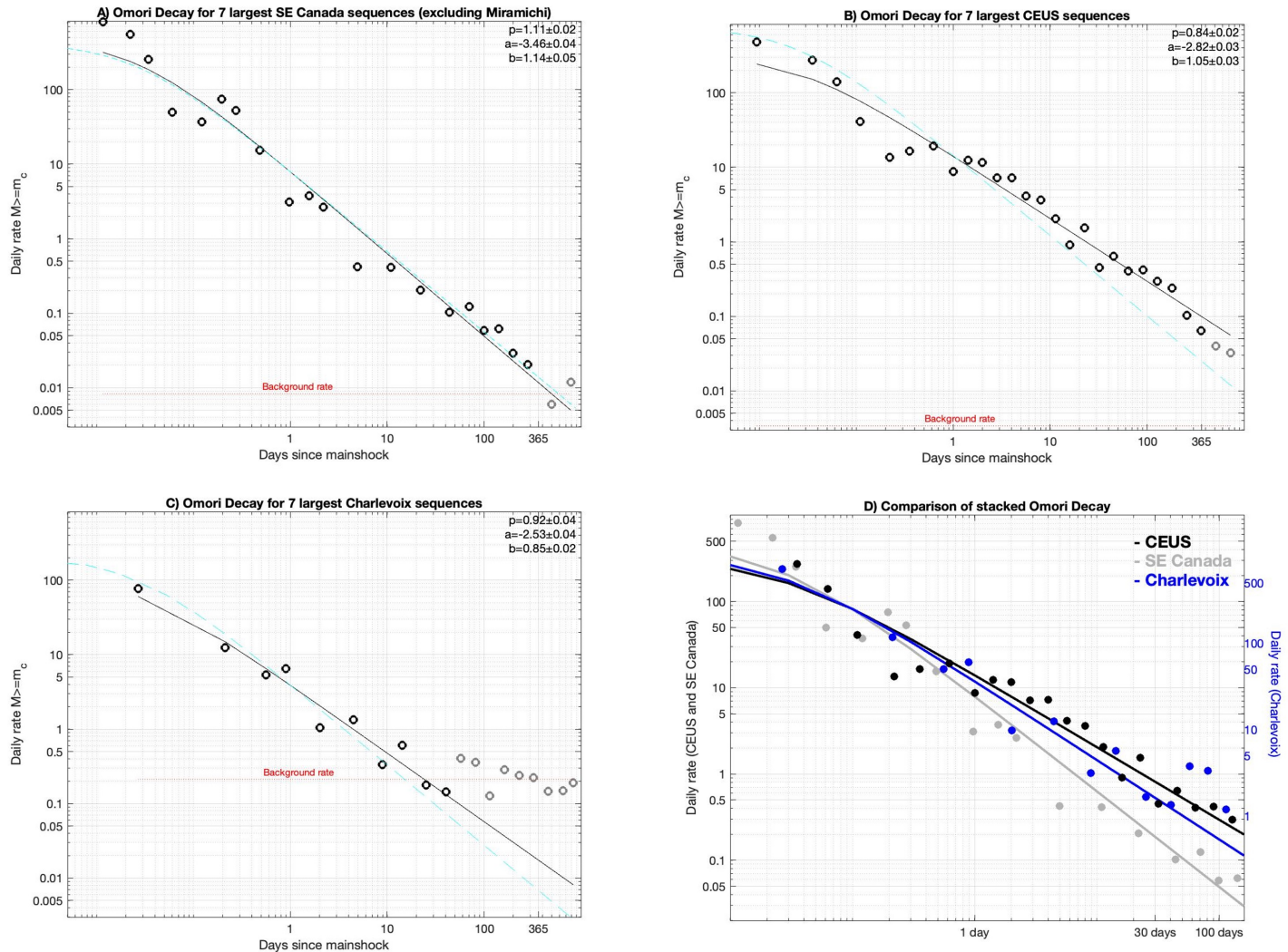


Figure 33: Omori Decay of seven-sequence stacks from A) SE Canada (excluding the Charlevoix region and the Miramichi sequence) $M_{\text{main}} 4.39-5.84$, B) CEUS $M_{\text{main}} 4.83-5.65$, and C) Charlevoix $M_{\text{main}} 3.71-4.75$. The seven largest mainshocks, by magnitude, are used in each region. D) Comparison of Omori Decay in the three regions. Gray: SE Canada. Black: CEUS. Blue: Charlevoix. Circles: Rate estimates from A-C.

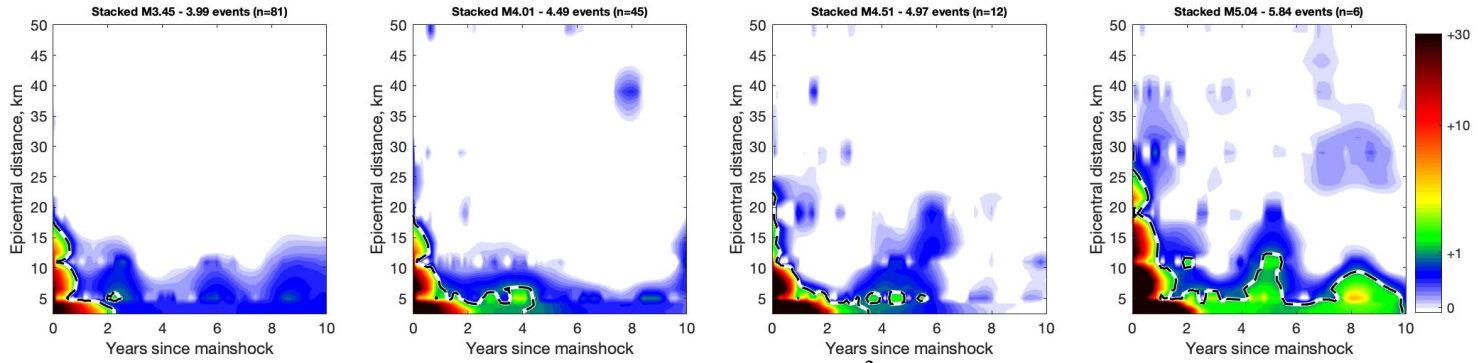


Figure 34: Average excess rate-density (annual #M2.5 / 2000 km²) for CENA sequences, binned by mainshock magnitude, as function of epicentral radius and time since mainshock. White regions denote activity rates equal to or lower than estimated long-term averages. Black/white dashed line: Rate density = estimated background rate density +1.0 M2.5+ event annually/2000 km². The Miramichi sequence is excluded from the M5+ stack, partially because of imprecise aftershock locations and partially because of its anomalous persistence.

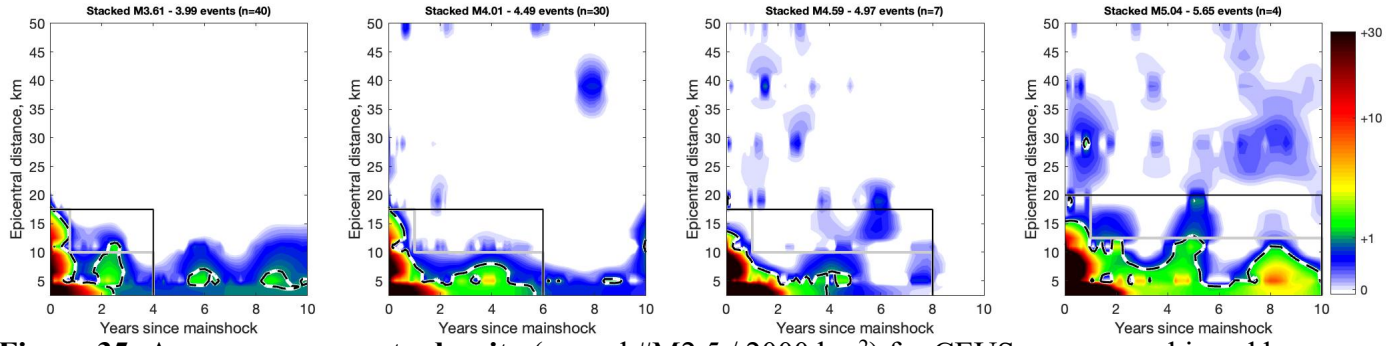
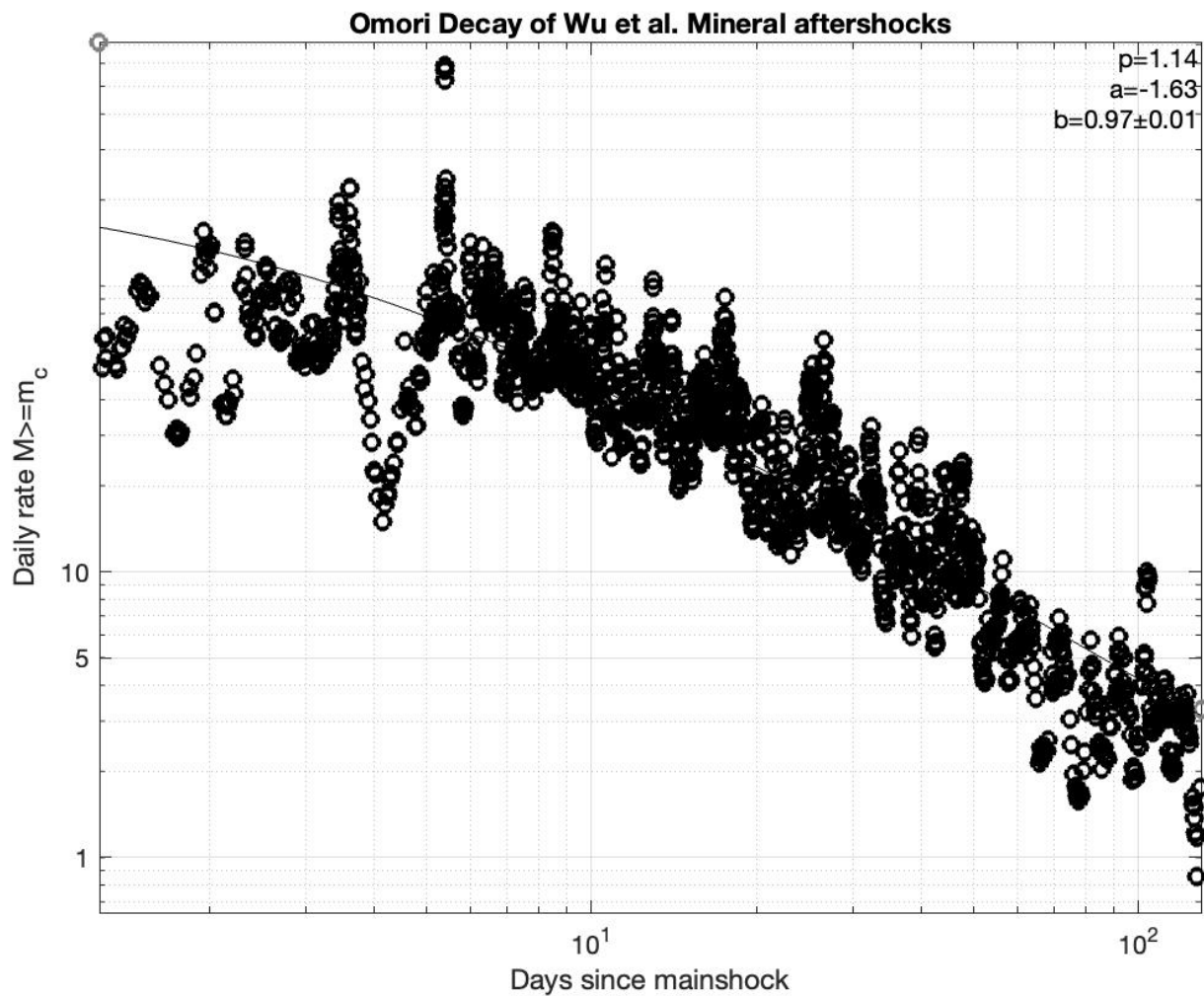


Figure 35: Average excess rate-density (annual #M2.5 / 2000 km²) for CEUS sequences, binned by mainshock magnitude, as function of epicentral radius and time since mainshock. Suggested declustering windows are shown as black (rectangular) and light grey (two-phase, boot-shaped) boxes.



Supplementary Figure S2.1: Omori Decay modeling of Mineral aftershocks using Wu et al.'s [2015] catalog, magnitude scale M_D^* , and $c=2.99$ days. The semi-automated algorithm employed here effectively reproduces Wu et al.'s findings. Using a common, consistent magnitude scale, $c=0.05$ days, and a substantially longer catalog, a much lower $p = 0.88$ is derived in the main text.

REFERENCES

- Boyd, O. S., Smalley, R., and Zeng, Y. Crustal deformation in the New Madrid seismic zone and the role of postseismic processes, JGR, 120.
- Cramer, C.H., and Boyd, O.S. (2014). Why the New Madrid earthquakes are M 7–8 and the Charleston earthquake is M ~7. BSSA 104(6).
- Davis, S. D., and C. Frohlich (1991). Single-link cluster analysis of earthquake aftershocks: Decay laws and regional variations, J. Geophys. Res. 96, no. B4, 6335–6350.
- Du Berger, R., D. W. Roy, M. Lamontagne, G. Woussen, R. G. North, and R. J. Wetmiller (1991). The Saguenay (Quebec) earthquake of November 25, 1988: Seismologic data and geologic setting, Tectonophysics 186, no. 1, 59–74.
- Ebel, J. E., Bonjer, K. P., & Oncescu, M. C. (2000). Paleoseismicity: Seismicity evidence for past large earthquakes, SRL, 71(2).
- Ebel, J. E. (2008) The importance of small earthquakes, SRL, 79(4).
- Ebel, J. E. (2011). A new analysis of the magnitude of the February 1663 earthquake at Charlevoix, Quebec, Bull. Seismol. Soc. Am. 101, 1024–1038, doi: [10.1785/0120100190](https://doi.org/10.1785/0120100190).
- Fereidoni, A., and G. M. Atkinson (2014). Aftershock statistics for earthquakes in the St. Lawrence Valley, Seismol. Res. Lett. 85, no. 5, 1125–1136.
- Frankel, A., C. Mueller, T. Barnhard, D. Perkins, E. V. Leyendecker, N. Dickman, S. Hanson, and M. Hopper (1996). 1996 National Seismic Hazard Maps—Documentation June 1996, U.S. Geol. Surv. Open-File Rept. 96-532, 110 pp.
- Gardner, J. K., and L. Knopoff (1974). Is the sequence of earthquakes in southern California, with aftershocks removed, Poissonian?, Bull. Seismol. Soc. Am. 64, 1363–1367.
- Hamburger, M.W., et al. (2011) Aftershocks of the 2008 Mt. Carmel, Illinois, Earthquake: Evidence for Conjugate Faulting near the Termination of the Wabash Valley Fault System. SRL, 82(5).
- Lamontagne, M., A. L. Bent, C. R. Woodgold, S.Ma, and V. Peci (2004). The 16 March 1999 mN 5.1 Côte-Nord earthquake: The largest earthquake ever recorded in the lower St. Lawrence seismic zone, Canada, Seismol. Res. Lett. 75, no. 2, 299–316.
- Lamontagne, M., H. S. Hasegawa, D. A. Forsyth, G. G. Buchbinder, and M. Cajka (1994). The Mont-Laurier, Québec, earthquake of 19 October 1990 and its seismotectonic environment, Bull. Seismol. Soc. Am. 84, no. 5, 1506–1522.
- Mueller, C. S. (2018). Earthquake catalogs for the USGS national seismic hazard maps. Seismological Research Letters, 90(1), 251-261.
- Omori, F. (1894). On the aftershocks of earthquakes: J. Coll. Sci. Imp. Univ. Tokyo 7, 111–200.
- Page, M. T., and Van der Elst, N.J. (2022). Aftershocks preferentially occur in previously active areas. The Seismic Record, 2(2).
- Petersen, M.D. et al. (2008). Documentation for the 2008 Update of the United States National Seismic Hazard Maps: USGS Open File Report 2014-1128.
- Petersen, M.D. et al. (2014). Documentation for the 2014 Update of the United States National Seismic Hazard Maps: USGS Open File Report 2014-1091.
- Reasenberg, P.A. and L.M. Jones (1989). Earthquake hazard after a mainshock in California, Science 243, 1,173-1,176.
- Stein, S., Liu, M., 2009. Long aftershock sequences within continents and implications for earthquake hazard assessment. Nature, 462.
- Wetmiller, R., J. Adams, F. Anglin, H. Hasegawa, and A. Stevens (1984). Aftershock sequences of the 1982 Miramichi, New Brunswick, earthquakes, Bull. Seismol. Soc. Am. 74, no. 2, 621–653.

- Yang, H., L. Zhu, and R. Chu (2009). Fault-plane determination of the 18 April 2008 Mount Carmel, Illinois, earthquake by detecting and relocating aftershocks. *Bulletin of the Seismological Society of America* 99, 3,413–3,420.
- Yeck, W.L., A. F. Sheehan, H. M. Benz, M. Weingarten, J. Nakai (2016) Rapid Response, Monitoring, and Mitigation of Induced Seismicity near Greeley, Colorado. *Seismological Research Letters*, 87(4): 837–847. doi: <https://doi.org/10.1785/0220150275>